FACULTY OF BIOSCIENCE ENGINEERING

FLOW CYTOMETRIC MICROBIAL MONITORING FOR SAFEGUARDING DRINKING WATER QUALITY

Jorien Favere

Student number: 01307110

Promotors: Prof. dr. ir. Nico Boon, Prof. dr. ir. Bart De Gusseme

Tutors: ir. Jasmine Heyse, Peter Rubbens

Master's Dissertation submitted in fulfilment of the requirements for the degree of Master of Science in Bioscience Engineering: Chemistry and Bioprocess Technology

Academic year: 2017 – 2018

UNIVERSITEIT GENT

Ghent, June 8th, 2018

The promotors,

Prof. dr. ir. Nico Boon

Prof. dr. ir. Bart De Gusseme

The tutors,

ir. Jasmine Heyse

Peter Rubbens

The author,

Jorien Favere

Acknowledgements

Thes-is the end... Met het afronden van mijn thesis sluit ik mijn studententijd af. Het waren vijf heerlijke jaren die voorbij gevlogen zijn. Het thesisjaar was een rollercoaster met ups en downs, waarin ik ongelofelijk veel heb bijgeleerd. Ik ben enorm dankbaar voor de kansen die ik tijdens mijn thesis heb gekregen, en ben trots op het eindresultaat.

Dit verhaal had ik nooit kunnen schrijven zonder mijn tutors. Zij kunnen niet genoeg bedankt worden. Jasmine, jij werd pas halverwege het jaar tot mijn tutor aangesteld en vervulde die rol subliem. Ik heb enorm veel van je bijgeleerd, jouw enthousiasme voor het onderzoek was aanstekelijk. Peter, dankjewel voor je begeleiding doorheen het jaar, jouw inbreng tilt mijn thesis echt naar een hoger niveau. Ook voor de steeds heldere uitleg, bij al die keren dat ik te pas en te onpas je bureau binnenviel. Benjamin, dankjewel voor de hulp en wijze raad, zelfs nadat je je doctoraat behaalde.

Professor Boon en professor De Gusseme, bedankt voor de unieke kansen die ik heb gekregen tijdens mijn thesis, om naar Washington DC te kunnen gaan en met de industrie samen te werken. Bedankt voor de waardevolle feedback. Jullie liefde voor het vak werkte motiverend!

Daarnaast wil ik graag de vakgroep CMET bedanken, voor de warme sfeer en behulpzaamheid. In het bijzonder Christine en Régine, voor alle praktische hulp voor, tijdens en na bij mijn trip naar Amerika. Ook Tom, voor de hulp bij de nitrificatie-experimenten.

I would like to thank everyone at DC Water. Especially Haydée, thank you for your guidance. You triggered my sense for research and got the best out of me. Garrett, thank you for your guidance, your help and big support. Rahil, thank you for your help during the nitrification experiments, even sacrificing your weekends.

Tot slot wil ik mijn ouders, zussen en vriend bedanken voor de steun doorheen het jaar.

Contents

Table of Abbreviations

AOB	Ammonia oxidizing bacteria
AOC	Assimilable organic carbon
ATP	Adenosine triphosphate
DBP	Disinfection by-product
DWD	Drinking Water Directive
DWDS	Drinking water distribution system
FCM	Flow cytometry
FL-1	Green fluorescence
FL-3	Red fluorescence
FSC	Forward scatter
HNA	High nucleic acid
HPC	Heterotrophic plate count
LNA	Low nucleic acid
NOB	Nitrite oxidizing bacteria
NPOC	Non-purgeable organic carbon
OPU	Operational phenotypic unit
PcoA	Principal coordinates analysis
PI	Propidium iodide
RF	Random Forest
RQ	Research question
SDWA	Safe Drinking Water Act
SG	SYBR Green I
SGPI	SYBR Green I and propidium iodide
SSC	Side scatter
TAN	Total ammonia nitrogen
TOC	Total organic carbon

Abstract

Safeguarding the drinking water quality is still a challenge worldwide. Unwanted microbial contamination of drinking water and invasion of pathogens are one of the most widespread risks to public health. It is therefore of utmost importance monitor, in order to maintain the drinking water quality, and especially the microbial drinking water quality. Current microbial monitoring techniques are shortcoming in terms of accuracy and/or speed. Flow cytometry (FCM) overcomes these limitations and is therefore a promising monitoring technique. In combination with advanced data analysis, FCM can be used to characterize a community based on morphological traits of the cells, using phenotypic fingerprints. In this dissertation, we have evaluated the value of FCM when applied as a tool for monitoring the microbial drinking water quality.

In order to frame the performed research, a literature study was performed, discussing drinking water in all aspects and the applicability of FCM as a monitoring tool.

In a first part, the objective was to relate changes in the physicochemical drinking water quality to changes in the bacterial community. This was evaluated in a monitoring campaign at dead ends (*i.e.* hydrants at the ends of the pipelines where water may be stagnant for longer periods) of the drinking water distribution network of DC Water (Washington DC, USA). Bacterial regrowth and/or biofilm disruption caused increased bacterial abundances when the hydrants were flushed after one week of stagnation. The regrowth was facilitated by reduced residual disinfectant concentrations. Furthermore, iron was found to directly influence the bacterial abundance at low concentrations. Changes in the bacterial community were shown to be mainly influenced by either the flush duration or by external effects (*e.g.* temperature), depending on the water age at the hydrant.

In a second part, the aim was to assess to what extent automated online FCM can be used to detect the influence of operational changes on the drinking water bacterial community. Therefore, online flow cytometric measurements were performed in full-scale water towers of the drinking water transport network of FARYS (Flanders) and Pidpa (Flanders) and in a lab-scale setup. The influence of the source water mixing ratio on the bacterial dynamics could be characterized. Operational changes were reflected in the bacterial abundance and/or the phenotypic diversity, measured using FCM.

Thirdly, as a proof-of-concept, we demonstrated the possibilities of FCM fingerprinting as a basis for predictive water composition modelling. Our study showed that it was possible to use microbial community fingerprinting as a basis for predicting the mixing ratio of drinking water.

Overall, this study demonstrated for the first time the added value of FCM fingerprinting in safeguarding drinking water quality. This offers new prospects for routine and continuous monitoring of the microbial drinking water quality.

Samenvatting

Bewaking van de drinkwaterkwaliteit is nog steeds een wereldwijde uitdaging. Microbiële contaminatie en invasie van pathogene bacteriën vormen de meest voorkomende risico's voor de publieke gezondheid. Monitoring is daarom van groot belang om de drinkwaterkwaliteit, en specifiek de microbiële kwaliteit, te garanderen. De huidige monitoringstechnieken schieten tekort op vlak van accuraatheid en/of snelheid. Flow cytometrie (FCM) heeft deze beperkingen niet en is daarom een veelbelovende monitoringstechniek. In combinatie met geavanceerde data-analyse kan FCM gebruikt worden om een bacteriële gemeenschap te karakteriseren. Op basis van de fenotypische eigenschappen van de aanwezige bacteriën wordt een "fenotypische vingerafdruk" van de gemeenschap gemaakt. In deze studie werd de waarde van FCM als microbiële monitoringstechniek in drinkwater geëvalueerd.

Om het uitgevoerde onderzoek te kaderen werd eerst een literatuurstudie gedaan, waarin alle aspecten van drinkwater worden besproken, alsook het gebruik van FCM als monitoringstechniek.

In een eerste onderdeel werden veranderingen in de fysicochemische drinkwaterkwaliteit gelinkt aan veranderingen in de bacteriële gemeenschap. Dit onderzoek werd gevoerd in samenwerking met DC Water (Washington DC, USA) tijdens een monitoringscampagne op de brandkranen van doodlopende delen van pijpleidingen in het distributienetwerk. Op deze plaatsen kan het drinkwater voor een langere tijd stilstaan, wat voor microbiële problemen kan zorgen. Bacteriële hergroei en/of het loskomen van de biofilm zorgden voor een verhoogde bacteriële abundantie wanneer de kranen gespoeld werden na één week stagnatie. De hergroei werd gefaciliteerd door verminderde residuele chloorconcentratie. Verder had ijzer in lage concentraties een directe invloed op de bacteriële abundantie. Veranderingen in de bacteriële gemeenschap werden hoofdzakelijk veroorzaakt door de spoeltijd of door externe factoren (vb. temperatuur), afhankelijk van de waterleeftijd aan de hydrant.

In een tweede luik werd nagegaan in welke mate online FCM gebruikt kan worden om de invloed van operationele veranderingen op de bacteriële drinkwatergemeenschap te detecteren. Om dit na te gaan werden metingen verricht in watertorens van FARYS (Vlaanderen) en Pidpa (Vlaanderen), en in een laboschaal opzet. Uit de resultaten van deze studie blijkt dat flow cytometrische fingerprinting een voldoende gevoeligheid heeft om kleine operationele veranderingen, zoals aanpassingen van inkomende wateren of verandering in de grootte van het inkomend debiet, te detecteren.

Tot slot werd, als een *proof-of-concept*, aangetoond dat het mogelijk is om de watersamenstelling van gemengde drinkwaters te voorspellen door middel van FCM fingerprinting.

Deze studie toont in zijn geheel voor het eerst de toegevoegde waarde van FCM als monitoringstechniek voor de microbiële drinkwaterkwaliteit aan. Dit opent perspectieven voor zowel routinematige als continue monitoring van de microbiële gemeenschap in drinkwater-distributienetwerken.

1. Drinking water

It is a basic human right to have access to safe and clean drinking water (WHO 2011). This might seem self-evident, however, safeguarding drinking water quality is still a challenge both in developed and developing countries. New challenges are arising with urbanization, population growth and global warming (Sedlak 2014; van der Wielen & van der Kooij 2013). The drinking water sector is thus an important but vulnerable public service.

What follows is a literature study to frame the performed drinking water research, comprising drinking water sources, production, distribution and legislation, with an emphasis on the drinking water microbial community. Also FCM will be discussed both its applicability as a drinking water monitoring tool and the relation to the currently used monitoring techniques. As measurements were performed in both the USA and Belgium, the differences in approach will be discussed and referred to throughout the literature study.

1.1 Sources & treatment

Only 2.5% of the total water resources on Earth consist of freshwater. Nearly 70% of these freshwater resources are stored in inaccessible glaciers and deep groundwater aquifers (Oki & Kanae 2006). As a result, less than 1% of the freshwater is available for direct human consumption (United Nations 1997). Surface water and groundwater provide the major sources of drinking water. In Belgium and the Netherlands roughly one third of the drinking water is produced from surface water, whereas two thirds is produced from groundwater (Dufour 1998). This ratio is reversed for the United States (US EPA 2003b). The risk of depleting the freshwater resources due to the increasing demand, droughts, and pollution has led to the application of water reuse technologies (Wade Miller 2006).

Drinking water production consists of a series of individual steps, called a "treatment train" (US EPA 2003b). Depending on the source water, different treatment steps are combined. In the US, surface water is mostly treated by applying subsequent coagulation, sedimentation and filtration. For example, in Washington DC the water is collected from the Potomac River (USACE 2013). The treatment train is depicted in **figure 1.1**. The raw surface water is first screened in order to remove the largest debris prior to entering the plant. The treatment consists of a gravitational pre-sedimentation, followed by coagulation (using aluminium sulphate) and flocculation in order to settle and consolidate suspended solids. Subsequently there is a sedimentation step, after which

the cleared water flows from the top of the sedimentation basin towards the gravitational sand filters.

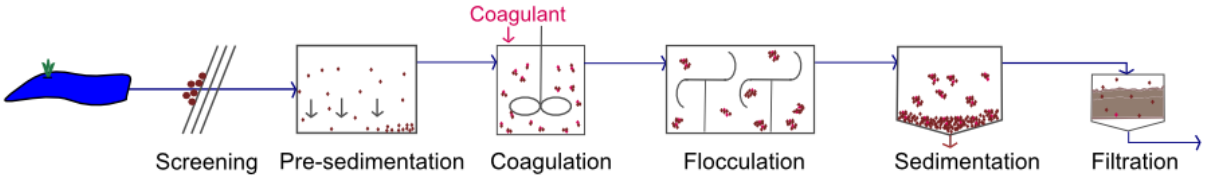

Figure 1.1 – Conventional treatment train of surface water. The treated water flows afterwards to disinfection, after which it is distributed.

On the contrary, in Europe, the treatment of surface water is mostly a combination of conventional treatment techniques that are used in the US, and more advanced treatment techniques, such as activated carbon filtration or membrane filtration, *e.g.* for desalination (van der Hoek et al. 2014). For example, in Antwerp surface water from the Albert Channel is treated according to the treatment train used in Washington DC (**figure 1.1**), followed by an additional filtration step using activated carbon filtration. This drinking water is produced by Water-link and distributed by FARYS.

Groundwater usually requires less treatment, since it has already undergone a natural "treatment" by percolating through the soil (Water in the West 2013). It is often treated using aeration and rapid sand filtration (**figure 1.2**), or it can even be disinfected as such (Dufour 1998). Aeration and rapid sand filtration is used by FARYS to remove iron and manganese from groundwater resources in Mainvault. Pidpa, an Antwerp water utility, uses this process combined with a decanting step for iron removal to treat groundwater. In the US, 55% of the groundwater does not undergo any treatment before disinfection, whereas in Europe this is only 25% (van der Hoek et al. 2014; Water in the West 2013). Extensive groundwater use, however, may result in water depletion and soil dehydration (Dufour 1998).

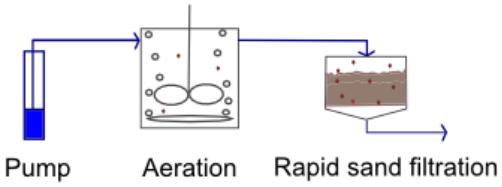

Figure 1.2 – Conventional treatment train of groundwater. The treated water flows afterwards to disinfection or is directly distributed.

1.2 Disinfection

After treatment, the water is disinfected in order to inactivate the microorganisms, since these might pose a risk to public health. Unwanted microbial contamination of drinking water and invasion of pathogens are the most widespread risks to public health, apart from specific chemical

contaminations (Reiff 1995; WHO 2011). For example, in Flanders and the Netherlands there were some recent incidents caused by *Escherichia coli* contamination (*e.g.* FARYS – Oostakker, 2017; EVIDES – Maassluis, 2017).

In large distribution systems, disinfection is often a combination of two processes: primary disinfection or pre-disinfection and secondary disinfection or post-disinfection (EPA 2011). Primary disinfection is applied in order to kill or inactivate microorganisms after the production process. During secondary disinfection, disinfection residual is added to the water at the production plant. This residual is retained throughout the distribution network in order to suppress low-level contamination and regrowth (WHO 2011). In Europe, it is common practice to combine different treatment and disinfection techniques to create a multi-barrier system, whereas in the US more emphasis is placed on secondary disinfection of the distribution network (Amy 2007).

The most used disinfectants are chlorine, which is applied in Belgium, and chlorine derivatives, such as chlorine dioxide or chloramine. Chlorine is introduced into the system as a hypochlorite solution (OCl^-) or as chlorine gas (Cl_2) (EPA 2011). Chlorine hydrolyses to hypochlorous acid (HOCl), which causes cell membrane damage (Venkobachar et al. 1977). Booster chlorination, *i.e.* the strategic addition of chlorine at different locations in the network, is sometimes applied to increase the disinfectant residual throughout the distribution network (Amy 2007; Tryby et al. 1999). The reaction of chlorinated substances with organic matter in the water may lead to the formation harmful disinfection by-products (DBPs) such as trihalomethanes (*e.g.* chloroform) and haloacetic acids (*e.g.* dichloro acetic acid) (Williams et al. 1997). Furthermore, when a hypochlorite solution is used, inorganic DBPs such as chlorate can be formed, which are potentially carcinogenic (Bolyard et al. 1992). To avoid the formation of organic DBPs, chlorine dioxide (ClO_2) can be used (Benarde et al. 1967). However, inorganic DBPs such as chlorite and chlorate can be formed as well (WHO 2005b).

An emerging disinfection approach, which is currently applied in Washington DC, is the combination of chlorination and the addition of ammonia, which leads to the formation of (mono)chloramine (NH_2Cl) as a secondary disinfectant (**eq.1**) (Amy 2007).

$$Cl_2 + NH_3 \rightarrow NH_2Cl + Cl^- + H^+ \qquad \textbf{(eq. 1)}$$

Monochloramine has a less strong taste and odour compared to chlorine and other chloramines, making it a preferred disinfectant residual in the distribution network (EPA 2011; Vikesland et al. 2001). Furthermore, monochloramine is less reactive than chlorine, resulting in less DBP

formation (Kool et al. 1999). However, the reaction of natural organic matter with monochloramine may still induce the formation of carcinogenic N-DPBs, such as N-nitroso dimethylamine (Choi & Valentine 2002; Chuang et al. 2013).

As an alternative to chlorine, ozone (O_3) can be used as a disinfectant. Ozonation has been proven to be a more effective technique against some harmful protozoan parasites compared to chlorination (Betancourt & Rose 2004). However, ozonation is more expensive than chlorination and carcinogenic bromate can be formed when bromide is present in the water (WHO 2005a).

Next to chemical disinfection, several physical methods such as UV radiation and membrane filtration can be used (Choi & Choi 2010; Jacangelo et al. 1997). UV radiation requires only short contact times, is effective against protozoan parasites and does not induce the formation of DBPs. Drawbacks are the lack of residual disinfectant in the distribution system and the interference by turbidity (Lorenzo-Lorenzo et al. 1993). Membranes, especially low-pressure microfiltration and ultrafiltration membranes, can be used for disinfection through different modes of action, such as size exclusion and adsorption or repulsion of specific substances depending on the membrane characteristics (*e.g.* charge) (Betancourt & Rose 2004; Jacangelo et al. 1997). Similar to UV radiation, membrane disinfection does not induce DBP formation and is effective against all kinds of microorganisms. However, membranes are prone to fouling and leakage. It is thus important to combine membrane filtration with appropriate pre-treatment of the source water (Van Der Bruggen et al. 2003). Furthermore, a waste stream (concentrate), *e.g.* when using reverse osmosis, is generated. Also, no disinfection residual is retained in the DWDS.

There is a worldwide difference in "philosophy" concerning the moderation of DBP formation, and secondary disinfection. In the US, DBP formation is limited through the removal of natural organic matter before chlorination. The aim is to eliminate live microbial presence in the distribution systems by adding ample (secondary) disinfectant. On the contrary, in Europe, the emphasis is placed on the elimination of disinfection residual in the DWDS (Amy 2007). Their aim is to produce "biologically stable" water, which means that there is "no change in the concentration and composition of the microbial community in the water during distribution", without the use of secondary disinfectants (Lautenschlager et al. 2013, p. 3016). In order to produce biologically stable water, the emphasis is currently placed on the extensive limitation of assimilable organic carbon (AOC), as this is considered to be the main limiting nutrient for microbial growth (Hammes & Egli 2007; van der Kooij et al. 1982). Since only organic carbon is limited in the distribution system, bacterial processes that require other nutrients may still take

place, such as ammonia-nitrogen conversion during autotrophic nitrification. This implies for the European approach that, if pathogen contamination takes place, the consequences for human health might be very serious due to the lack of residual disinfection (LeChevallier 1999).

1.3 Distribution

After disinfection, the drinking water is distributed to the customers through drinking water distribution systems (DWDS). These networks include a piping system, pumps, valves, and storage facilities such as water towers. In Washington DC, two different companies are responsible for production (US Army Corps of Engineers) and distribution (DC Water) (USACE 2013). In Flanders, multiple companies execute both the production and distribution of drinking water (*e.g.* Pidpa), or water utilities produce only a part of the drinking water that they distribute and buy water from other producing utilities (*e.g.* FARYS that collaborates with Water-link). In order to provide water of good quality at the taps, frequent monitoring within the distribution system is necessary.

As the water is transported through the DWDS, it undergoes chemical (*e.g.* DBP formation), physical (*e.g.* colour change) and biological (*e.g.* regrowth) transformations, which affect the water quality and may cause a potential threat to public health (AWWA 2002a). Within the distribution network, the water residence time will thus have a substantial influence on the water quality. The water age, *i.e.* the time the water spends in the DWDS, is determined by the size of the network, the system operation and the water demand. The capacity of the DWDS is often large in order to meet peak demands (*e.g.* in case of fire or other emergencies) and to anticipate future needs (*e.g.* population growth), resulting in increased water ages (AWWA 2002a).

Interaction of the drinking water with the piping infrastructure can induce corrosion of cast iron pipes (AWWA 2002b). Iron corrosion can lead to pipe damage, less energy-efficient water transportation, and depletion of disinfectant residual and other oxidizing agents (Sarin et al. 2004). Corrosion can also lead to an increase in surface roughness of the pipe walls, which indirectly may support biofilm formation (Sarin et al. 2004). Furthermore, corrosion products may cause aesthetic water quality issues, such as colour, taste, and odour abnormalities. Moreover, leaching of chemicals might cause serious health issues (AWWA 2002b). To prevent corrosion, a lining (*e.g.* cement lining) can be applied in combination with orthophosphate addition at the treatment plant. Orthophosphate will reduce iron oxidation by forming a passivation layer on the iron surface (Volk et al. 2000). Under specific conditions, such as low pH and temperature, phosphate, in the form of polyphosphate, can however react with the lining and consequently accelerate the corrosion and

leaching process (Cantor et al. 2000). Calcium hydroxide can be added in order to increase the pH, and in this way limit the reaction of orthophosphate to polyphosphate (USACE 2013). Alternatively, plastics such as PVC, can serve as a corrosion-resistant piping material in drinking water applications. In this case, contamination of the water can still occur through permeation of chemicals originating from the external environment, and leaching of chemicals from the plastic (AWWA 2002b).

Independent of a performant treatment and disinfection, contaminants can intrude the DWDS because of short pressure transients. These are abrupt pressure changes caused by a sudden change of the water's velocity (Karim et al. 2003). Sudden movements that disturb the water flow, such as the closure of a valve, can cause direct contamination (*e.g.* intrusion through an air-valve) or affect the bulk water quality (*e.g.* resuspension of the sediment) (US EPA 2003a). Through connections between drinking water and non-potable water supply sources, such as the use of drinking water as feed water in industrial systems, contaminants can enter the system when the connection is not secured. This is called "backflow". Backflow can be caused by either an increased external pressure (*i.e.* backpressure), or by a low or negative pressure in the pipe (*i.e.* backsiphonage) (US EPA 2001, 2010)

1.4 Microbial growth in DWDS

Growth in the drinking water distribution system is limited by the nutrient availability, the presence of growth-inhibitors such as disinfectant residual, the presence of other microorganisms and environmental conditions (Boe-Hansen et al. 2002). Consequently, drinking water is an oligotrophic (*i.e.* poor in nutrients) environment wherein, despite disinfection and intensive DWDS maintenance, the indigenous microbial community can reach population densities of up to 10^6 cells/mL. The community is mostly harmless (Berney et al. 2008; Hammes et al. 2008). Long water ages and moderate temperatures (15 - 25°C, *e.g.* when a surface water source is used in summer) will stimulate microbial growth within the DWDS (Camper et al. 1986). This is the case in low velocity or stagnant water zones, such as at the end of a pipeline in the system, termed "dead end". The long water age induces loss of disinfectant residual and the stagnant water can heat up to ambient temperature more easily, and consequently facilitate proliferation of microorganisms (AWWA 2002a; Liu et al. 2016).

In general, "bacterial regrowth" is the recovery of cells after disinfection (Characklis 1988). Extensive bacterial regrowth within the distribution network can result in physicochemical, aesthetical or operational problems (Prest et al. 2016). It is thus necessary to understand the

microbial growth and ecology of drinking water bacteria to ensure the safety of the drinking water (Berry et al. 2006).

The biggest microbial risk to public health is the presence of waterborne pathogens. For example, the *Centre for Disease Control and prevention* reported that "during 2013-2014, in the US, 42 drinking water associated outbreaks have been reported, accounting for at least 1006 cases of illness and 13 of death" (Benedict et al. 2017, p. 1). Enteric pathogens, such as *Escherichia coli*, enter the drinking water distribution system through inadequate disinfection or by accidental contamination. However, these pathogens are unable to proliferate within the oligotrophic environment of drinking water distribution systems (US EPA 2002a). To minimize outbreaks, it is of utmost importance to disinfect in a right way (Teunis et al. 1997). Some opportunistic pathogens, such as *Legionella pneumophila*, and *Pseudomonas aeruginosa* can survive both treatment and disinfection, through for example parasitism of amoebae (Cervero-Aragó et al. 2015). Furthermore, opportunistic pathogens are able to proliferate within the network as they can use dead organic matter as a nutrient source (Moritz et al. 2010; US EPA 2002a; Wang et al. 2013).

It is therefore essential to monitor the presence of these pathogens. *E. coli* and *Enterococci* serve as indicator organisms for faecal contamination. Since the infective dose can be low (*e.g.* $< 10^2$ cells for *Legionella* spp. as aerosol), it is not always possible to register smaller risks (Rusin et al. 1997; US EPA 2002a). Furthermore, because pathogens often adhere to pipe walls or suspended solids (*e.g. Legionella* spp.), their concentration in the water may vary and the risk is not always properly estimated through average monitoring results (Moritz et al. 2010; US EPA 2002a).

In general, microbial growth can occur in four different phases: as a biofilm attached to the pipe walls, dissolved in the bulk water, attached to suspended solids or as loose deposits (**figure 1.3**) (Liu et al. 2016). Biofilm formation is the most prevalent form of growth. In these biofilms microorganisms are protected from shear stress and changes in water composition by the extracellular polymeric substances (Berry et al. 2006; Liu et al. 2016). Biofilms can, besides causing illnesses caused by pathogen invasion, affect the taste and odour of the water and accelerate corrosion during "biocorrosion" (Beech & Sunner 2004).

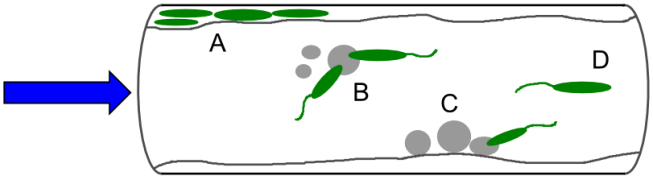

Figure 1.3 – Forms of microbial growth in DWDS. (**A**) Biofilm formation, (**B**) attached to suspended solids, (**C**) attached to loose deposits, (**D**) dissolved in the bulk water. Based on Liu et al. 2016.

Microbial growth in DWDS may cause a depletion of disinfectant residual and an increase of disinfection by-products. Drinking water produced from surface water sources, such as the Potomac (Washington DC) or the Albert Channel (Water-link), has a higher risk towards microbial regrowth since it is higher in temperature during summer, and contains more nutrients. Not only the AOC concentration is higher, bacterial processes that use other nutrients such as phosphorus and nitrogen may also take place. As a specific case hereof, nitrogen can be used by nitrifying bacteria in chloraminated drinking water during nitrification. Due to monochloramine auto decomposition in the network, ammonia is provided as a nutrient to the system (**eq. 2**) (Hoefel et al. 2005; Vikesland et al. 2001). Dosing chlorine and ammonia in a weight ratio of 5:1 almost completely eliminates the presence of free ammonia in the DWDS (Kirmeyer 2004).

$$3NH_2Cl \rightarrow N_2 + NH_3 + 3Cl^- + 3H^+ \qquad \textbf{(eq. 2)}$$

Nitrifying bacteria oxidise the added ammonia to nitrite and subsequently nitrate (**eq. 3, eq. 4**). Both substances are toxic to humans when ingested, especially to infants. Upon ingestion, nitrate is metabolized to nitrite (or nitrite may be ingested as such) that binds to hemoglobin in the blood, resulting in oxygen transport difficulties. This may lead to cyanosis, also known as "blue baby syndrome", which eventually may cause death (Fan & Steinberg 1996). Both substances are also potentially carcinogenic (IARC 2010). Besides this, nitrification will decrease the pH through the generation of protons, which may result in a faster chloramine decay and facilitated corrosion of iron piping (Vikesland et al. 2001). Degradation of disinfectant residual gives rise to adverse health effects through the overall increase of microbial abundance, including pathogens. To overcome this, more disinfectant is added, which in turn may lead to an increase of DBP (AWWA 2013; Berry et al. 2006).

The nitrifying community consists of mostly autotrophic, slow growing, biofilm forming bacteria (AWWA 2013). Ammonia oxidizing bacteria (AOB) or archaea (AOA), and the nitrite oxidizing bacteria (NOB), will oxidize ammonia to nitrite (**eq. 3**) and nitrite to nitrate, respectively (**eq. 4**) (Rabaey & Verstraete 2015):

$$NH_3 + O_2 \rightarrow NO_2^- + 3H^+ + 2e^- \qquad \textbf{(eq. 3)}$$

$$NO_2^- + H_2O \rightarrow NO_3^- + 2H^+ + 2e^- \qquad \textbf{(eq. 4)}$$

Nitrification is favoured by a slight alkali pH (7.0 - 8.0), since NH_3 is preferred to NH_4^+ as substrate (Zhang et al. 2009). Additionally, nitrification is favoured under moderate temperatures, though, nitrifiers can also thrive in colder waters (Lipponen et al. 2002). High water ages might promote

biofilm formation and proliferation of nitrifying bacteria. Furthermore, iron, which may enter the water through highly corroded pipes, can be used as an electron donor to regenerate ammonia from nitrite. Also, corrosion by-products, such as Fe^{2+} can accelerate chloramine decay (Zhang et al. 2009).

To control nitrification, drinking water suppliers often make use of periodic "breakpoint chlorination". This is the addition of chlorine until the chlorine supply exceeds the chlorine demand, leading to an increase of free chlorine residual (Kirmeyer et al. 1995). Alternatively, drinking water providers can temporarily switch from chloramination to chlorination (US EPA 2002a).

1.5 Legislation

In the *Guidelines for Drinking Water Quality* the World Health Organisation (WHO) defines "safe drinking water" as "not representing any significant risk to health over a lifetime of consumption, including different sensitivities that may occur between life stages" (WHO 2011, p. 1). This document outlines the scientific water quality assessment and is internationally recognized as a rough guide for national drinking water standards and legislation.

1.5.1 United States

The United States Environmental Protection Agency (US EPA) published the *Safe Drinking Water Act (SDWA)*, which determines the legal standards for water quality on a national level (US Congress 1996). It states that public water systems are responsible for the water quality delivered at the tap. The act includes legal maximum contaminant levels for more than 90 biological, chemical, physical and radiological contaminants.

The *National Primary Drinking Water Regulations (NPDWR)* regulate the contaminants which may have a primary effect on human health. For each contaminant, it includes the non-enforced Maximum Contaminant Level Goal (MCLG) and the enforced Maximum Contaminant Level (MCL). Furthermore, it comprises treatment techniques that should be applied for the removal of certain contaminants (US EPA 2004a). The NPDWR encloses specific rules, such as the *Disinfectant/Disinfection By-Product (D/DBP) Rule* and *The Revised Total Coliform Rule (RTCR)*. The latter sets a MCLG of zero for total coliforms and a MCL based on the absence/presence of total coliforms in 100mL (US EPA 2013). The D/DBP Rule establishes standards for D/DBP, and requires to meet the limits through regular sampling. The maximum residual disinfectant level for free chlorine and chloramines is 4mg/L each (US EPA 1998).

Since 1905, standard methods used for routine analysis and quality control for regulation compliance are described in the *Standard Methods for the Examination of Water and Wastewater* (Rice et al. 2012).

Next to the SDWA, the *Surface Water Treatment Rules* and the *Ground Water Rule* have been established to improve the drinking water quality and provide protection from pathogens in the source water, by requiring resp. filtration and disinfection or solely disinfection (US EPA 2002b, 2006).

1.5.2 European Union and Belgium

In the European Union, the *Drinking Water Directive (DWD)* (Council Directive 98/83/EC) is the legislative framework to safeguard the drinking water quality. Its objective is to "protect human health from adverse effects of any contamination of water intended for human consumption by ensuring that it is wholesome and clean" (European Communities 1998, art. 1). To comply with this directive, the water quality is assessed by regular monitoring of 48 essential indicator parameters. Equivalent to the US, guideline values and enforced limits are defined (*e.g.* absence of *E. coli* in 100mL).

Since many countries in the EU get their water from neighbouring countries, the *Water Framework Directive* (2000/60/EC) aims to protect and conserve the quality all of the water resources in the EU by international water resource management (European Parliament 2000).

In Belgium, the DWD is adopted in the national legislation as the *Royal Decree on drinking water* (established January 14th, 2002). The regional drinking water standards for Flanders are specified in the *Decree concerning the quality and distribution of water intended for human consumption* (established December 13th, 2002, extended in February 2008). The enforced limits are more stringent and extensive than the DWD dictates. For example, the chlorine residual in the distribution system cannot exceed 0.25mg/L and the monochloramine disinfection dose should be maximal 1.5mg/L (Decreet 2002a; Koninklijk besluit 2002).

Furthermore, the Flemish government established a *Decree concerning water intended for human consumption* (established May 24th, 2002), wherein the responsibilities of public water providers and the selling price of drinking water are described. Similar to the US, public water systems are responsible for the water quality from source to tap (Decreet 2002b).

2. Monitoring drinking water

To maintain good water quality within the distribution system, drinking water providers need reliable monitoring techniques.

2.1 Current monitoring systems

Over the past two centuries, plenty of tools have been developed to assess the microbial safety of drinking water. Heterotrophic plate count (HPC) is a cultivation-based method that is used to evaluate microbial drinking water safety (Koch 1883). HPC characterizes a microbial community by inoculating and incubating a water sample on a semi-solid growth medium and subsequently assessing colony formation. A similar technique is selective plate counting, which makes use of selective media to target specific groups of bacteria. A crucial limitation of these techniques is referred to as "The Great Plate Count Anomaly", which states that less than 1% of the bacteria present in oligotrophic freshwater systems are cultivable on solid media (Amann et al. 1995; Jones 2006; Staley & Konopka 1985). Furthermore, the number of microorganisms and the grown genera will vary depending on the incubation temperature and time, the composition of the growth medium, and the inoculation method (Allen et al. 2004; Reasoner 2004). In other words, there is a discrepancy of a few orders of magnitude between the microbial community in the water and the one measured through HPC (Allen et al. 2004; Bartram et al. 2003).

Furthermore, HPC results are not of hygienic value (Bartram et al. 2003). Hence, during the 20th century, methods that use faecal bacteria as indicator organisms for the detection of contamination in drinking water have been developed (Bartram et al. 2003). Faecal coliforms, such as *Escherichia* spp. and *Enterobacter* spp., are being used because of their ease of detection and the strong correlation of their presence with both recent faecal contamination and enteric pathogen presence (Rompré et al. 2002). Next to the use of classical methods such as membrane filter technique and multiple-tube fermentation, most used procedures to detect the presence of coliforms are based on enzymatic reactions (Rompré et al. 2002). Where the enzyme β-D-glucuronidase is mostly limited to *E. coli*, the enzyme β-D-galactosidase is considered as a characteristic of the coliform bacteria group. When grown on a selective substrate, exclusively coliforms or *E. coli* are able to convert it into a coloured derivative and can subsequently be visually detected (Rompré et al. 2002). This method makes it possible to detect viable but non-cultivable coliforms, though it is more expensive compared to HPC (George et al. 2000).

Due to their simplicity and low cost, HPC and total coliform detection are currently used as standardized techniques to evaluate the microbial drinking water safety (Allen et al. 2004). Both

techniques have a long time delay (2 - 3days) due to the required incubation step. (Rompré et al. 2002). Although these methods serve as a good indication of contamination, it is not possible to determine which microorganisms are present (except for the indicator organisms) and there is no direct relation to the presence of other than faecal pathogens (Bartram et al. 2003).

An alternative approach to assess microbial presence and viability in drinking water in a quantitative way is adenosine triphosphate (ATP) analysis. ATP is a universal metabolite that serves as an energy carrier, and is present in all viable cells (Karl 1980). First, intracellular ATP is extracted using chemicals or enzymes. Next, the reaction with the luciferin-luciferase complex in the presence of Mg^{2+} and oxygen is carried out, resulting in an excited enzyme complex. The intensity of the light that is emitted when the enzyme complex returns to its ground state is measured (Hammes et al. 2010; Whitehead et al. 1979). This reaction is fast and robust, which makes ATP measurements a very straightforward method to quantify the active biomass concentration in water (Chappelle & Levin 1968; Hammes et al. 2010). Still, there are some critical obstacles. First of all, this technique has a low sensitivity in aquatic environments due to the low bacterial abundance (Hammes et al. 2010). Next to this, ATP is present both intracellularly and extracellularly, which makes it hard to interpret results and to draw correct conclusions regarding the amount of active bacteria (Sakakibara et al. 1997). Also, the ATP concentration in a cell may vary depending on its physiology (Hammes et al. 2010; Sakakibara et al. 1997).

For non-routine monitoring, molecular techniques, such as sequencing and genetic fingerprinting, can be used to determine the microbial community composition without cultivation. These methods incorporate the use of nucleic acid extraction and subsequent amplification of target genes by polymerase chain reaction, which makes them time consuming (Douterelo et al. 2014; Muyzer 1999). Moreover, an enrichment step is required to be able to use these techniques for analysis of drinking water due to the low cell densities (Dewettinck et al. 2001). An overview of the monitoring techniques, in comparison to flow cytometry is given in **table 1.1**.

Table 1.1 – Comparison of methods used for bacterial monitoring in drinking water (Buysschaert 2018; Van Nevel, Koetzsch et al. 2017).

	Time-to-result	**Accuracy**	**Labour intensity**
HPC	Days	-	Medium
ATP	Minutes	+	Low
Sequencing	Days – Weeks	+++	High
FCM	Minutes	++	Low

2.2 Flow cytometry

Flow cytometry (FCM) is a fast, cultivation-independent technique that is mostly used in clinical applications. The technique has been used to characterize suspended bacteria for the first time in 1977, but was only applied for drinking water monitoring at the beginning of the 21st century (Van Nevel et al. 2017b). FCM can be used to characterize and quantify the microbial community in drinking water processes and distribution systems (Douterelo et al. 2014; Prest et al. 2013; Van Nevel et al. 2016).

2.2.1 General principle

FCM is an optical technique that is used to analyse single particles, usually cells. Via a sample introduction probe the sample is injected, after which the fluidics system guides the sample to the detector. The drag effect of the sheath fluid will cause the particles to align into a single stream in order to improve the resolution of the optics (**figure 1.4**) (BD biosciences 2000; Rahman 2014). This principle is called "hydrodynamic focusing" (Shuler et al. 1972). By using a peristaltic pump system, the velocity of the sample can be adjusted. Higher sample introduction velocities give rise to bigger core diameters, resulting in a shorter analysis time, but less accurate measurements (Rahman 2014).

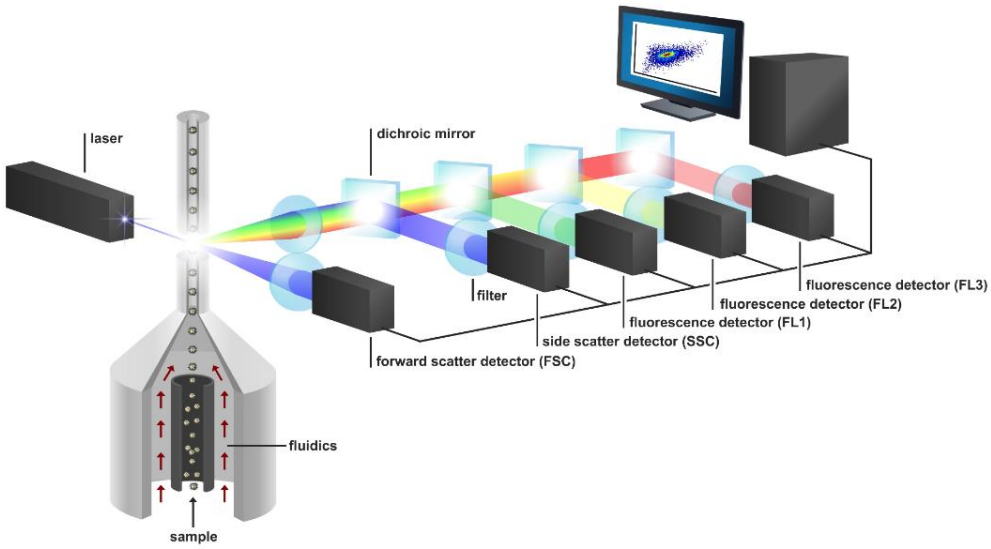

Figure 1.4 – Working mechanism of a flow cytometer with three fluorescence detectors (De Roy 2014).

After alignment of the sample in the flow cell centre, it is transported to a beam of light. Interaction of the particles with the incoming light will result in scattered light and fluorescence. Forward scatter (FSC) is collected along the axis of the incoming light. The signal is related to the particle's surface, and thus gives an indication of its size. The side scatter (SSC) is detected perpendicularly to the incoming laser beam and is related to the particle's granularity. Fluorescence is induced

through fluorochromes, which can be added prior to analysis or can be inherently present in the cells, such as autofluorescent proteins (*e.g.* a green fluorescent protein) (Gatza et al. 2013; Harms et al. 2001). The fluorescence intensity of a particle is proportional to the amount of attached stain (Müller & Nebe-Von-Caron 2010).

Stains can bind to several biomolecules, such as nucleic acids, lipids and proteins (Veal et al. 2000). By using one or more fluorescent stains differentiation of particles or cells can be accomplished. This can be done by using stains that interfere with cellular processes, such as membrane potential or enzymatic activity (George et al. 2000). A more specific example is "immunological labelling", where fluorochromes are conjugated to antibodies, which bind to specific proteins (BD biosciences 2000).

Fluorescence (FL) is measured by several detectors, that all comprise a specific part of the spectrum. The partition of different wavelengths is executed by a series of dichroic mirrors, which fulfil a dual function: filtering and focusing of the desired part of the spectrum to the detector, and reflecting the remaining radiation (BD biosciences 2000).

As an example, the combination of the nucleic acid stains Sybr Green I (SG) and propidium iodide (PI) allows the discrimination between intact and permeabilized cells. SG stains both intact and damaged or permeabilized cells. PI is not able to penetrate through intact cell membranes and will only stain permeabilized cells. Intact cells will thus be SG stained, whereas permeabilized cells will be SGPI stained. Light emitted from a 488nm laser will excite SG, and SG will on its turn emit light within the green spectrum. This light will consequently excite PI. This phenomenon known as "fluorescence resonance energy transfer (FRET)" (**figure 1.5**) (Stocks 2004). Since the emitted radiation of SG is used to excite PI, the green fluorescence will be quenched. The emission of PI is situated in the red spectrum, leading to an additional differentiation (Van Nevel 2014). Hence, permeabilized cells will typically have a reduced green intensity and a higher red intensity. As a result, two different "populations" are visible on the green versus red fluorescence plot: one having permeabilized membranes and one having intact membranes. Since membrane permeability is a generally accepted criteria for viability, SGPI staining can be used for the assessment of cell viability (Grégori et al. 2001).

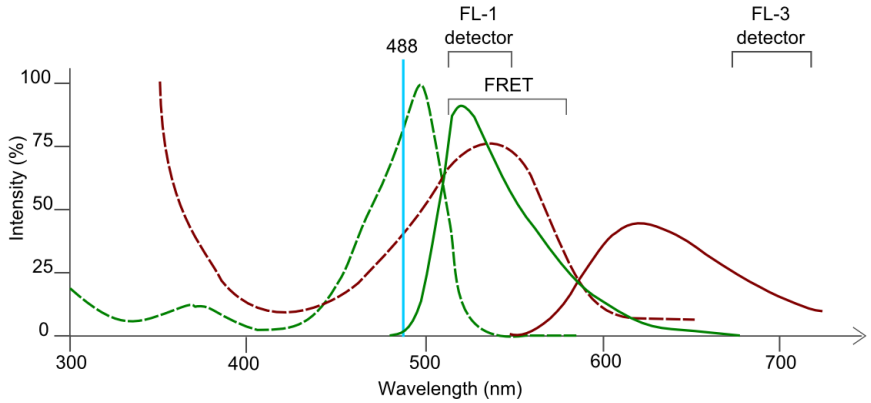

Figure 1.5 – Spectrum chart of the absorbance and emittance intensity of SG (green) and PI (red), relative to the excitation intensity of SG. Dotted lines represent absorbance spectra, whereas full lines represent emittance spectra. The incoming light has a wavelength of 488 nm. The absorbance spectrum of PI (red, dotted) overlaps with the emission spectrum of SG (green, full), resulting in FRET. Based on BD biosciences 2018.

Flow cytometry has several advantages over the conventional techniques that are applied in drinking water analysis. First, there is no cultivation step, which ensures that also viable but non-cultivable microorganisms are detected. Secondly, it is a fast technique, resulting in remarkable time savings compared to conventional methods (Van Nevel et al. 2017a). Furthermore, stains can be combined to assess multiple features simultaneously, such as live/dead staining with SGPI. For microbiological applications however, this is in general not very straightforward due to the lack of standardization (Buysschaert et al. 2016). Lastly, FCM is sensitive enough to be directly applied in relatively low density systems such as drinking water (Van Nevel et al. 2017b).

2.2.2 Data analysis

Hammes & Egli (2010) stated that the major problem of flow cytometry is "the relative ease with which an immense wealth of data can be generated" (p. 1085). Hence, the advantage of FCM as a high-throughput technique can be translated into its biggest challenge: the correct (1) processing and (2) interpretation of the multiparametric data (De Roy et al. 2012; Shapiro 2005). FCM data analysis is a time-consuming process that can be considered as an additional source of variation (Bashashati & Brinkman 2009).

The data generated by FCM is commonly presented on a single-parameter histogram or as a two-dimensional dot plot, often referred to as a "fingerprint" (**figure 1.6**) (Shapiro 2005).

Interfering particles such as humic acids, dust, and salt crystals can scatter light or bind to stains and emit fluorescence (Van Nevel 2014). This background noise is separated from the cell population of interest in the so-called "gating" process. Gating is selecting the region that contains the cells or particles of interest, mostly based on two-dimensional intensities of scatter or fluorescence signals (**figure 1.6**). Gating is mostly performed manually, though this is subjective and will increase the variability of the results. To overcome this limitation, multiple automated

gating procedures have been developed. These are either based on supervised gating, relying on a training set, or unsupervised gating, using cluster analysis (Bashashati & Brinkman 2009). It should be noted that the background might provide an additional source of information, which is currently not fully exploited (Van Nevel 2014). Besides this, the operator can change the voltage of the detector channels. An increase of voltage will result in a more sensitive response, but may also induce more background. These sources of variation make it difficult to directly compare results between different studies.

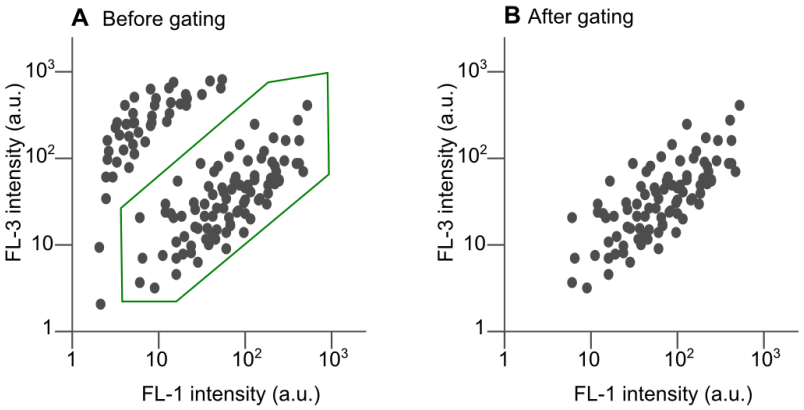

Figure 1.6 – Visualization of the gating process on the two fluorescence parameters FL-1 (green fluorescence) and FL-3 (red fluorescence). (**A**) 2D representation of an FCM sample containing the population of interest and background, before gating. (**B**) Isolation of the population of interest after gating.

Several recently developed pipelines interpret the data though the calculation of a "cytometric fingerprint". The word "fingerprint" can be used for any unique image or dataset of a sample generated using FCM (Van Nevel 2014). In this study, it is used to refer to the unique discretized data frame that is obtained after data processing. Consequently, in this study, we define "fingerprinting" as the discretization of the FCM data to extract the variables of interest.

These fingerprints are used for comparing between samples, and can be used for the calculation of the so-called "phenotypic diversity" metrics using the Phenoflow pipeline. This pipeline has been recently developed by Props et al. (2016) and will be discussed in the following paragraphs.

The fluorescence and scatter intensities are transformed according to arcsinh(x), after which they are rescaled to [0, 1] by dividing the intensities by the maximal green fluorescence intensity over the entire dataset. After this transformation, the bivariate parameter spaces are discretized. This can be done manually by selecting regions of interest (*e.g.* CyBar algorithm) or by the dividing the 2D-space using a binning grid, consisting of "equal space bins" (*e.g.* 128x128 bins) or "equal frequency bins" (**figure 1.7**) (Koch et al. 2014; Props et al. 2016; Rogers & Holyst 2009). The creation of the latter grid is accomplished by probability binning, iteratively partitioning the two-dimensional cloud in two parts (alternately parallel to one of the axis), so that each "daughter bin"

contains the same amount of data points, until a specified number of bins is reached (Rogers et al. 2008).

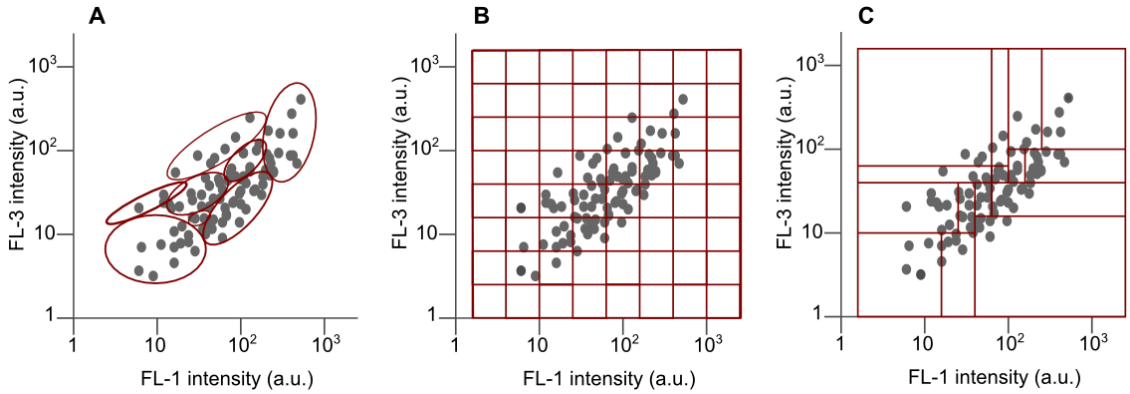

Figure 1.7 – Illustration of the different options that can be used for discretising the parameter spaces. (**A**) Manual selection of different clusters using the CyBar algorithm. (**B**) Equal space binning using the Phenoflow R package. (**C**) Equal frequency binning using the FlowFP R package.

When using the Phenoflow pipeline, discretization is performed using either equal space binning or equal frequency binning. Subsequently, for each bin, a bivariate Gaussian distribution is fitted using kernel density estimation with a fixed bandwidth (**figure 1.8, B**). The community density is then obtained by summation of the densities of all the bins. Next, the density of each bin is concatenated into a one-dimensional vector called the "phenotypic fingerprint" (**figure 1.8, C**). The bins or gates used to create the phenotypic fingerprint may represent operational phenotypic units (OPU). This way, the phenotypic fingerprint resembles the typical output of sequencing pipelines, which are a matrix or vector containing the relative abundances of operational taxonomic units that are assumed to represent different species. Correspondence between the phenotypic and genotypic diversity was shown by Props et al. (2016). Hence, established ecological biodiversity metrics can be calculated from the phenotypic fingerprint.

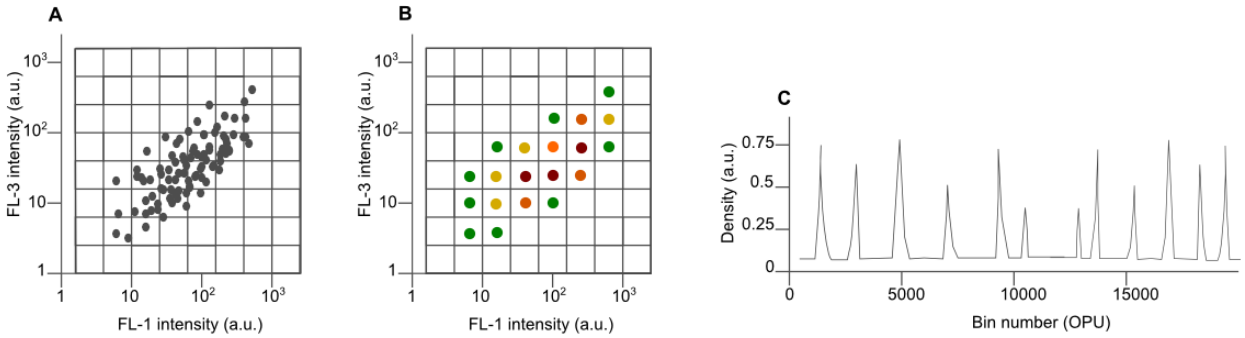

Figure 1.8 – Fingerprinting process. (**A**) Discretization using equal space binning. (**B**) Kernel density estimation for each bin (green = low density, red = high density). (**C**) Fingerprint containing the densities for each bin (16,384 bins using a 128x128 grid).

Biodiversity is used to indicate the variability amongst species within a community, taking into account both the evenness (indicating the relative abundances of species) and richness (indicating the amount of different species) of the community. As a general concept, biodiversity can be

expressed on three levels: alpha diversity or the within-sample diversity, beta diversity or the relative dissimilarity between samples' diversity, and gamma diversity, the regional diversity (Whittaker 1972). The Hill numbers are the preferred measures to evaluate the alpha biodiversity, since they can be interpreted as the "effective number of species", *i.e.* the number of equally abundant species needed to create the same amount of diversity (Hill 1973). Alpha diversity considers both richness and evenness. The larger the Hill order, the lesser rare species are taken into account. The Hill diversity metrics for q in [0, 2] represent the richness, the exponential of the Shannon entropy and the inverse of the Simpsons index, respectively (**table 1.2**).

Table 1.2 - Hill order ($q \leq 2$) and the corresponding diversity metric, as to be calculated from the phenotypic fingerprint. With S the number of non-empty bins and p_i the probability of abundance for bin i.

Hill order (q)	**Diversity metric (D_q)**
0	$D_0 = S$
1	$D_1 = e^{-\sum_{i=1}^{S} p_i \ln(p_i)}$
2	$D_2 = \frac{1}{\sum_{i=1}^{S} p_i^2}$

To evaluate beta-diversity, or in other words, the dissimilarity between the samples, the Bray-Curtis dissimilarity is used (Bray & Curtis 1957). The Bray-Curtis dissimilarity will equal to zero for identical fingerprints, and will equal one in case two samples have no non-empty bins in common (Greenacre & Primicerio 2014). To calculate the Bray-Curtis dissimilarity between the phenotypic fingerprints of two samples A and B, the following formula is used, where S is the number of non-empty bins and p_i is the relative abundance for bin i (Greenacre & Primicerio 2014) (**eq. 5**):

$$D_{AB} = \frac{\sum_{i=1}^{S} |p_{A,i} - p_{B,i}|}{\sum_{i=1}^{S} (p_{A,i} + p_{B,i})} \qquad \textbf{(eq. 5)}$$

In this study, "phenotypic diversity" refers to both the phenotypic alpha and beta diversity. The Hill number D_2 relates the best to the genotypic diversity and is the least sensitive to the sample size (**appendix 2**). It is generally highly correlated to D_1 and D_0, D_2 will be used in this study to evaluate the phenotypic alpha diversity.

2.2.3 Online monitoring

To better understand the microbial dynamics over time in the DWDS, and their causes, such as changes in raw water composition or contamination, FCM can be customized into a high-frequency online technique (Besmer et al. 2016). The use of online FCM in drinking water applications has only recently been developed. Hammes et al. (2012) developed a prototype robot

for online staining, mixing, incubation, cleaning and measurement of drinking water on a lab-scale. The online monitoring system is controlled through a script, enabling the user to write an operating code for the desired implementation (*e.g.* dilution and incubation times). Besmer et al. (2014) first used this technique for long term (12 days, measurement every 15 minutes) monitoring of a drinking water ecosystem.

II. Objectives

As described in the literature study, abnormalities in the microbial drinking water community can lead to a variety of issues. Therefore, monitoring is essential, however, current microbial monitoring techniques are shortcoming in terms of accuracy and/or speed. Flow cytometry (FCM) overcomes these limitations and is therefore a promising technique for microbial drinking water quality monitoring. The main objective of this thesis is to assess the value of FCM as a tool for microbial drinking water quality monitoring.

In the drinking water distribution network of DC Water (Washington DC, USA), FCM analyses will be performed in combination with physicochemical analyses in a long-term sampling campaign. The objective of this part is to relate changes in the physicochemical drinking water quality to changes in the bacterial community. More specific, the aim is to answer the following research questions (RQ):

RQ 1: What is the influence of the residual disinfectant concentration on the drinking water bacterial community?

RQ 2: What is the influence of the flush duration on the drinking water bacterial community?

RQ 3: What is the seasonal effect on the drinking water bacterial community?

RQ 4: What is the influence of the water age on the drinking water bacterial community?

RQ 5: What is the influence of the iron concentration on the drinking water bacterial community?

As a case study, the occurrence and extent of nitrification in DC Water drinking water will be assessed, as this is a microbial process that may affect public health.

In a second part, monitoring will be performed in water towers of FARYS (Flanders) and Pidpa (Flanders), and in a lab-scale water tower. The aim is to assess to what extent online flow cytometry can be used to detect the impact of operational changes on the drinking water bacterial community. Therefore, the following research questions will be answered:

RQ 6: Is online FCM able to detect operational changes in drinking water distribution networks?

RQ 7: Can the FCM fingerprint be used as a basis for predictive modelling of the water composition?

1. Physicochemical analyses

The physicochemical properties of drinking water samples from DC Water were analysed using optical detection methods, a pH/temperature probe and titration (**table 3.1**).

Table 3.1 – Parameters that were assessed for the drinking water of DC Water. "Free ammonia" refers to the Total Ammonia Nitrogen (TAN), consisting of nitrogen in the form of NH_3 and NH_4^+.

Parameter	**Measured as**	**Method**	***In situ/ ex situ***
pH		pH/temperature probe	*In situ*
Temperature		pH/temperature probe	*In situ*
Total chlorine	mg/L Cl_2	Hach® SL1000	*In situ*
Monochloramine	mg/L Cl_2	Hach® SL1000	*In situ*
Nitrite	mg/L NO_2^--N	Hach® SL1000	*In situ*
Orthophosphate	mg/L PO_4^{3-}	Hach® SL1000	*In situ*
Free ammonia	mg/L NH_3-N	Hach® SL1000	*In situ*
Total iron		Hach® powder pillows	*In situ*
Nitrate		Hach® powder pillows	*In situ*
Alkalinity	mg/L $CaCO_3$	Titration with sulfuric acid	*Ex situ*

Most parameters were analysed using a Hach® SL1000 portable colorimeter (Colorado, United States), which has four Chemkey™ slots and two probe connections. Using Chemkeys™ (**table 3.2**) and IntelliCAL™ probes, the analyser is capable of simultaneously measuring up to six parameters. The Chemkeys™ contain reagents, which react with the substances in the sample and form coloured products (**table 3.2**). The light intensity absorbed by the reaction products is proportional to the concentrations of the substances in the drinking water. The results are automatically gathered within 10 minutes and saved as Excel files.

A Hach® digital titrator with a sulfuric acid cartridge (1.6 N H_2SO_4) was used for total alkalinity measurement. The total alkalinity is defined as the buffer capacity of the water, *i.e.* the total concentration of bases derived from weak acids present in the water. The total alkalinity can be expressed in mg/L $CaCO_3$, as all buffer species can be represented in function of the buffer capacity of the carbonate anion (Dickson 1981). Sulfuric acid is gradually added to 100mL of sample whilst monitoring the pH using a pH probe. At a pH of 4.5, the total alkalinity (in mg/L $CaCO_3$) is displayed on the digital titrator. The samples were, conform the analysis requirements, cooled during transport and were analysed in the lab within six hours.

Table 3.2 – Used Hach® SL1000 Chemkeys™ for each parameter.

Chemkey	Active substances	Range of detection
Free Chlorine	DPD (N, N-diethyl-p-phenylene diamine)	0.04 - 4.6 mg/L Cl_2
Monochloramine	Cyanoferrate catalyst, indophenol	0.04 - 4.6 mg/L Cl_2
Nitrite	Sulfanilic acid, chromotropic acid	0.005 - 0.6 mg/L NO_2^--
High Range Orthophosphate	Molybdate under acidic conditions	2.0 - 30.0 mg/L PO_4^{3-}
Low Range Orthophosphate	Molybdate under acidic conditions	0.20 - 4.00 mg/L PO_4^{3-}
Free Ammonia	Cyanoferrate catalyst, indophenol, hypochlorite	0.05 - 0.5 mg/L NH_3-N

To determine the iron and nitrate concentration, Hach® powder pillows (Colorado, United States) containing Permachem® reagents were used (**table 3.3**). One powder pillow was added to 10 mL of sample, after which the light absorbance at 520nm was measured using the Hach® DR900 colorimeter. This protocol is a standardized Hach® method. The results were corrected for interference using a blank sample, *i.e.* where no reagents were added.

Table 3.3 – Powder pillow reaction details.

Parameter	Powder pillow	Colorimetric method	Reaction time
Iron	FerroVer® Iron Reagent	1-10 phenanthroline method	3 minutes
Nitrate	NitraVer® Nitrate Reagent	Cadmium reduction and gentisic acid coupling	6 minutes

2. Flow cytometry

For flow cytometric analysis, the samples were stained with two nucleic acid stains. The stain that was used for total cell analysis is SYBR® Green I (SG (Invitrogen, Belgium), 100x diluted in 0.22µm-filtered dimethyl sulfoxide, 0.99vol% final concentration). For live-dead analysis, SYBR® Green I was combined with propidium iodide (SGPI (Invitrogen, Belgium), 100x diluted in 0.22µm-filtered dimethyl sulfoxide, 0.99vol% final concentration). Samples were subsequently incubated in the dark for 20min at 37°C for experiments performed in Belgium and 13min at 35°C for experiments performed in the US. Samples were analysed immediately after incubation (Prest et al. 2013). Three flow cytometers were used in this study.

An Accuri™ C6 flow cytometer (BD Biosciences, Belgium) and an Accuri™ C6 Plus flow cytometer. They are both equipped with four fluorescence detectors (533/30nm, 585/40nm, > 670nm and 675/25nm), two scatter detectors, a blue 20mW 488nm laser and a red 12.5mW 640nm laser. The flow cytometers were operated with MilliQ (Merck Millipore, Belgium or

MilliporeSigma, Massachusetts, USA) as sheath fluid. QC was performed on a daily basis using BD™ CS&T RUO beads (BD Biosciences, Belgium). Samples were run in fixed volume mode (50µL).

A FACSVerse™ flow cytometer (BD Biosciences, Belgium) with eight fluorescence detectors (527/32nm, 783/56nm, 586/42nm, 700/54nm, 660/10nm, 783/56nm, 528/45nm and 488/45 nm), two scatter detectors, and a blue 20mW 488nm laser, a red 40mW 640nm laser and a violet 40mW 405nm laser. The flow cytometer was operated with FACSFlow™ solution (BD Biosciences, Belgium) as sheath fluid. QC was performed on a daily basis using BD FACSuite™ Research beads (BD Biosciences, Belgium). Samples were run in "high flow rate" mode, using a fixed preview time of 10 seconds, and 60 seconds measuring time with a maximal event acquisition of 10,000 events.

For online FCM measurements, an onCyt© (onCyt Microbiology AG, Switzerland) staining robot was coupled to an Accuri™ C6 flow cytometer or an Accuri™ C6 Plus flow cytometer (BD Biosciences, Belgium). Staining was performed using a 1000x dilution SYBR® Green I concentrate (Invitrogen, Belgium), in TRIS buffer with pH 8.2, 10vol% final concentration. Samples were incubated for 20 ± 2 minutes at 37°C. To prevent bacterial growth in the sheath fluid during the online measurements, a bacteriostatic concentrate solution (BD Biosciences, Belgium) was added. The onCyt© robot consists of three "chambers", wherein the first chamber the FCM measurement takes place. The chambers can be used as incubation chambers. A Cavro® XCalibur Pump (Tecan Trading AG, Switzerland) with 12 channels connects the necessary fluidics, air and waste with the three chambers. The pump regime is regulated using the onCyt© software.

3. Experimental setups

3.1 DC Water, Washington DC, USA

3.1.1 Drinking water distribution network

In Washington DC, the drinking water is produced from surface water of the Potomac River, upstream of the city. The water is treated by the US Army Corps of Engineers (The Washington Aqueduct). There are two treatment plants: the Dalecarlia Aqueduct treatment plant and the McMillan treatment plant (**figure 3.1**). Both plants also serve as a reservoir and are connected to a pumping station. DC Water provides drinking water for about one million people in total. The Washington Aqueduct and DC Water share responsibilities concerning distribution: The Washington Aqueduct operates three reservoirs throughout the city (Foxhall, Fort Reno and Van Ness reservoir) and the Dalecarlia Aqueduct pumping station. DC Water operates four pumping

stations (Anacostia, Bryant Street (McMillan), 16th Street & Alaska, and Fort Reno pumping station), and eight reservoirs and elevated tanks. The distribution network is divided into seven pressure zones according to the elevation level (**figure 3.1**).

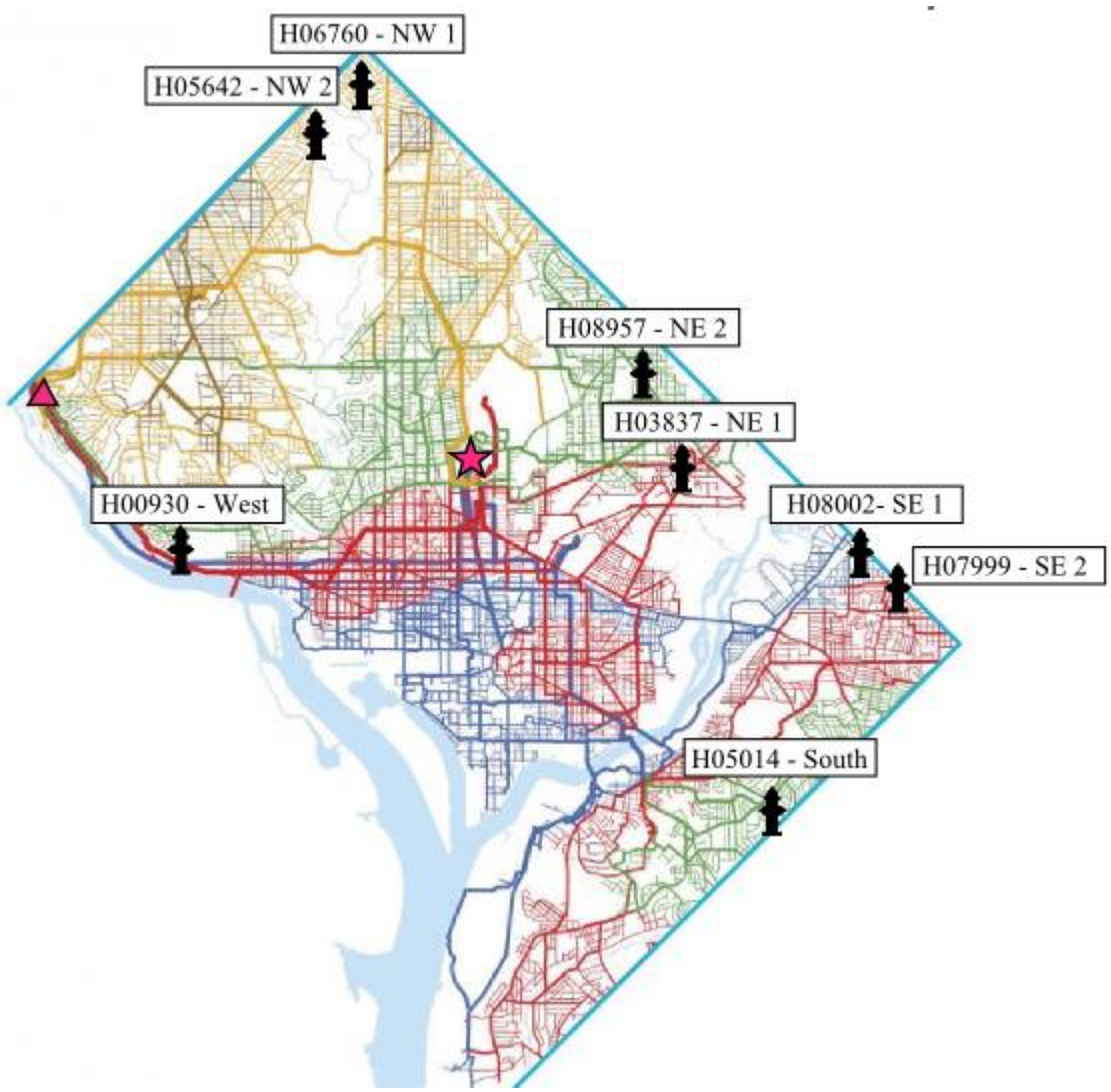

Figure 3.1 – Map of the drinking water distribution network of Washington, DC (based on DC Water 2017). The main feeders (pipes) are indicated as bold lines. The network is coloured according to the pressure zones. *Purple*: low service area, *red (south)*: Anacostia first high service area, *green (south)*: Anacostia second high service area, *red (north)*: first high service area, *green (north)*: second high service area, *yellow*: third and fourth high service area. The treatment plants are indicated with symbols. △: Dalecarlia Aqueduct treatment plant, ☆: McMillan treatment plant. The black hydrants represent the dead end sampling locations with hydrant identification number and location based name.

For each hydrant, the water age (*i.e.* the time water takes to travel from the respective reservoir to the hydrant), was estimated using a hydraulic model built by DC Water. The outcome is shown in **table 3.4** for all hydrants.

Table 3.4 – Water age predictions of the hydraulic model of DC Water. The water age is calculated as the time (h) that the water takes to travel from the respective reservoir to the hydrant. The average water age was used as a rough estimation of the true water age at the hydrants. Hydrants NW 1 and NW 2 have relatively high water ages due to the isolation of this neighbourhood. The water age for hydrants NE 1 and NE 2 is relatively short, since these hydrants are located close to the Bryant St. Reservoir. The water age at hydrant NE 2 is somewhat higher because of the oversized piping compared to the demand (residential zone). Hydrant West is almost directly supplied from the main feeder at Dalecarlia Reservoir, resulting in a very low water age. The water age at hydrants SE 1 and SE 2 is longer due to the low demand area. The average water age at hydrant South is estimated to be higher than the model prediction due to old piping.

Hydrant	Pressure zone	Average water age (h)	Minimum water age (h)	Maximum water age (h)
NW 1	3rd High	70	20	105
NW 2	3rd High	100	80	120
NE 1	1st High	60	20	90
NE 2	2nd High	75	65	90
South	A2 High	>65	40	80
West	1st High	35	10	60
SE 2	A1 high	90	85	95
SE 1	Low	95	90	100

3.1.2 Sampling procedure

During fifteen weeks, from July 3rd until October 14th, eight hydrants spread across the city were sampled (**figure 3.1**). The eight hydrants that were sampled are dead end hydrants, which means that they are located at the dead ends of the pipelines. They were chosen based on the location and pressure zone (**figure 3.1**). An overview of the hydrants and their properties is given in **table 3.5**.

Table 3.5 – Overview of the sampled dead end hydrants with the sampling characteristics. The hydrant identification code is used in communication between DC Water employees. For an easier understanding, names based on each hydrant location will be used throughout this master thesis.

Hydrant ID	Hydrant name	Pressure zone	Sampling
H00930	West	1st high	Monday
H06760	NW 1	3rd high	Tuesday
H05642	NW 2	3rd high	Tuesday
H03837	NE 1	1st high	Wednesday
H08957	NE 2	2nd high	Wednesday
H08002	SE 1	Low	Thursday
H07999	SE 2	Anacostia 1st high	Thursday
H05014	South	Anacostia 2nd high	Monday

Every hydrant was sampled weekly at a fixed day. During sampling, the hydrants were flushed at maximal flow rate and samples were taken after 1, 15 and 30 minutes of flushing. For every sample, the chemical parameters (**table 3.1**) were assessed. A 100mL sample was taken in a sterile vessel containing 0.80g sodium thiosulfate ($Na_2S_2O_3$) powder for chlorine quenching (Idexx, Virginia, USA). A 1L sample was taken in a non-sterile, Milli-Q (MilliporeSigma, Massachusetts, USA) rinsed sampling bottle. Both samples were stored and cooled at 5 ± 2°C.

In the lab, FCM analysis was performed on the 100mL quenched sample using an Accuri™ C6 Plus flow cytometer. Samples were stained with SG and analysed in duplicate. From the 17th of August on, a SGPI stained sample was analysed additionally. Afterwards, alkalinity was measured using a Hach® digital titrator.

3.2 Pidpa, Kalmthout, Belgium

3.2.1 Drinking water distribution network

Pidpa is one of the biggest Flemish drinking water utilities, providing drinking water to almost 1,200,000 people in the province of Antwerp (**figure 3.2**).

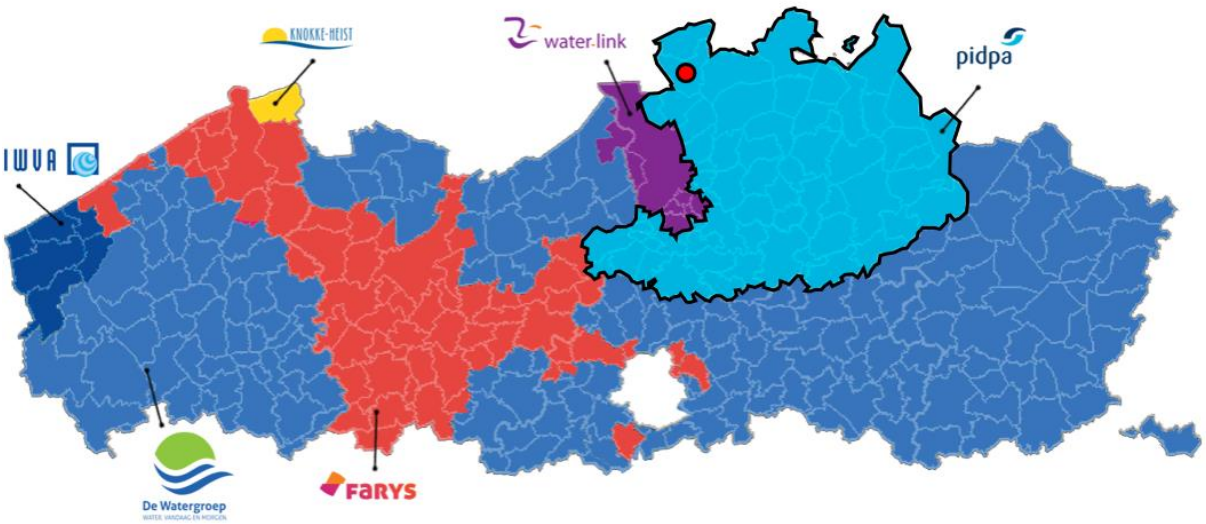

Figure 3.2 – Drinking water providers in Flanders and their provision area. Pidpa provides drinking water to a large part of the province of Antwerp. ●: Sampled water tower in Kalmthout.

3.2.2 Online sampling procedure

A water tower located in Kalmthout (**figure 3.2**) was sampled during 15 days. The samples were taken from the rising pipe in the water tower. Via this pipeline, the water tower is emptied and filled, depending on the pressure in the drinking water network. This system is operated by a valve that is situated underneath the storage tank. The water tower is usually filled during the night and emptied during the day. A sensor inside the tank monitors changes in water level.

A sample was taken from the rising pipe every 15 minutes using an Accuri™ C6 Plus flow cytometer coupled with an onCyt© staining robot. Staining was performed using SG.

3.3 FARYS, Gent, Belgium

3.3.1 Drinking water distribution network

The Flemish drinking water utility FARYS has a distribution network which extends from the provinces Vlaams-Brabant and Henegouwen/Hainaut up to the coastal area (**figure 3.2, 3.3**). FARYS provides drinking water for about 600,000 people. The water is produced from both surface water and groundwater. The groundwater production facilities of FARYS are located in Mainvault (Henegouwen, Wallonia), Beersel (Vlaams-Brabant, Flanders), Ronse and Oudenaarde (Oost-Vlaanderen, Flanders). In addition, FARYS buys drinking water produced from groundwater from the water utility Vivaqua in Espinette (Waals-Brabant, Wallonia). Drinking water produced from surface water is bought from other drinking water utilities, such as Water-link (producing from the Albertkanaal, Antwerp, Flanders) and De Watergroep (producing in Kluizen, Oost-Vlaanderen, Flanders). In total, FARYS distributes about 85,000,000 m^3/year.

The experiments were performed at the water tower located in Kattenberg, Gent (**figure 3.3**). This water tower was selected because two different feed streams enter the water tower. One feed is produced from surface water by the utility Water-link, and is transported by the the main feeder which starts at Buggenhout and runs along Aalst (Oost-Vlaanderen). This drinking water stream will further be referred to as “surface water”. The second feed water stream is produced from groundwater by FARYS and Vivaqua, coming from the production plants in Mainvault (Henegouwen) and Espinette (Waals-Brabant). It is mixed in two large buffers of 15,000 m^3 each in Brakel (Oost-Vlaanderen). It is transported to the water tower in Gent by the main feeder coming from Brakel. This drinking water stream will further be referred to as “groundwater”.

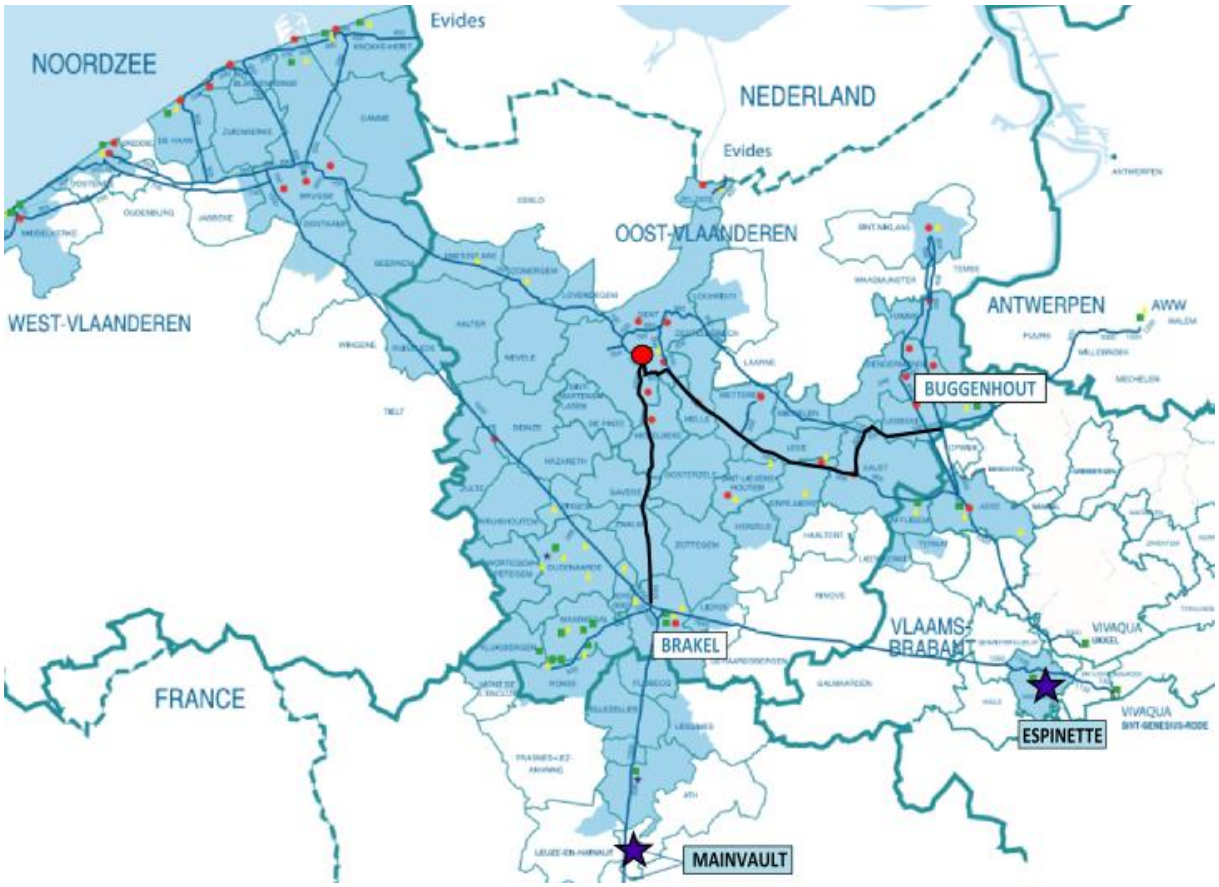

Figure 3.3 – Map of the drinking water transportation network of FARYS, Belgium. ●: Water tower at Kattenberg, Gent. ★: FARYS's and Vivaqua's groundwater production facilities Mainvault and Espinette. Black lines: Main feeders from Brakel ("groundwater") and Buggenhout ("surface water") which enter the water tower at Kattenberg.

3.3.2 Experimental setups

Offline experiments were performed by grab sampling both of the incoming feed streams, and the outgoing stream on four different days. Within six hours after sampling, a FCM analysis of all incoming drinking water streams was performed using a FACSVerse™ flow cytometer. Furthermore, the incoming water streams were mixed in vitro in nine concentrations ranging from 10% to 90%, increasing with steps of 10%. Samples were analysed in five to eight replicates. Online FCM measurements were performed over five days, using an Accuri™ C6 flow cytometer equipped with an onCyt© staining robot. The two incoming streams and the outgoing stream were sampled every 40 minutes.

The mixing ratio of the outgoing stream is not known, since the full-scale water tower reservoir serves as a buffer to the system. The online incoming and outgoing water flow rates, measured and provided by FARYS, were used to model the mixing ratio of the outgoing stream. Differential equations were used to calculate the percentage of surface water in the exiting water. In this approach, perfect mixing was assumed. The volume of the water tower (V) changed over time in function of the incoming "groundwater" (GW) and "surface water" (SW), and outgoing (OUT)

flow (Q) (**eq. 6**).

$$\frac{dV(t)}{dt} = Q_{GW}(t) + Q_{SW}(t) - Q_{OUT}(t) \quad \textbf{(eq. 6)}$$

As the flows of the incoming water streams varied over time, the mixing ratio is not constant. For example, the outgoing mass of "surface water" (m_{SW}) varied over time, with c_{SW} the fraction of incoming water produced from surface water in the outgoing stream (**eq. 6**).

$$\frac{dm_{SW}(t)}{dt} = \frac{d(V(t)*c_{SW}(t))}{dt} \quad \textbf{(eq. 7)}$$

Combining **eq. 6** with **eq. 7** gives the following (**eq. 8**), where $c_{SW,SW}$ is the fraction of surface water in the "surface water" stream (=1) and $c_{SW,GW}$ is the fraction of surface water in the "groundwater" stream (=0):

$$\frac{dV(t)}{dt} * c_{SW}(t) + V\frac{(t)*dc_{SW}(t)}{dt} = Q_{GW}(t) * c_{SW,GW}(t) + Q_{SW}(t) * c_{SW,SW}(t) - Q_{OUT}(t) * c_{SW}(t) \quad \textbf{(eq. 8)}$$

As the fraction of "surface water" in the "groundwater" and "surface water" feed was resp. zero and one, the equation can be reduced to a first order differential equation (**eq. 9**).

$$\frac{dc(t)}{dt} = \frac{Q_{SW}(t)}{V(t)} - \frac{Q_{OUT}(t)}{V(t)} * c_{SW}(t) \quad \textbf{(eq. 9)}$$

Based on this equation, the percentage of surface water in the outgoing stream was modelled.

A lab scale version of the water tower Kattenberg was built. As incoming streams, two 10L bottles grab samples were taken from the incoming streams of the full-scale tower, produced from surface water and groundwater, respectively. These bottles were connected to a glass vessel with a total volume of 540mL. Two peristaltic pumps were used: a Watson-Marlow 101U (Watson-Marlow®, England), and a Masterflex® L/S® (Cole-Parmer Instrument Co., Illinois, USA). A hydraulic retention time of four hours was chosen, as a rough estimation of the actual hydraulic retention time in the water tower. The total flow (0.135L/h) was divided between the two types of drinking water. Similar to the offline measurements, the drinking waters were mixed in eight different ratios ranging from 10% to 80% "groundwater", increasing with steps of 10% (**table 3.6**). Every ratio was run for 12 hours (three times the hydraulic retention time) to ensure the water composition in the lab water tower had reached equilibrium. To maintain these low flow rates (**table 3.6**), Masterflex® 6404-13 tubing with inner diameter of 0.8mm and outer diameter of 1.6mm (Cole-Parmer Instrument Co., Illinois, USA) was used. More information on the pump calibration is described in **appendix 1**.

The microbial composition of both of the incoming feed waters and the water of the lab scale water tower was online monitored using an Accuri™ C6 flow cytometer combined with an onCyt© staining robot. Every 40 minutes, a sample was taken from each stream.

Table 3.6 – Flow rates and the cumulative volume over time of the incoming feed drinking waters, produced from surface water and ground water respectively.

Q_{surf} (%)	Q_{surf} (L/h)	Q_{ground} (%)	Q_{ground} (L/h)	$V_{surf,cum}$ (L)	$V_{ground,cum}$ (L)
90	0.122	10	0.014	1.46	0.16
80	0.108	20	0.027	2.75	0.49
70	0.095	30	0.041	3.89	0.97
60	0.081	40	0.054	4.86	1.62
50	0.068	50	0.068	5.67	2.43
40	0.054	60	0.081	6.32	3.40
30	0.041	70	0.095	6.80	4.54
20	0.027	80	0.108	7.13	5.83

The setup was built in a temperature-controlled room at 15°C, in order to approximate the actual temperature of the water tower, and to eliminate the influence of temperature fluctuations on the microbial community. The experiment was conducted over a period of seven days (**table 3.7**).

Table 3.7 - Execution times of different mixing regimes in the semi-continuous lab-scale water tower.

Day	% Surface Water	% Groundwater
MON 09 APR 20:00	90	10
TUE 10 APR 08:00	80	20
TUE 10 APR 20:00	70	30
WED 11 APR 08:00	60	40
WED 11 APR 20:00	50	50
THU 12 APR 08:00	40	60
THU 12 APR 20:00	30	70
FRI 13 APR 08:00	20	80

4. Data analysis

The flow cytometric data was analysed in R (v3.4.4). The Flow Cytometry Standard (.fcs) files were imported using the flowCore package (v1.44.2).

The background data was removed by manually drawing a gate on the FL-1 (green) and FL-3 (red) fluorescence channels (**appendix 2**). The data was subsequently analysed using the Phenoflow

package (v1.1.1) and the FlowFP package (v1.36.0). Both packages convert the single-cell data into a phenotypic fingerprint using different algorithms. Fingerprinting was performed based on the FL-1 and FL-3 fluorescence channels, and the FSC and SSC. When using probability binning, 2^7 recursions were performed, and when using equal space binning, a grid consisting out of 128x128 bins was used. For experiments using the BD Accuri™ C6 & C6 Plus flow cytometers, the signal height values were used in further calculations since the detectors are more sensitive towards the signal heights. Similarly, for experiments using the FACS™ flow cytometer the signal area values were used. The threshold for total cell counts used for calculation of the diversity indices was relatively low due to the overall low cell counts in the drinking water (**appendix 2**). The Phenoflow package allows the calculation of diversity metrics such as alpha- and beta diversity. Significance of the differences in phenotypic fingerprint were examined using PERMANOVA. Using the vegan package (v2.5.2), the Bray-Curtis dissimilarity between different phenotypic fingerprints was calculated. Significance between two groups was calculated using the Wilcoxon Rank Sum test, from the R stats package (v3.4.4). Random Forest predictions were performed in R using the R package RandomForest (v4.6.14). Predictions were made using mtry = 6, based on fingerprints generated using the FlowFP package, with an adapted grid made out of 2^5 bins.

1. DC Water

The aim of the DC Water monitoring campaign was to evaluate the effect of external influences such as disinfectant concentration, water temperature and water age on the drinking water quality, and specifically on the drinking water bacterial community. Specific attention was given to areas suffering from discoloured drinking water, most likely related to (microbially induced) corrosion of cast iron piping. Drinking water utilities typically try to reduce this effect for the customers by flushing the network using fire hydrants. The drinking water quality of eight dead end hydrants, spread out over Washington DC, was monitored over 15 weeks (**figure 3.1**). Every hydrant was sampled once a week. During sampling, the hydrants were flushed and a sample was taken at 1, 15 and 30 minutes of flushing. The physicochemical properties and the biological characteristics of the drinking water were assessed. The significance level is set at $\alpha = 5\%$ for statistical calculations performed in this study. The effect of external influences on the microbial drinking water quality is examined on the basis of specific research questions as defined in the objectives (**section II**). D_2 was calculated to evaluate the phenotypic alpha diversity, which was highly correlated to D_1 and D_0 ($r_p(D_1,D_2) = 0.97$, $r_p(D_0,D_2) = 0.75$, $p < 0.001$) (**appendix 2**).

1.1 The effect of flushing on the chemical profile of the hydrants.

DC Water, which is responsible for drinking water distribution in Washington DC, implements flushing of hydrants as a strategy to maintain the drinking water quality. The effect of flushing on the water quality was evaluated by comparing the samples taken at 1 and at 30 minutes. DC Water uses total chlorine concentration as the main parameter for evaluating the drinking water quality during routine measurements. Therefore, the effect of flushing on the total chlorine concentration was evaluated in this section.

Over the duration of the sampling campaign, the average total chlorine concentration at the Dalecarlia production plant was 3.73mg/L (**figure 4.1**). At the hydrants, the total chlorine concentration is highly correlated to the measured monochloramine concentration ($r_p = 0.998$, $p < 0.001$). Moreover, on average 77.75% of the total chlorine was still present in the form of monochloramine. An increase of the total chlorine concentration was observed after 30 minutes of flushing (**figure 4.1**). Samples at 15 minutes of flushing had intermediate chlorine concentrations. At hydrants SE 1, SE 2 and NW 2, the total chlorine concentration at 30 minutes of flushing was still relatively low (*e.g.* 0.17mg/L at NW 2). For all of the hydrants, except for NW 2, the difference in chlorine concentration was significant. The extent of the difference is hydrant-dependent.

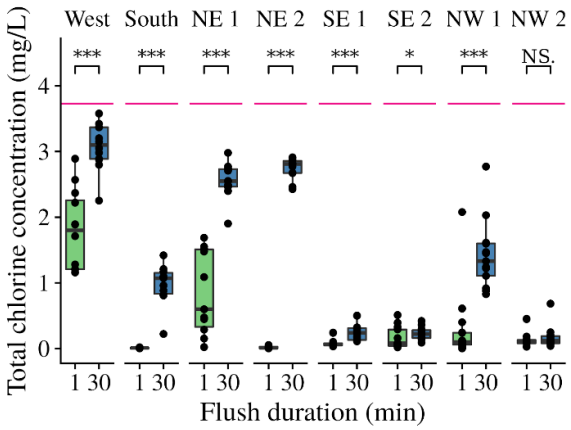

Figure 4.1 – The effect of flushing (samples taken at 1 and 30 minutes of flushing) on the total chlorine concentration for the eight dead end hydrants. The dotted pink line indicates the average chlorine concentration at the production plant (Dalecarlia). Significance of the differences between flush durations for each hydrant was evaluated using the Wilcoxon Rank Sum test, significance is marked as "***" < 0.001 < "**" < 0.01 < "*" < 0.05 < "NS.".

These results indicate that there is a loss of residual chlorine in the distribution network. This loss may be attributed to reactions of the residual disinfectant in the bulk water, such as auto decomposition of monochloramine and microbial activity, and to reactions of the disinfectant residual with the pipe wall during transportation (Clark et al. 1993; Vikesland et al. 2001; Wang et al. 2012). For example, monochloramine can serve as an oxidant during iron pipe wall corrosion (Westbrook & Digiano 2009). The pipe size and the flow rate will both influence the extent of chloramine residual loss (Clark et al. 1993; Rossman et al. 1995). This implies that the water retention time (or water age) will affect the extent of chlorine residual loss. DC Water provided model predictions of the water age of all of the hydrants (**table 3.4**). The water age is calculated as the time (h) for the water to travel from the respective reservoir to the hydrant. The average water age was used as a rough estimation of the true water age at the hydrants. The average water age was highly negatively correlated to both the total chlorine concentration at 1 minute of flushing (r_p = -0.79, $p < 0.05$) and at 30 minutes of flushing (r_p = -0.82, $p < 0.05$). This means that hydrants with a high water age hydrants (*e.g.* due to the distance to the plant) typically have low chlorine concentrations, even after flushing 30 minutes. Shang et al. (2008) modelled the effect of the water age on the monochloramine auto decomposition reaction and found losses of more than 2mg/L at a water age of 60 hours. This is within the same range as the concentrations measured in this study. Note that the model did not take into account other reactions besides monochloramine auto decomposition. This may explain why the observed decrease at some hydrants was bigger than 2mg/L. More recently, Westbrook et al. (2009) evaluated monochloramine decay in a pipe-section reactor. Their results indicate that monochloramine decay due to pipe wall interactions could occur up to 2 - 3 orders of magnitude faster than bulk decay in a thoroughly mixed flow regime. Other studies also indicated that the relative contribution of wall decay may be bigger compared to bulk

decay in full-scale distribution systems (Castro & Neves 2003; Hallam et al. 2002). The water age will strongly affect the extent of both the auto decomposition decay reaction and the pipe-wall interactions and consequently affect the disinfectant residual concentration at the hydrant.

To conclude, disinfectant residual loss may occur through a combination of pipe wall interactions and bulk reactions. The extent of both processes is strongly dependent on the water age. The disinfectant residual concentration before and after flushing will consequently be lower at higher water age hydrants and *vice versa*. Practically, this implies that flushing for more than 30 minutes is needed to restore the monochloramine residual concentration at high water age hydrants such as SE 1, SE 2 and NW 2.

As described in the literature study, the pH may be a valuable indicator for the detection of water quality deterioration, *e.g.* caused by microbial activity such as nitrification. Therefore, the effect of flushing on the pH was evaluated. An increase in pH after 30 minutes of flushing was observed (**figure 4.2, A**). For all hydrants, the pH difference between 1 and 30 minutes of flushing is significant. Note that the pH of hydrant NW 1 was higher than the others. The alkalinity in the network varied in the range of 70 - 120mg $CaCO_3$/L. No clear effect of flushing on the total alkalinity was observed (**figure 4.2, B**). For only two of the hydrants (West and South), there was a significant correlation between flushing and the alkalinity.

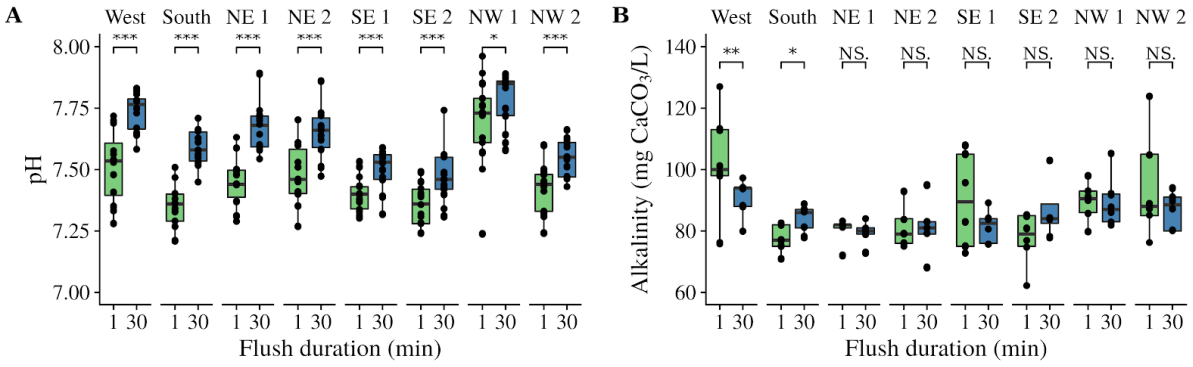

Figure 4.2 – Effect of flushing on the (**A**) pH and (**B**) the total alkalinity of the eight dead end sampling hydrants separately. Significance of the differences between flush durations for each hydrant was evaluated using the Wilcoxon Rank Sum test, significance is marked as "***" < 0.001 < "**" < 0.01 < "*" < 0.05 < "NS.".

The decreased pH at 1 minute of flushing may be due to protons generated during microbiological processes such as nitrification and during monochloramine auto decomposition (Vikesland et al. 2001). The elevated pH at hydrant NW 1 can be explained by the cement lining, which is a mixture of Portland cement and clean sand, at this hydrant. Hereby, lime ($Ca(OH)_2$), which is formed during the cement hardening, is leached from the cement lining into the drinking water, causing a rise in pH and alkalinity (Douglas et al. 1996). Neville (2001) states that leaching will be increased

at prolonged water ages, as it is the case for this hydrant. However, the increase in pH was not confirmed by an increase of the total alkalinity (**figure 4.2, B**). The assumed leaching does however not affect the water quality (pH < 8.5, no alkalinity increase) (Douglas et al. 1996; US EPA 2004b). Note that the piping at hydrant SE 1 and a part of the piping at SE 2 is also cement-lined, however for these sampling points no elevated pH was observed. The water mains of the other hydrants consist of unlined cast iron piping. Different studies indicate that leaching of cement linings may occur extensively up to 30 years after pipe installation, however, the pipes at DC Water are up to 100 years old (Douglas et al. 1996; Muster et al. 2011). This might explain the rather limited differences in pH. Furthermore, total alkalinity may be influenced by water temperature (r_p = -0.27, $p < 0.001$) rather than the piping material in this case, as the solubility of $CaCO_3$ will decrease with increasing temperature (Lee et al. 2006).

To conclude, flushing results in a pH increase. A lower pH may indicate overall water quality deterioration, whereas a higher pH can indicate leaching of cement lining. The pH after flushing should consequently be evaluated relative to the pH before flushing.

1.2 RQ 1: What is the influence of the residual disinfectant concentration on the drinking water bacterial community?

Since the total chlorine concentration is currently used as an indicator for drinking water quality, the relationship between chlorine concentration and the drinking water bacterial community was examined. The bacterial cell density and phenotypic diversity was assessed using flow cytometry. A negative exponential behaviour of the cell density in function of the total chlorine concentration was observed (**figure 4.3**). Furthermore, samples taken at 1 minute of flushing typically contained more cells and contained, as previously discussed, a lower chlorine concentration.

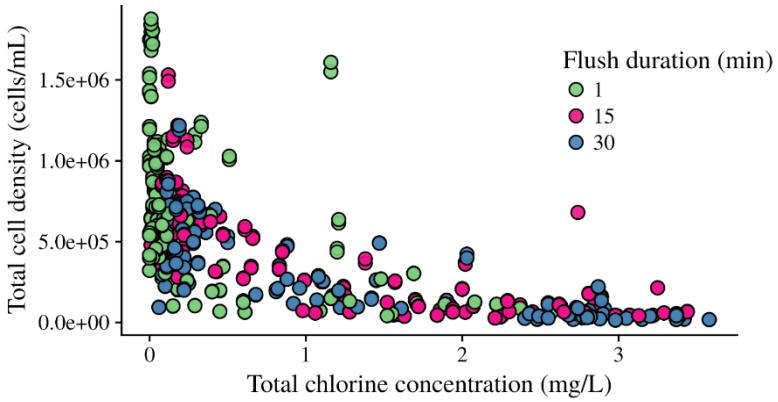

Figure 4.3 – Total cell density (cells/mL) in function of the total chlorine concentration for all hydrants. The data points are coloured according to flush duration.

The effect of chlorine on the intact cell fraction was assessed by analysing FCM data obtained from samples stained with SGPI. The intact cell fraction was calculated as the intact cell density

divided by the sum of the intact and permeabilized cell densities. A decreasing trend in the intact cell fraction in function of the total chlorine concentration was observed (r_p = -0.72, $p < 0.001$) (**figure 4.4, A**). The mean intact cell fraction is 0.69 ± 0.18. This decreasing trend is more obvious when the intact cell densities are plotted in function of the total chlorine concentration (**figure 4.4, B**).

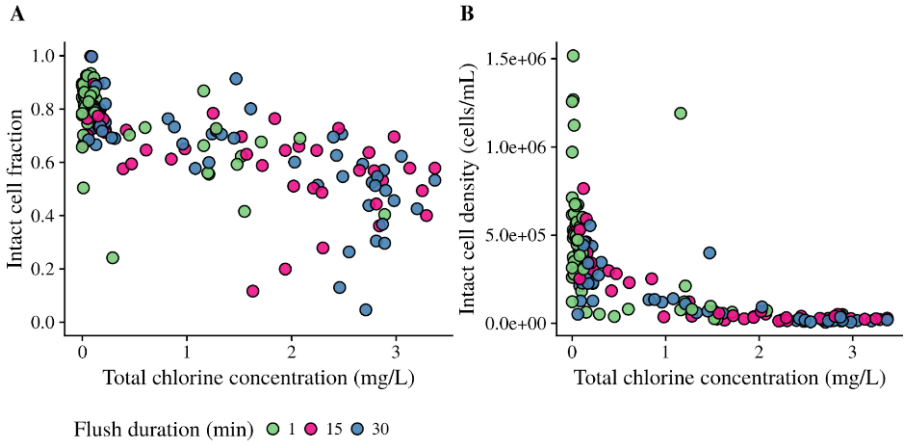

Figure 4.4 – (**A**) Intact cell fraction and (**B**) intact cell density in function of the total chlorine concentration for all of the hydrants, coloured according to flush duration.

To assess the effect of disinfectant residual on the diversity of the bacterial community, the phenotypic alpha diversity D_2 was evaluated in function of the total chlorine concentration. No trend was observed (**figure 4.5**). D_2 of the intact bacterial community showed a similar profile (s_D = 22.53%). When grouping the data per hydrant to account for hydrant-specific differences, the relation between chlorine concentration and D_2 was hydrant-dependent (**figure 4.5, B**). Additionally, the flush duration did not seem to have a clear effect on D_2 (**figure 4.5, A**, further discussed in **section IV.1.3**).

The phenotypic beta diversity (*i.e.* the between sample diversity) was assessed using the Bray-Curtis dissimilarity between the SG stained samples. Bray-Curtis dissimilarities were visualised by principal coordinates analysis (PCoA). The data was visualized per hydrant as differences between the hydrants may mask the effect of chlorine concentration on the microbial community. Overall, no general relation between chlorine concentration and phenotypic beta diversity was observed (**figure A7.1**, in appendix). However, hydrant South and NE 2 showed a discrimination between samples that could respectively gradually or clearly be explained by a difference in chlorine concentration (**figure 4.6**). Furthermore, a gradient was observed in the phenotypic beta diversity profile of hydrants SE 1 and SE 2 in function of the chlorine concentration, indicating that the phenotypic community structure will gradually change with an increasing chlorine concentration (**figure 4.6**).

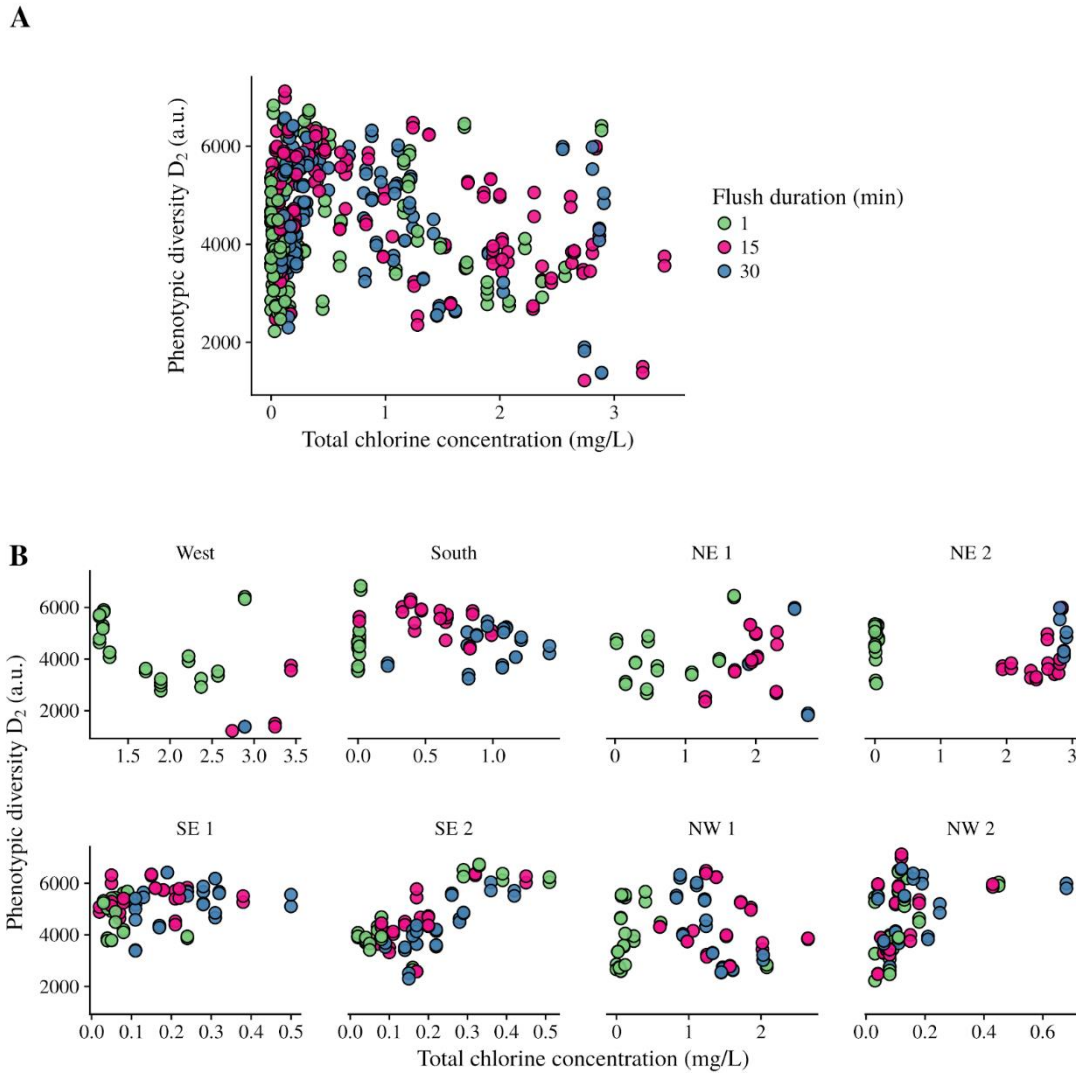

Figure 4.5 – Phenotypic alpha diversity D_2 in function of the total chlorine concentration, coloured by flush duration (**A**) and hydrant location (**B**). D_2 was calculated using 999 bootstraps for each sample.

The results show that the total bacterial abundance will increase exponentially with a decreasing disinfectant residual (**figure 4.3**). Zhang et al. (2002) reported similar observations for a full-scale DWDS: a strong negative linear correlation between the log of HPC counts and the total chlorine concentration. Chiao et al. (2014) observed a comparable negative exponential relationship between total cell counts and monochloramine exposure when used as a primary disinfectant. Thus, the total bacterial abundance is strongly affected by the disinfection residual in the DWDS. Monochloramine is used in DC Water as secondary disinfectant to control bacterial growth rather than actively killing bacterial cells. Therefore, it is suggested that the results from the present study should be interpreted as "less disinfectant residual will lead to more bacterial regrowth in the distribution system".

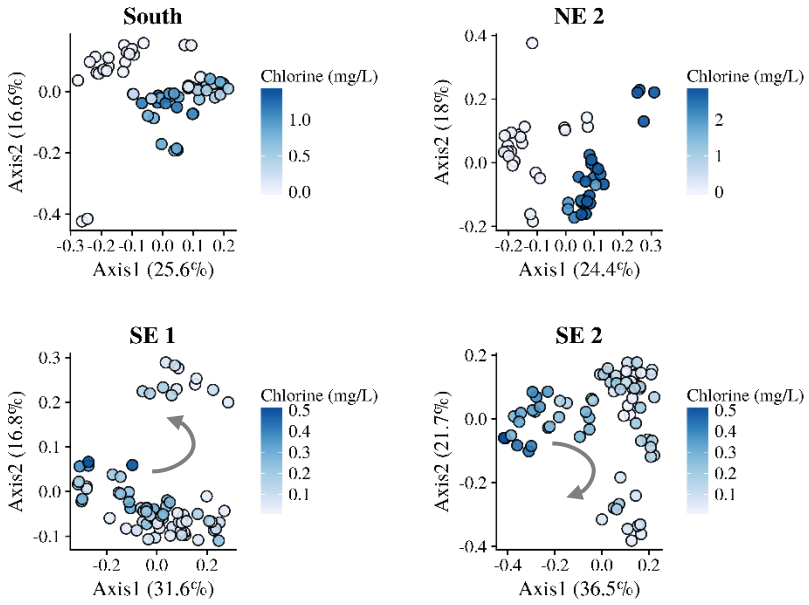

Figure 4.6 – PCoA ordination of phenotypic fingerprints of hydrant South, NE 2, SE 1 and SE 2, coloured according to the total chlorine concentration. Since the total chlorine concentration range is different for every hydrant, the scale of the PCoA gradient is adjusted based for each hydrant. The grey arrow shows the gradient, indicating that the phenotypic community structure will gradually change with an increasing chlorine concentration. All samples, taken at 1, 15 and 30 minutes of flushing, were taken into account.

The intact cell fraction decreased in function of the total chlorine concentration (**figure 4.4, A**). The disinfecting effect of monochloramine is due to damaging the bacterial cell membrane through the oxidation of functional groups (*e.g.* amine functionalities of the transmembrane proteins) and the degradation of the nucleic acids and intracellular proteins (Nie et al. 2016; Ramseier et al. 2011). Furthermore, Gatza et al. (2013) reported that using chlorine disinfection, the permeabilized fraction measured using FCM will increase with an increasing disinfectant concentration. The results from the present study comply with this. Cells will thus be permeabilized by monochloramine. A loss of chlorine residual at the hydrants will thus facilitate regrowth, resulting in an increase of the living cell fraction. Just after primary disinfection and secondary disinfection residual addition, the effect of chlorine on the bacterial abundance is high: Gillespie et al. (2014) assessed the viability of the bacterial community in chloraminated drinking water reservoirs before entering the DWDS. They reported intact cell fractions of only 5 - 10% using FCM. However, the results in these study show a much higher intact cell fraction of 0.69 ± 0.18. This indicates the occurrence of bacterial regrowth within the DC Water distribution system, despite secondary disinfection. Remarkably, Berney et al. (2008) reported similar intact cell fractions in samples collected in a non-chlorinated DWDS using FCM (62 - 98%).

In a next step, the phenotypic alpha diversity of the bacterial community was evaluated. No relation was observed between D_2 and the disinfectant residual concentration (**figure 4.5**). McCoy et al. (2012) evaluated the temporal variability of the bacterial diversity in a chlorinated DWDS using

sequencing. In their results, changes in the bacterial diversity could be attributed to a change in disinfection dose. The results obtained in the present study indicate that changes in the phenotypic alpha diversity may be occurring, however, a general trend for all hydrants was not observed. This difference may be explained due to a different disinfection strategy. Also the distribution system, pipe age and materials may differ. Furthermore, the phenotypic diversity may differ from the genotypic diversity obtained using sequencing (see **section I**). Thus, the results of the present study suggest that the phenotypic alpha diversity will not change unambiguously in function of the disinfectant residual concentration.

A change in the phenotypic bacterial community structure in function of the disinfectant residual concentration was observed at four hydrants. Chiao et al. (2014) examined the bacterial community composition in the drinking water effluent of a biological activated carbon filter. In their findings, the community composition changed in function of the monochloramine concentration. In another study performed by Yang et al. (2017), the selectivity of monochloramine disinfection for specific bacterial groups was shown in treated wastewater effluent. Both studies hypothesize that the bacterial community changes in function of monochloramine exposure. The results from the present study are in line with these findings, however, the differences were less pronounced, as a community shift could only be detected at four out of eight sampling points. McCoy et al. (2012) indicate that shifts in the bacterial community may be related to changes in the chlorine concentration, as not all bacterial classes are equally chlorine-resistant.

To conclude, less disinfectant residual will lead to bacterial regrowth in the distribution system and consequently increase the intact cell fraction. Despite secondary disinfection, the living bacterial cell fraction is comparable to the living cell fraction in non-chlorinated DWDS. Disinfection residual may cause changes in the phenotypic diversity, however, a general trend was lacking. Furthermore, phenotypic changes in the bacterial community may be related to the disinfectant residual concentration. This will be assessed in the following research questions.

1.3 RQ 2: What is the influence of the flush duration on the drinking water bacterial community?

Since DC Water uses flushing as a strategy to maintain the drinking water quality, the effect of the flush duration on the bacterial community was evaluated. The change in total cell density after 30 minutes of flushing is shown in **figure 4.7**. For all hydrants except for NW 2, the cell density was significantly different between samples taken at 1 and 30 minutes of flushing. Samples taken at 15 minutes had an intermediate cell density.

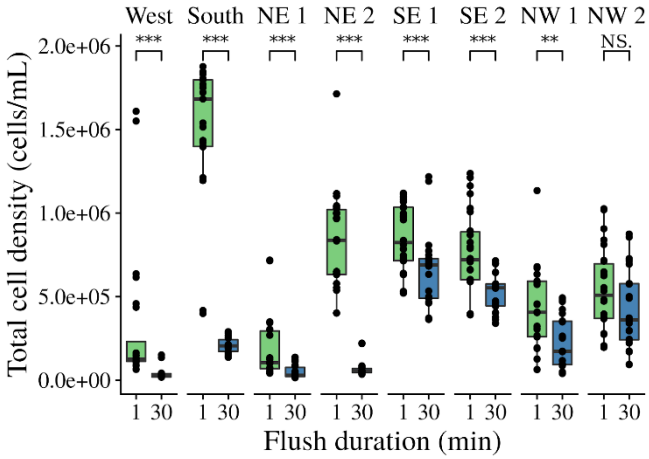

Figure 4.7 – Total cell density in function of flush duration for all hydrants. Significance of the differences between flush durations for each hydrant was evaluated using the Wilcoxon Rank Sum test, significance is marked as "***" < 0.001 < "**" < 0.01 < "*" < 0.05 < "NS.".

To detect changes in the phenotypic fingerprints that are related to the flush duration, the phenotypic beta diversity was calculated and visualised using PCoA for all of the hydrants separately (**figure A7.2** in appendix). The flush duration had a clear effect on the phenotypic fingerprint for three of the hydrants (West, South and NE 2) (**figure 4.8**).

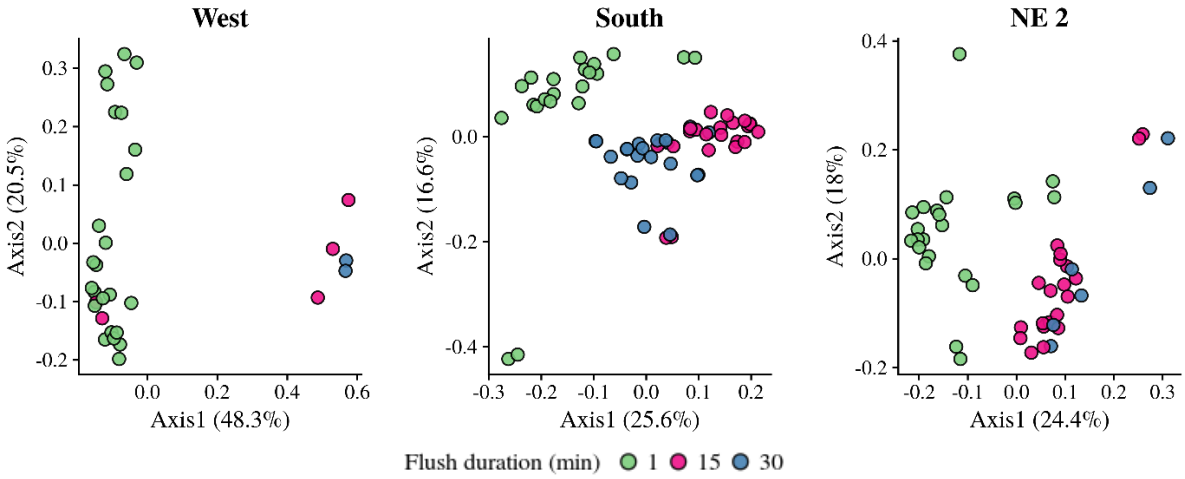

Figure 4.8 – PCoA ordination of phenotypic fingerprints of hydrants West, South and NE 2, coloured according to flush duration.

Statistical significance of the differences between the samples taken at different flush durations was assessed using PERMANOVA, p-values were adjusted using the Bonferroni correction. Homogeneity of variance between groups (flush duration) was assessed and confirmed (except for West), prior to PERMANOVA analysis. The samples taken at different flush durations are significantly different for hydrants South ($p_{1\text{-}15}$, $p_{1\text{-}30}$, $p_{15\text{-}30} < 0.01$) and NE 2 ($p_{1\text{-}15}$, $p_{1\text{-}30} < 0.01$, $p_{15\text{-}30} < 0.05$). For hydrant West, the samples taken at 1 minute of flushing are significantly different from the others ($p_{1\text{-}15}$, $p_{1\text{-}30} > 0.05$). Note that at hydrant West, homogeneity of variance was not confirmed as only a few samples taken at 15 and 30 minutes of flushing are taken into account due to the overall low cell counts (**appendix 2**). Consequently, for this hydrant, no conclusions about

the significance of the effect of the flush period can be made. However, difference were visually observed. For the other hydrants, flush duration did not explain differences in the fingerprints.

Additionally, the Bray-Curtis dissimilarity matrix was calculated using probability binning ($n_{recursions} = 7$, $n_{bins} = 2^7 = 128$) as this allows to better detect small changes in cell abundance of highly abundant phenotypes (see **section I**). Samples were pooled based on the flush duration prior to calculation of the Bray-Curtis dissimilarity. The Bray-Curtis dissimilarity matrix is presented as a heat map in **figure 4.9** for hydrants West, South, NE 2 and NE 1. These hydrants show the biggest difference between fingerprints, depending on the flush duration. No clear differences were observed for the other hydrants (**figure A7.3** in appendix). Hydrant NE 1 shows clear differences in the Bray-Curtis analysis, which were not observed in the phenotypic beta diversity.

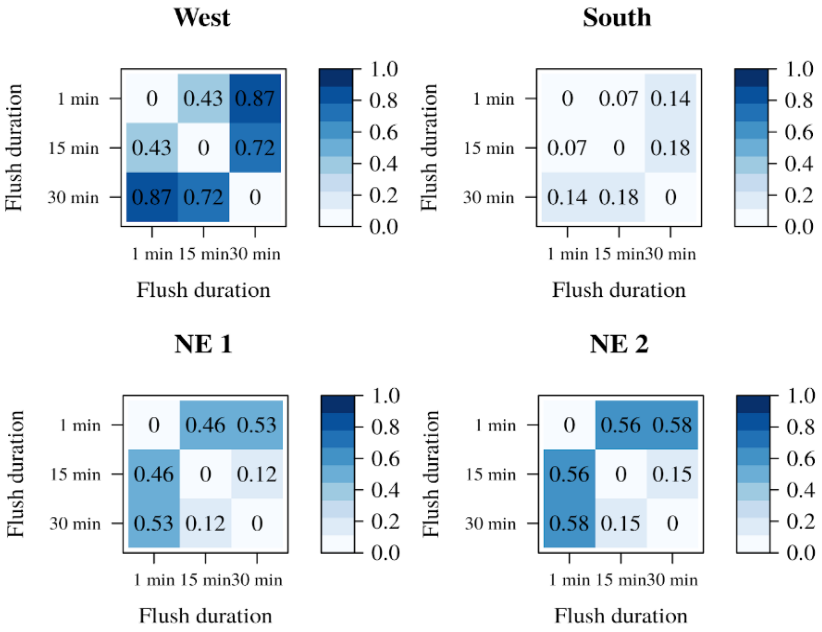

Figure 4.9 – Heatmap of the Bray-Curtis dissimilarity matrix for hydrant West, South, NE 1 and NE 2, calculated between flush durations. The Bray-Curtis dissimilarity ranges from 0 to 1. Light: lower dissimilarity, indicating more similar phenotypic fingerprints, dark: higher dissimilarity, indicating more different phenotypic fingerprints. The samples were pooled per flush duration prior to analysis.

Next, the relation between flushing and the phenotypic alpha diversity of the bacterial community was examined (**figure 4.10**). D_2 is significantly different between 1 and 30 minutes of flushing at hydrant SE 1, whereas this is not the case for the other hydrants. In some cases, D_2 increases with flush duration.

At hydrant West, no significant change in cell counts was found after flushing (**figure 4.7**), but a decrease in D_2 was observed (**figure 4.10**). This confirms the observed phenotypic change in bacterial community of this hydrant. For hydrants South, NE 1 and NE 2, the difference between phenotypic fingerprints is not reflected by a change in D_2.

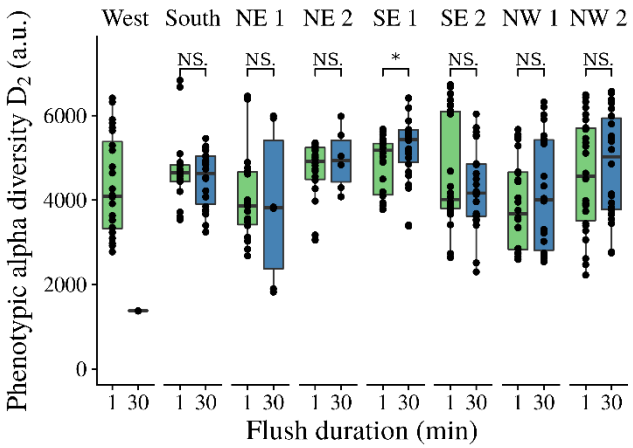

Figure 4.10 – Effect of the flush duration on the phenotypic alpha diversity D_2. Significance of the differences between flush durations for each hydrant was evaluated using the Wilcoxon rank-sum test, significance is marked as "***" < 0.001 < "**" < 0.01 < "*" < 0.05 < "NS.". For hydrant West, only two samples were taken into account at 30 minutes of flushing, thus no significance between flush durations was calculated.

These results indicate that flushing affects the bacterial abundance. A decrease in cell density was observed after flushing at most of the hydrants. This is in accordance with research performed by Lautenschlager et al. (2010) and Prest et al. (2013), who showed that overnight stagnation in household pipes resulted in an increase of the total cell density. The decrease in cell density after flushing that was reported by Prest et al. (2013) was within the same range as observed in this study (up to a factor 6-7 decrease). Other authors report that bacterial growth in drinking water is limited due to the nutrient limitation of the oligotrophic environment (Boe-Hansen et al. 2002). Both Lautenschlager et al. (2010) and Prest et al. (2013) suggest that the changes in cell densities might be caused by a combination of bacterial regrowth and biofilm detachment due to the sudden hydraulic changes. In our study, hydrants were flushed at full flow rate, thus detachment of the biofilm may have occurred (Lehtola et al. 2006, 2007). Also, decreases in disinfection residual (see s**ection IV.1.2**) may have facilitated bacterial regrowth at the hydrants. Thus, the combination of (limited) bacterial regrowth and biofilm detachment may explain the higher cell densities at 1 minute of flushing.

Furthermore, **figure 4.8** indicates that phenotypic changes in the bacterial community are related to the flush duration. This suggests that the microbial community of the bulk stagnant water (samples at 1 minute) differs from the bulk water in the network (samples at 15 and 30 minutes). Douterelo et al. (2013) evaluated the effect of different hydraulic regimes on the bacterial community in a lab-scale piping system. In their study, there was an observed difference between the bacterial biofilm community before and after flushing and significant differences were found between the microbial composition of the biofilm and the bulk water. In the present study, only bulk water samples were taken, as these are considered to be representative for the drinking water

quality at the tap. As suggested before, due the hydraulic change caused by flushing, the biofilm at the hydrant can detach and increase the cell density. Thus, the difference between the microbial communities before and after flushing may be explained as a difference between the detached biofilm (1 minute) and bulk community (30 minutes). However, this hypothesis may only be true for hydrants where a difference was observed. Hydrants NW 1, NW 2, SE 1 and SE 2 did not show differences in het microbial community before and after flushing. As differences in cell density were also attributed to bacterial regrowth, selective bacterial regrowth may have occurred and caused changes in the bacterial community.

To conclude, differences in the bacterial community are hypothesized to be attributed to on the one hand a difference between disrupted biofilm and bulk water, and on the other hand to selective bacterial regrowth.

The phenotypic alpha diversity D_2 did not significantly change in relation to the flush duration for most of the hydrants. This result is confirmed by a full-scale study performed by Douterelo et al. (2014), where no significant difference in bacterial richness and diversity was observed with an increasing hydraulic shear stress in cast iron pipes. Note that their results were obtained using sequencing, whereas the results from the present study were obtained using FCM.

To address the cause of the observed phenotypic community shift at some hydrants, a contrast analysis was performed on the pooled fingerprints of the samples at 1 and 30 minutes of flushing (**figure 4.11**). The results were obtained using SG staining. As SG is a stoichiometric stain (*i.e.* a cell with more nucleic acids will be more intensely coloured), the bivariate FL-1 versus FL-3 space of drinking water can divided into low and high nucleic acid bacteria, with the separation situated around FL-1 = 85 (Wang et al. 2009). When comparing the bivariate FCM plots at 1 and 30 minutes of flushing, a relatively higher abundance of HNA bacteria (high nucleic acid, FL-1 > 85) was observed at 1 minute of flushing, whereas LNA bacteria (low nucleic acid, FL-1 < 85) were relatively more present at 30 minutes of flushing.

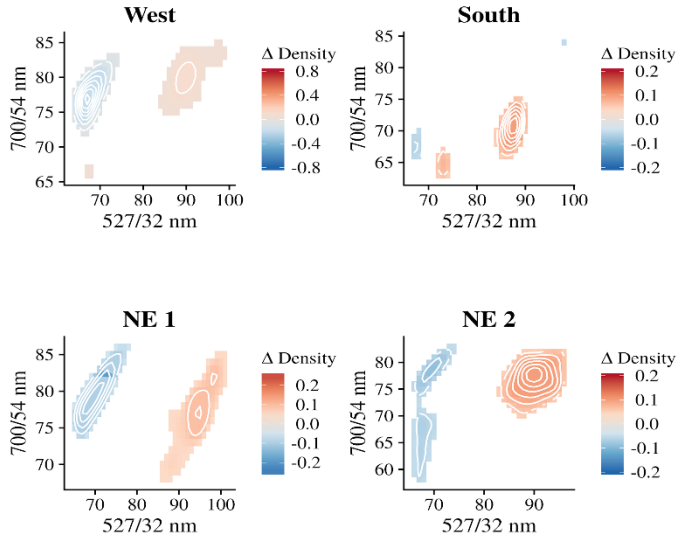

Figure 4.11 – Contrast analysis between the pooled fingerprints at 1 and 30 minutes of flushing of hydrants West, South, NE 1 and NE 2. A Δdensity > 0 (red) means a higher abundance at 1 minute of flushing, a Δdensity < 0 (blue) indicates that the abundance is higher at 30 minutes of flushing. If the difference in density between the two flush durations was lower than 0.05, no contrast value is shown.

For the hydrants where the microbial community changed in relation to the flush duration, the HNA bacteria were found to be relatively more prevalent at 1 minute of flushing, whereas the LNA bacteria were relatively more abundant in samples taken at 30 minutes of flushing. The interpretation of the distinction between LNA and HNA bacteria is not straightforward (Wang et al. 2009). Proctor et al. (2018) recently proposed that LNA bacteria share similar characteristics, such as small cell size and metabolic dependency on other bacteria. Wang et al. (2009) showed that both LNA and HNA bacteria are able to grow in an oligotrophic drinking water environment, however, the specific growth rate of HNA was observed to be higher than the specific growth rate of LNA. Thus, the observed shift in the bacterial community may be explained as growth of HNA bacteria was favoured during regrowth. This is in compliance with the results of previously performed regrowth experiments in literature, where a community shift was observed due to the selective regrowth of HNA bacteria (Prest et al. 2013; Wang et al. 2009). On the other hand, Ramseier et al. (2011) hypothesized that LNA bacteria are more resistant towards a higher disinfectant exposure than HNA. As bacterial classes that are more prevalent in the bulk phase have been shown to have a greater chlorine resistance, bulk water samples at 30 minutes of flushing may contain more LNA bacteria (Douterelo et al. 2013; McCoy et al. 2012). Thus, a second hypothesis from the obtained results may be that the disrupted part of the biofilm contains a higher relative abundance of HNA, which will increase the relative HNA abundance at 1 minute of flushing.

To conclude, flushing will result in a decrease of bacterial cell density at most hydrants. The phenotypic alpha diversity of most hydrants did however not change in relation to the flush duration. For some hydrants, the phenotypic structure of the microbial community differed before and after flushing, which was explained by an increase of the HNA bacteria fraction. A relative increase of the HNA bacteria before flushing may be attributed to a combination of selective (faster) regrowth of HNA bacteria and biofilm detachment. Hereby, it is hypothesized that the detached biofilm community would contain a higher relative HNA abundance than the bulk community. Both processes are believed to cause changes in the microbial community at some hydrants.

Effect of additional flushing

Because of the consistently low chlorine concentrations, compared to the production plant, measured at some of the hydrants during the sampling campaign, it was decided to flush two of the hydrants more frequently to improve chlorine residual (**table 4.1**).

Table 4.1 – Details of additionally flushing during the DC Water summer sampling campaign. Hydrant NW 2 was additionally flushed 2 times a day, but this was after two weeks raised to 3 times a day. Hydrant SE 2 was not flushed on Sundays because it is located next to a church. "Week" refers to the number of weeks after the start of the sampling campaign, starting from June 26th (week 1). The flush duration was 45 to 60 minutes.

Hydrant	Date installed	Week	Flushing frequency	Days of operation
NW 2	08/08/2017	7	2 times a day	7 days per week
	22/08/2017	9	3 times a day	7 days per week
SE 2	16/08/2017	8	3 times a day	Monday- Saturday

The effect of additional flushing was evaluated on three levels: the total chlorine concentration (since this is the criterion used by DC Water), the total cell density and the phenotypic alpha diversity D_2 (**figure 4.12**).

Additional flushing did not increase the total chlorine concentration at both hydrants (**figure 4.12, bottom**). Total cell density and D_2 showed a drop around week eight for hydrant SE 2, however, both parameters increased again. For NW 2, no decrease was observed in the total cell density, even after flushing three times a day. D_2 decreased, however, increased again after four weeks.

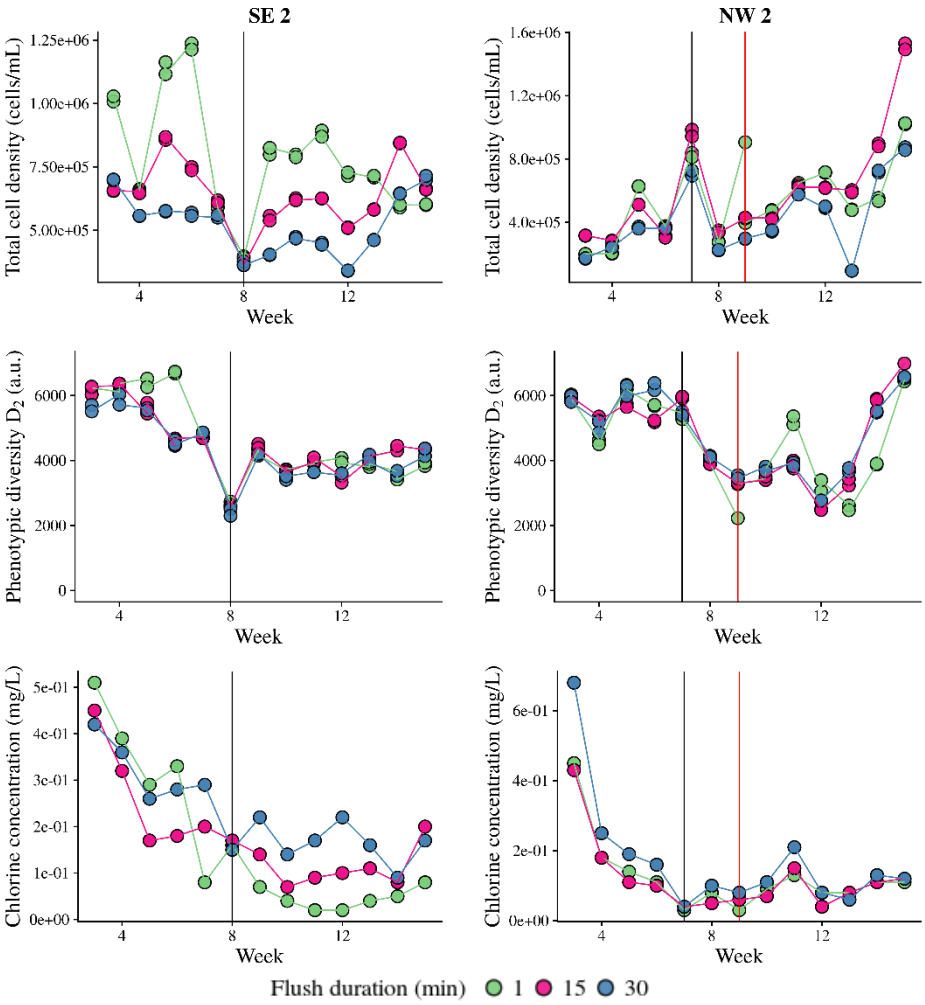

Figure 4.12 – Total cell density, phenotypic alpha diversity D_2 and chlorine concentration over time for hydrants SE 2 and NW 2, coloured according to flush duration. SE 2, black line: start of additional flushing campaign, NW 2, black line: start of flushing two times a day, red line: increasing to three times a day.

These results indicate that additional flushing has no effect on the chlorine concentration nor on the bacterial cell counts. The potential effect on D_2 and cell density is not clear. The decreasing trend in both parameters may be coincidental, as for hydrant SE 2 the decrease was already noticed in week 7, and at hydrant NW 2 the D_2 and cell counts increased back to the same level near the end of the sampling period. At both hydrants, the water age is high (SE 2 = 90h, NW 2 = 100h, **table 3.4**). As the hydrants are flushed every 4 to 6 hours, the elevated cell densities may be caused by biofilm disruption instead of bacterial regrowth, since the time that the water is stagnant is so limited because of the high flushing frequency. However, additional flushing does not seem to completely remove the biofilm from the pipe wall, as the measured cell densities are not clearly changing. This corresponds with the results from a study performed by Douterelo et al. (2013), where increased hydraulic changes were not able to remove biofilms from the piping. Also, Manuel et al. (2007) found that the daily flushing regime (flow rate) is critical for the development of the biofilm. In their study, hydraulic changes, were not able to remove the biofilms.

Practically, this implies that flushing for up to 60 minutes, even multiple times a week, is not sufficient to improve the chlorine residual and to clearly affect the cell counts and phenotypic diversity of the microbial community at both hydrants. Thus, flushing for a longer time may "refresh" the water, and increase the monochloramine residual concentration. As monochloramine in particular is very effective at penetrating biofilms, an increased residual could decrease the biofilm formation at the dead ends (Lee et al. 2018, 2011). The evaluation of the long-term effect of flushing for a considerably longer time on the drinking water quality may be of additional value from both an academic and industrial point of view.

1.4 RQ 3: What is the seasonal effect on the drinking water bacterial community?

As the monitoring campaign continued for 15 weeks (June 26th – October 5th), long-term changes in the bacterial community were evaluated. For all hydrants, there was a significant difference between phenotypic fingerprints of different weeks. A trend over time was observed in the PCoA profile of hydrants SE 1, SE 2, NW 1 and NW 2 in function of the monitoring week (**figure 4.13**).

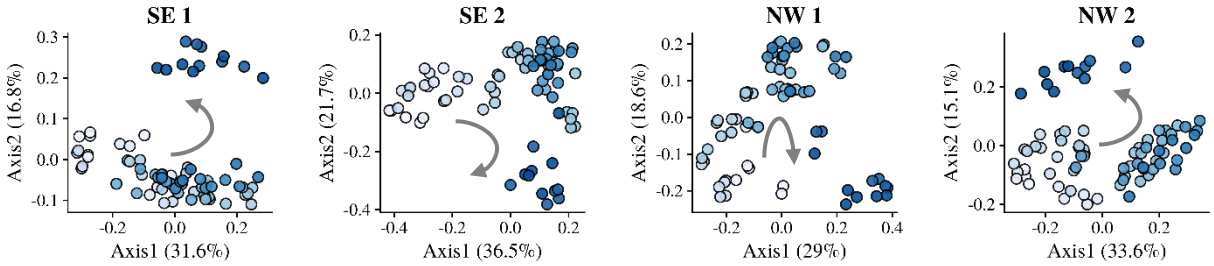

Figure 4.13 – PCoA ordination of the phenotypic fingerprints for every hydrant, coloured by "week", starting from July 10th (white) until October 2nd (dark blue). The arrows indicate that the phenotypic community structure gradually changes in function of the week number.

The results indicate that changes in the bacterial community in the drinking water are related to changes over time. As Pinto et al. (2014) indicated, the water temperature may induce seasonal changes in the drinking water community. The temperature was the main (measured) physicochemical parameter that clearly changed over time (**figure A7.4** in appendix). Therefore, the water temperature is evaluated as a potential factor that influences the community dynamics over time. The water temperature decreased over the course of the monitoring campaign with around 4°C (r_p = -0.77, p < 0.001). Nescerecka et al. (2018) performed a long-term FCM monitoring campaign on a full-scale DWDS with a surface water source. They observed that the fluctuations in temperature were closely related to fluctuations in cell density. This was not observed in the present study (**figure A7.5, A7.6** in appendix). However, their study was performed over the course of one year, whereas only 15 weeks were monitored in the present study. It is therefore suggested that the timespan of the present study is too short to reflect seasonal changes in the bacterial abundance. The water age of the sampling points from Nescerecka et al. (2018)

varied between 32 and 50 hours, which is lower than the water ages at the hydrants that were sampled in this study (**table 3.4**). It is hypothesized that in the present study, the increased cell densities are believed to result from regrowth, which is facilitated by the long water ages. Consequently, temperature fluctuations may be less reflected in changing cell densities.

Although there was no clear relationship between the population density and the water temperature, the microbial community was observed to change in function of the monitoring week. Pinto et al. (2014) performed a 15-month monitoring campaign on a full-scale DWDS. They observed that the microbial community changed over time, with a yearly recurring pattern. Moreover, they noted that during summer, the water temperature was the main physicochemical parameter that influenced the microbial community structure.

To conclude, seasonal fluctuations had a significant effect on the phenotypic structure of the bacterial community at all hydrants. This may be related to changes in temperature. It is however not the explaining factor for the discrimination of all of the hydrants. For some hydrants, samples are rather separated based on the flush duration than due to seasonal changes. Pinto et al. (2014) showed that samples taken at one year apart were clustered together. To extend the knowledge about such recurring patterns, further monitoring over a period of at least one year would be of added value. Note that other water constituents besides temperature, such as the TOC concentration of the surface water source, may possibly induce changes in the bacterial community over time.

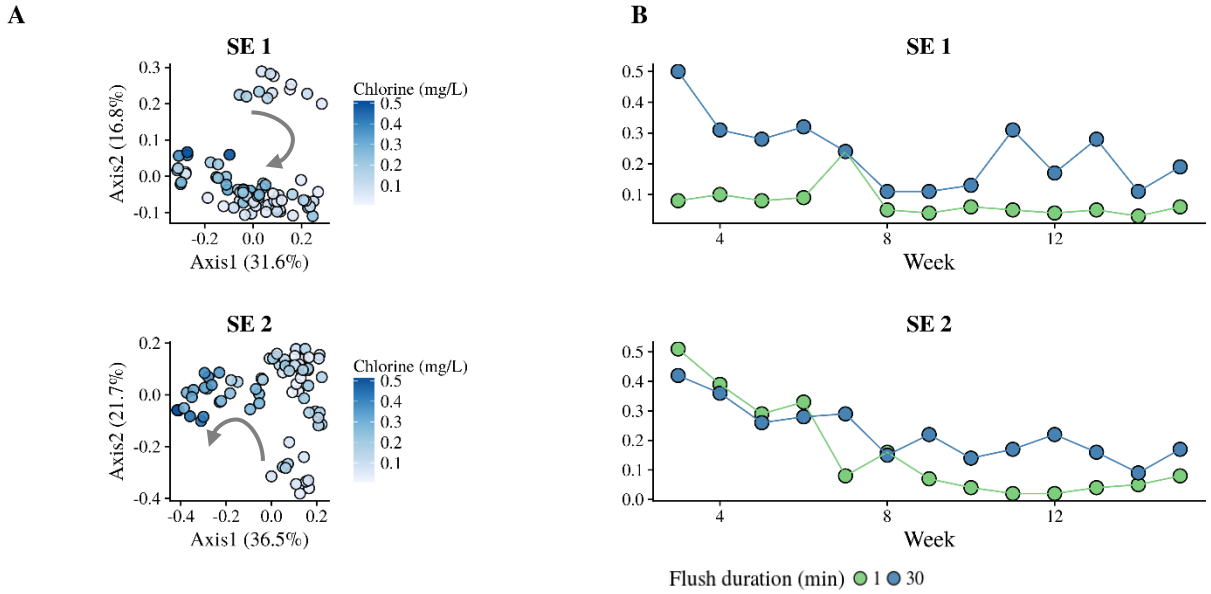

Figure 4.14 – (**A**) PcoA ordination of the phenotypic fingerprints of hydrants SE 1 and SE 2, coloured by chlorine concentration (left). (**B**) Total chlorine concentration (mg/L) for hydrants SE 1 and SE 2 over time (right). The grey arrow indicates the cyclic change of the phenotypic fingerprints with increasing chlorine concentration.

Furthermore, as previously discussed, for hydrants SE 1 and SE 2 the opposite of the time-wise gradient was seen, according to the chlorine concentration (**figure 4.14, left**). This is, however, linked to the seasonal gradient since for both hydrants, the chlorine concentration decreased over time (**figure 4.14, right**). This trend (and also the gradient) is more abundant at hydrant SE 2. Thus, the changes in chlorine concentration are believed to be only a partial contribution to the temporal effect on the phenotypic fingerprint. Seasonal fluctuations are therefore considered as a possibly more holistic explanation of the gradient in the phenotypic fingerprint of the bacterial community. Practically this means, as McCoy et al. (2012) suggest, that drinking water quality should be evaluated through a combination of variables, *i.e.* chlorine concentration, water temperature and the deviation of the phenotypic community structure of the seasonal baseline, which should be determined in yearly monitoring campaign.

Additionally, the Bray-Curtis dissimilarity was calculated between different weeks for each hydrant. Since temporal fluctuations were significant for all hydrants separately (results not included), the Bray-Curtis dissimilarity matrix for all of the hydrants together, pooled by week, was calculated and visualized as a heat map (**figure 4.15**). A "separation" of the fingerprints can be drawn after week nine (August 22nd), somewhat in the middle of the summer sampling campaign. Phenotypic fingerprints before and after week nine differ clearly.

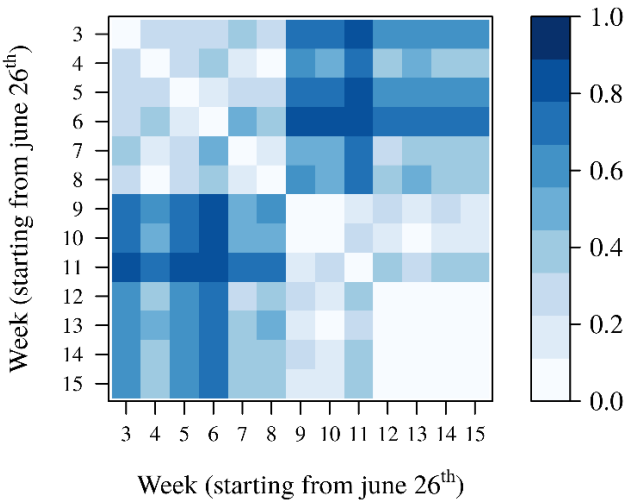

Figure 4.15 – Bray-Curtis dissimilarity matrix for all the sampling hydrants over time. Red: similar phenotypic fingerprints, yellow: different phenotypic fingerprints. FCM measurements started at week three, counting from June 26th (week 1). Only the samples taken after 1 minute of flushing were taken into account, as these are assumed to be representative for the stagnant water in the hydrants.

The gradient that is observed in the Bray-Curtis dissimilarity matrix confirms the previously proposed hypothesis that seasonal influences will cause changes in the bacterial community. The "separation" after week nine was not explained by a temperature change, nor was it caused by additional flushing. It may be caused by a change in the production process, however this could not be confirmed by DC Water.

1.5 RQ 4: What is the influence of the water age on the drinking water bacterial community?

DC Water provided model estimations of the water age at the hydrants (**table 3.4**). The water age is defined as the time (h) for water to travel from the respective reservoir to the hydrant. The average water age was used as a rough estimation of the true water age at the hydrants. The influence of the water age on the chemical composition of the water has been previously discussed (**section IV.1.1**). To evaluate the effect of the water age on the bacterial community, the Bray-Curtis dissimilarity between samples taken at 1 and 30 minutes of flushing was plotted in function of the average water age (**figure 4.16**). This way, the relative effect of flushing on the bacterial community is shown in function of the water age. There is a moderate negative linear correlation ($r_p = -0.62$, $p < 0.05$) between the Bray-Curtis dissimilarity and the average water age.

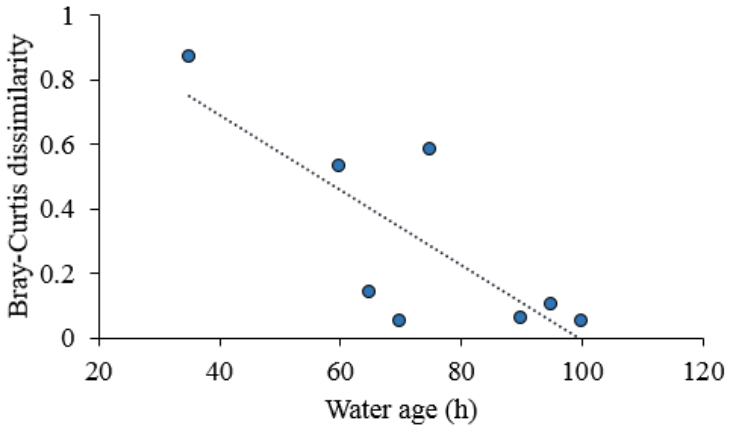

Figure 4.16 – Bray-Curtis dissimilarity in function of the average water age for all of the sampling hydrants. The Bray-Curtis dissimilarity is the dissimilarity between the bacterial communities at 1 and 30 minutes of flushing.

These results indicate that water age has an overall moderate effect on the size of the change in phenotypic fingerprints between 1 and 30 minutes of flushing. In literature, a "short" water age is defined as a water age shorter than three days (72h) (EPA, 2002). Four hydrants are comprised in this category: West, South, NE 1 and NW 1. Hydrants NE 2, NW 2, SE 1 and SE 2 are defined as long water age hydrants. A pronounced effect of flushing was observed at the short water age hydrants (exception for NW 1) and NE 2. The effect of flushing on the bacterial community can be interpreted as a spatial effect, *i.e.* location-dependent, since it shows how much the community has differed from the water community upstream in the pipeline. The seasonal effect was seen at long water age hydrants (without NE 2) and NW 1. Pinto et al. (2014) examined temporal and spatial effects on the bacterial community in a full-scale DWDS. In their results (average HRT between 2h and 7h), the seasonal effects dominated the spatial (*i.e.* location-dependent) effects on the drinking water community. However, they suggest that it is unlikely that annual effects would always dominate spatial DWDS influences. They suggested to monitor the drinking water quality

in a high resolution to get a better insight in the contribution of spatial and temporal effects on the bacterial community. The present study is therefore a valuable addition to their research, as both effects have been detected at the sampling hydrants on a phenotypic level. However, the present study showed that the water age is a more decisive factor than the exact geographical location (*e.g.* South and SE 2 are both far away from the production plant, but are subjected to different effects due to their difference in water age, **figure 3.1**). In other words, water age instead of the exact geographical location will determine to what extent both spatial and temporal effects will affect the microbial community.

To conclude, seasonal changes will have an influence on the changes in phenotypic fingerprint for all of the hydrants. However, this effect will be dominated by the effect of flushing at (in general) low water age hydrants (NE 1, South and West). For most of the high water age hydrants (SE 1, SE 2, NW 2), the changes in phenotypic fingerprint are solely explained through the temporal effects. Thus, the bacterial community is steered by the flush duration or the seasonal effect, depending on the water age at the hydrant. The water age plays an important indirect role in the explanation of the changes in the bacterial community.

Practically, this means that flushing for 30 minutes will be effective at short water age hydrants to restore the drinking water quality. For long water age hydrants, 30 minutes of flushing is not sufficient. To save time and water, the necessary flush duration can be determined for each hydrant separately by monitoring the chlorine concentration (standard measurement), total cell counts (FCM) and the beta diversity (FCM).

1.6 RQ 5: What is the influence of the iron concentration on the drinking water bacterial community?

Since elevated iron concentrations at 1 minute of flushing were observed at hydrants South and NE 2, the effect of iron on the drinking water bacterial community is evaluated (**figure 4.17**). Furthermore, the samples taken at 1 minute showed an elevated cell density when compared to samples taken at 30 minutes for both of these hydrants (**figure 4.7**). Note that cell densities in the same range as hydrant NE 2 were observed at the other hydrants, however, the difference between 1 and 30 minutes of flushing was never that remarkable as for hydrants South and NE 2.

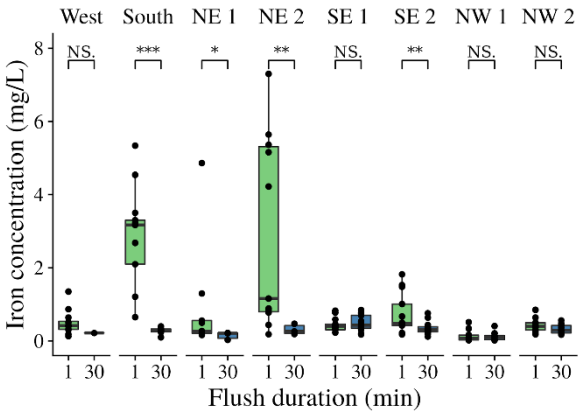

Figure 4.17 – Effect of flushing (1 minute versus 30 minutes of flushing) on the iron concentration for every sampling hydrant. Significance of the differences between flush durations for each hydrant was evaluated using the Wilcoxon Rank Sum test, significance is marked as "***" < 0.001 < "**" < 0.01 < "*" < 0.05 < "NS.".

The bacterial cell density was subsequently evaluated in function of the total iron concentration. A strong monotonically increasing relation between the bacterial cell density and the total iron concentration was observed ($r_s = 0.64$, $p < 0.001$) (**figure 4.18, A**). As only a small fraction of the samples contained an elevated iron concentration (*e.g.* 11% > 1mg/L), the samples containing less than 1mg/L iron were additionally evaluated in detail (**figure 4.18, B**). For those samples, a significant linear correlation of iron with the total cell density was observed ($r_p = 0.65$, $p < 0.001$).

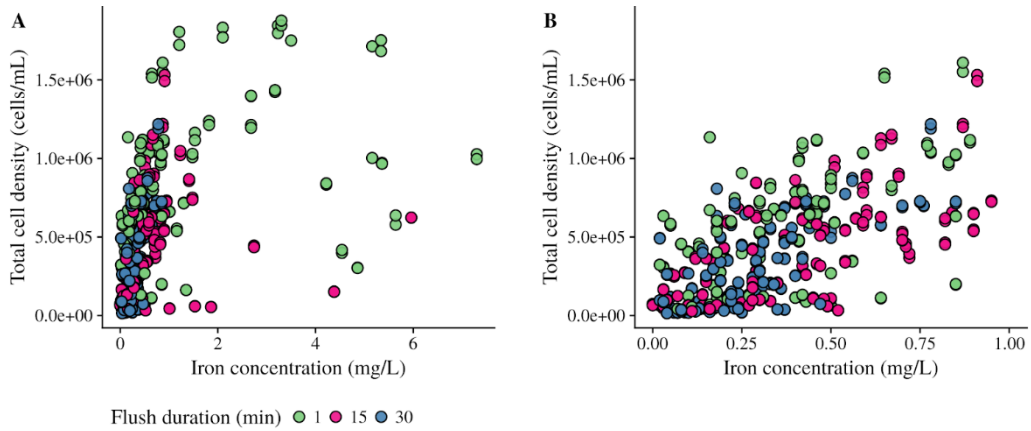

Figure 4.18 - Total cell density (cells/mL) in function of the total iron concentration for all of the sampling hydrants, coloured according to flush duration for (**A**) all samples and (**B**) samples containing less than 1mg/L iron. Most of the high iron samples were taken at 1 minute of flushing.

These results indicate that iron may be directly related to the total cell density at lower concentrations, whereas the relationship between iron and the total cell density is less clear at higher iron concentrations. In low concentrations, iron may promote bacterial growth as it serves as a micronutrient for bacteria, *e.g.* as cofactor in enzyme activity (Lankford & Byers 1973). Thus, at lower iron concentrations (< 1mg/L), iron may be used as a nutrient by the bacteria and consequently directly increase the bacterial abundance.

Higher iron concentrations (> 1mg/L) may indicate the presence of severely corroded cast iron piping. No direct influence of iron on the bacterial abundance was observed, however, a significant

monotonous relation was noted. These results imply that that iron does not directly serve as a rate-limiting nutrient for bacterial growth at higher concentrations. In a model study performed by Frateur et al. (1999), it was concluded that chlorine species can oxidize ferrous iron (Fe^{2+}), generated through corrosion, to ferric iron (Fe^{3+}), thus resulting in a chemical chlorine residual decay. As a consequence, the barrier against bacterial growth near the pipe wall will decline and the total cell density in the biofilm will increase (Clark & Haught 2005; Morton et al. 2005). Besides that, the biofilm can be protected from disinfectant residual and shear stress by corrosion pipe scales (Makris et al. 2014). Note that only bulk water samples were taken during the sampling campaign, so no conclusions about the biofilm can be drawn from this study. Furthermore, phosphorus present in the iron alloy may be leached from the piping during corrosion and consequently be used as a nutrient by bacteria (Morton et al. 2005). A correlation between iron and both phosphorous and residual chlorine was observed, which may confirm the proposed hypothesis (r_s(Fe,P) = 0.44, $p < 0.001$, r_s(Fe,Cl) = -0.43, $p < 0.001$).

To conclude, iron will directly influence bacterial growth at low (< 1mg/L) concentrations, and indirectly at high (> 1mg/L) concentrations. A remark that should be made is that the total iron was measured during sampling, however, only a fraction of the total iron concentration is readily available for microorganisms. This may explain the variability of the results obtained in the present study. For future research on the effect of iron on the bacterial abundance, it is therefore suggested to also measure the dissolved iron fraction, as this is a better estimation of the bioavailable iron fraction.

Besides affecting the bacterial abundance, iron could stimulate the growth of selective species (*e.g.* microbial induced corrosion by iron-oxidizing bacteria), and thus cause changes in the diversity of the bacterial community. Therefore, the phenotypic alpha diversity D_2 was evaluated in function of the iron concentration (**figure 4.19**). D_2 showed a monotonically increasing trend in function of the total iron concentration ($r_s = 0.55$, $p < 0.001$) (**figure 4.19, A**). As only a small fraction of the samples contained an elevated iron concentration, the samples containing less than 1 mg/L iron were additionally evaluated in detail (**figure 4.19, B**). For those samples, a significant linearly increasing correlation of iron with D_2 was observed ($r_p = 0.57$, $p < 0.001$).

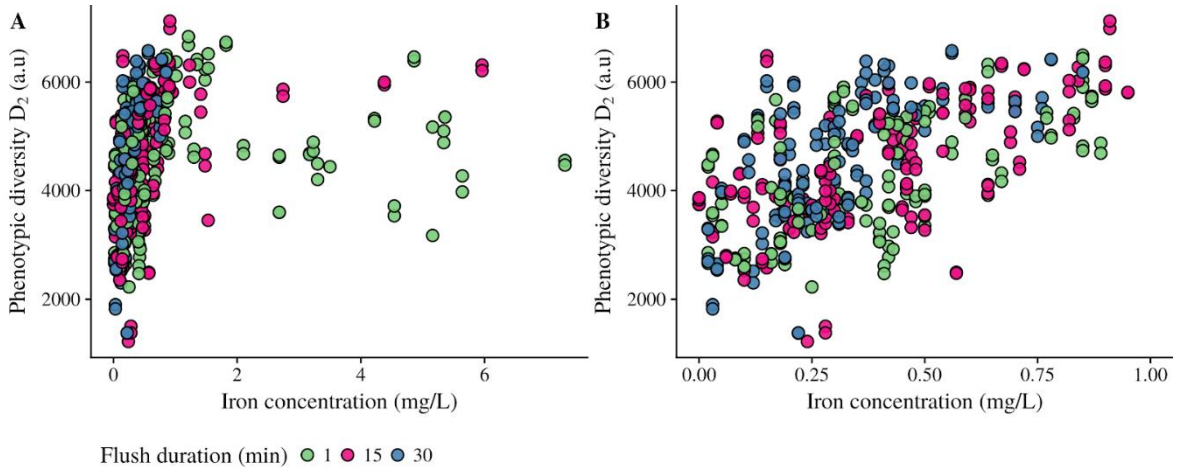

Figure 4.19 – Phenotypic alpha diversity D_2 in function of the iron concentration for all of the sampling hydrants, coloured according to flush duration for (**A**) all samples and (**B**) samples containing less than 1 mg/L iron.

To evaluate differences between the phenotypic fingerprints caused by a change in iron concentration, the beta diversity was evaluated using the Bray-Curtis dissimilarity and visualized using PCoA. Differences between fingerprints of hydrant South and NE 2 were not explained by a change in iron concentration (**figure 4.20**). For all of the other hydrants, differences were not mainly explained by a change in the total iron concentration either (**figure A7.7** in appendix).

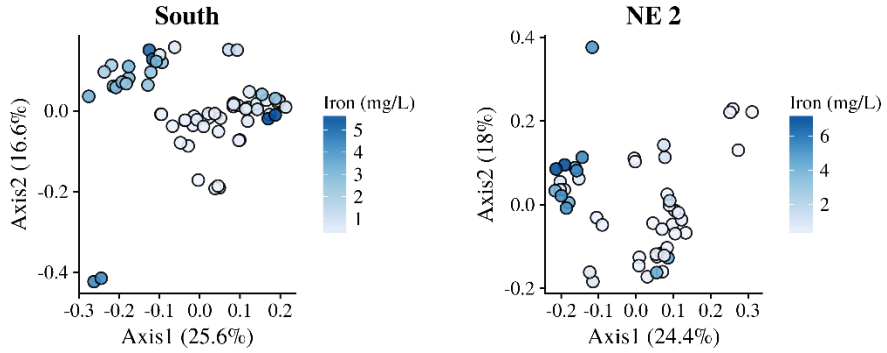

Figure 4.20 – PcoA ordination of the phenotypic fingerprints of hydrants South and NE 2, coloured according to the total iron concentration.

For low iron concentrations (< 1mg/L), the phenotypic alpha diversity increased in function of the total iron concentration. This indicates that the bacterial community will become more phenotypically diverse with an increasing iron concentration, next to a previously discussed overall increase in bacterial abundance. At higher iron concentrations (> 1mg/L), the relationship of D_2 with the iron concentration was less clear due to the high variability of the data. Furthermore, the phenotypic fingerprints did not differ clearly in function of the total iron concentration. These results imply that at higher concentrations elevated iron levels may not be directly influencing growth or diversity of the bacterial community. In **section IV.1.3**, the contrast analysis of both high-iron hydrants revealed that flushing caused changes in the bacterial community (**figure 4.11**). This was hypothesized to be the result of relatively more regrowth of HNA bacteria and their

higher abundance in the detached biofilm, resulting at a relatively higher HNA bacteria abundance at 1 minute of flushing compared to 30 minutes of flushing. These results indicate that selective regrowth is occurring, which may be attributed to the growth of iron-oxidizing bacteria at elevated iron hydrants. However, the impact on the phenotypic community structure was limited.

To conclude, the changes in the phenotypic beta diversity were not clearly directly related to iron concentration. However, for both high-iron hydrants, the bacterial community at 1 minute of flushing was phenotypically different from the community at 30 minutes of flushing. This was previously attributed to selective regrowth. Taking into account the results from the current analysis, the selective regrowth may indicate presence of iron-oxidizing bacteria and may suggest that more active (HNA) bacteria are responsible for the corrosion of the cast iron piping and the related higher iron concentrations. Nevertheless, the impact of iron on the phenotypic community structure was limited. For both hydrant South and NE 2, the differences in phenotypic fingerprints were rather influenced by the total disinfectant residual concentration and, from a possibly more holistic point of view, the flush duration. Remark that for both hydrants, as previously discussed, flushing induces significant changes in both the chlorine and iron concentration. The bacterial community shift may thus be attributed to a combined effect of both parameters (LeChevallier 1999; Masters et al. 2015; Westbrook & Digiano 2009).

1.7 Nitrification

Since monochloramine is used as secondary disinfectant in the distribution system of DC Water, ammonia is provided as a nutrient to the system. Therefore, nitrification may be taking place at the dead ends of the system. The water temperature during the sampling campaign was 25.6 ± 1.8 °C. Additionally, the water ages are high at the sampled hydrants. At some hydrants, the average water age exceeds 72 hours (**table 3.4**). These conditions are thus ideal for slow-growing nitrifying bacteria. Furthermore, nitrification typically lowers the pH due to the generation of protons. The lower pH at 1 minute of flushing (see **section IV.1.1**) could indicate that nitrification is indeed present.

To evaluate the occurrence of nitrification at the hydrants, the first sample (1 minute of flushing) is considered to be representative for the stagnant water pile in the dead end hydrant, whereas the sample taken at 30 minutes is considered to be representative for the "bulk water" in the pipeline. The NO_x production (*i.e.* NO_2^- + NO_3^- concentration at 1 minute of flushing minus the NO_2^- + NO_3^- concentration at 30 minutes of flushing) was taken as proxy for nitrification (**figure 4.21, A**). The total ammonia nitrogen (TAN) consumption (*i.e.* NH_4^+ + NH_3 concentration at 30 minutes of

flushing minus the $NH_4^+ + NH_3$ concentration at 1 minute of flushing) was calculated as cross-validation (**figure 4.21, B**).

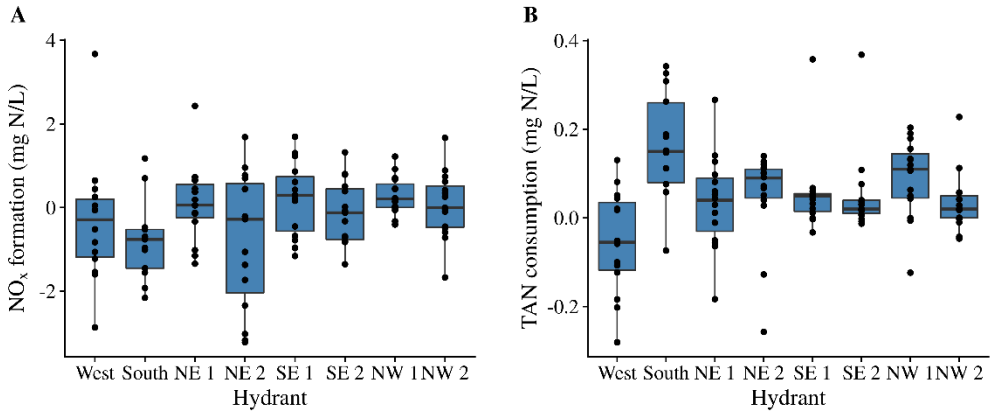

Figure 4.21 – (**A**) NO_x production. Negative values indicate that the NO_x concentration was higher at 30 minutes of flushing. (**B**) TAN formation. Negative values indicate that the TAN concentration was higher at 1 minute of flushing.

No correlation was observed between the NO_x production and the TAN consumption (r_p = -0.05, $p > 0.1$). Furthermore, the NO_x production and the TAN consumption followed irregular patterns over time (**figure A7.8, A7.9** in appendix), with rapidly disappearing peaks. The pH was not correlated to the NO_x production nor the TAN consumption (NO_x: $r_p = 0.06$, $p > 0.1$, TAN: $r_p = -0.25$, $p < 0.01$).

From these results, it may be suggested that inconsistent nitrification is taking place. However, the NO_x production was not related to the TAN consumption nor the pH. Both nitrite and nitrate concentrations are very variable (NO_2^-: 0.16 ± 0.12mg N/L, NO_3^-: 2.14 ± 0.87mg N/L). Besides, the used method for nitrate measurements is very susceptible to interference *e.g.* by iron. As nitrate contributes for the most part (86% on average) to the NO_x production, changes in its concentration have a big impact on the calculated NO_x production. Also, no data of nitrite and nitrate concentrations at the entrance of the distribution network was provided. From these uncertainties, it is hard to interpret the data and draw conclusions. Fluctuations in the NO_x production may therefore be caused by fluctuations in the incoming water or measurement errors, rather than nitrification activity during stagnation. Furthermore, the maximum contaminant level for nitrate and nitrite are resp. 10 and 1mg N/L in the USA (US EPA 2004a). The measured concentrations are situated below this level, thus not posing a risk to human health.

As it was not possible to draw conclusions concerning nitrification in the DWDS, drinking water samples were enriched and nitrifying activity was studied in the controlled lab environment. The experimental setup, results and brief discussion are described in **appendix 3**. From these results, the growth rate of the autotrophic AOB and their initial concentration in the water were determined, and were found to be similar for all hydrants (μ_{max} = 0.86 ± 0.11d^{-1}, $X_{o,AOB}$ = 0.03 ±

0.02mg COD/L). These results indicate that, even if the effects of nitrification were not observed, nitrifying bacteria may be present and be significantly active.

To control nitrifying activity, the application of zinc as a possible inhibitor was evaluated in a preliminary experiment. Zinc was chosen as it does not harm public health in low concentrations, and was previously demonstrated to show significant nitrification inhibition in wastewater and drinking water treatment applications (Grunditz et al. 1998; Sarker et al. 2018; Zhang & Edwards 2010). The experimental setup, results and brief discussion are described in **appendix 4**. In the USA, a secondary (non-enforceable) standard is determined at 5mg/L zinc, as it may cause a metallic taste (US EPA 2004b). In Flanders, the drinking water limit for zinc is also 5mg/L (Koninklijk besluit 2002). The obtained results were relatively variable, however, if one wants to apply zinc as a nitrification inhibitor in drinking water, it seems that higher concentrations than 3mg Zn/L need to be applied. This is in contrast with previously performed research, where zinc inhibition of nitrification in drinking water was observed at doses > 0.1mg/L (Zhang & Edwards 2010).

To conclude, the performed measurements are not a sufficient basis for reliable conclusions concerning nitrification in the DC Water drinking water network. However, the NO_x measurements did not imply public health risks. Nevertheless, it remains important to follow up nitrate and nitrite concentrations, especially in summer, as nitrifying bacteria may be present and be significantly active. As a preliminary experiment indicated that zinc could be used as a nitrification inhibitor in drinking water at concentrations >3mg/L, more research towards the effect of zinc on nitrification is necessary to understand and control nitrification in drinking water distribution systems.

2. FARYS water tower Kattenberg (Gent)

As described in **section III**, the water tower Kattenberg in Gent receives two types of drinking water produced from resp. groundwater coming from Brakel, and surface water coming from Buggenhout. Therefore, this water tower is an excellent location to examine the effect of mixing different types of water by flow cytometric monitoring. In **figure 4.22** both of the incoming feeders can be seen on the left side. "Elst" is drinking water produced from groundwater coming from Brakel. This drinking water stream will further be referred to as "groundwater". "Ukkel" is drinking water produced from surface water coming from Buggenhout, which will be referred to as "surface water". The tower complex has a total buffering capacity of 6,500 m³ (two smaller towers of 1,000 m³ each, a larger tower of 2,000 m³ and a buffering tank of 1,500 m³). On a monthly basis, 105,717 m³ groundwater and 316,159 m³ surface water entered the tower, meaning a respectively average intake of 3,524 m³/d groundwater and 10,539 m³/d surface water. Based on this average daily intake, the mixture consists of about 75% of drinking water produced from surface water. The water is distributed to the end customers by two outgoing distribution pipes, referred to as "Distributie 1" and "Distributie 2" (on the right on **figure 4.22**).

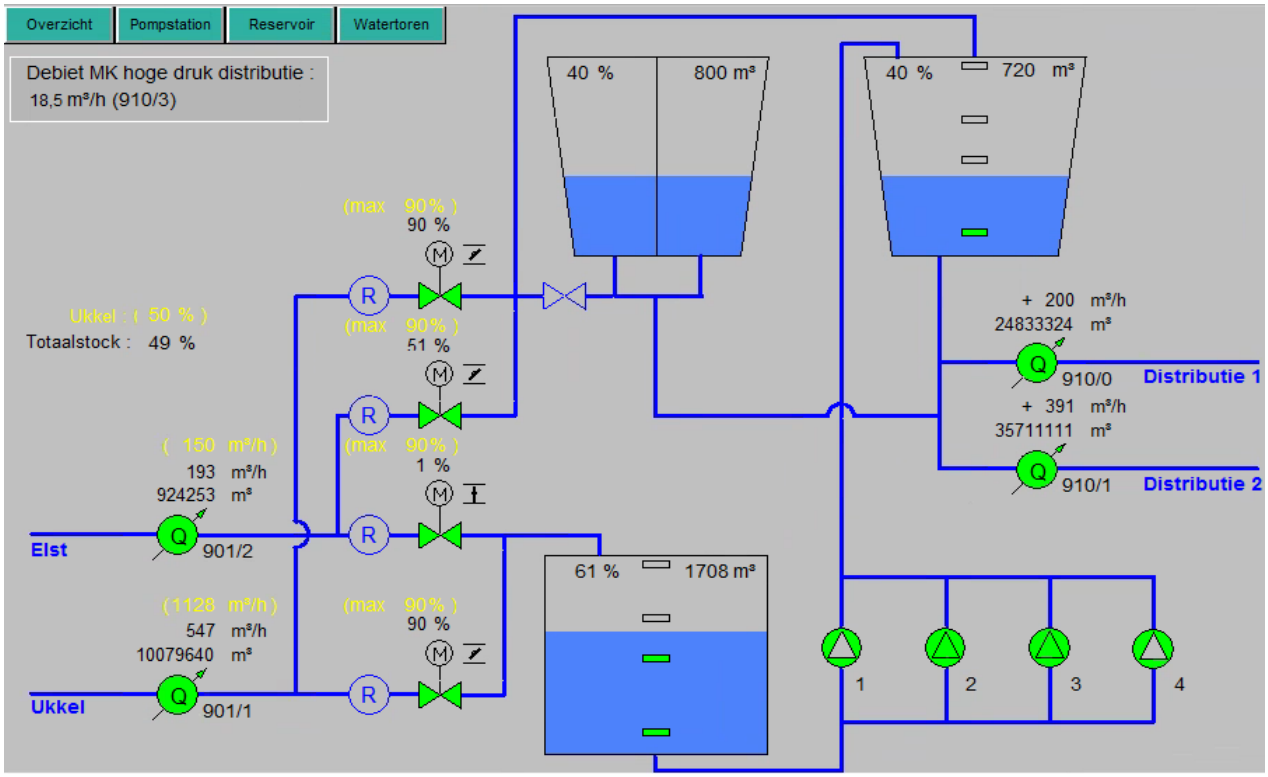

Figure 4.22 – SCADA overview of the FARYS water tower Kattenberg, consisting out of the three reservoirs. The incoming waters originate from "Ukkel" (*i.e.* "surface water" from production centre in Buggenhout) and "Elst" (*i.e.* "groundwater" from production centre in Brakel) on the left of the SCADA. The exiting water is distributed through two pipes, "Distributie 1" and "Distributie 2" on the right.

2.1 Online monitoring

The goal of the experiment was to evaluate to what extent flow cytometry can be used as an online tool to follow up the drinking water quality, and in drinking water distribution management. Based on online flow measurements, the hydraulic retention time (HRT) was calculated in this specific period and listed below (**table 4.2**).

Table 4.2 – Estimation of the HRT of the water tower Kattenberg based on the incoming and outgoing flows.

	HRT (h)	**"Groundwater" in (m^3/h)**	**"Surface water" in (m^3/h)**	**Exit (m^3/h)**
Max.	18.79	400	835	1236
Min.	2.90	88	68	193
Avg.	6.53	150.18	502.83	637.12
S_D	3.27	38.53	180.83	229.74

During the monitoring period, three events related to maintenance in the network occurred. On April 24th, the main feeder coming from Brakel was closed, meaning that the feed could be considered as nearly only "surface water" entering the tower between 07:34 and 23:19. The main feeder delivering "surface water" from Buggenhout was closed on April 26th, between 09:06 and 15:29, and on April 27th, between 09:13 and 12:30, meaning that only "groundwater" entered the tower. The periods with nearly 100% "surface water" and 100% "groundwater" are respectively highlighted in red and green in the figures below.

The outgoing flow over time showed a recurring pattern (**figure 4.23**). The pattern was diurnal (*i.e.* high during the day and low overnight) and in function of the water demand. Remark that the outgoing flow was not affected during works on the upstream main feeders (**figure 4.23**, red and green highlights).

The total cell density over time is given in **figure 4.24**. The cell density of the incoming water produced from groundwater was constant over time. It was lower ($3.1 \pm 0.8 * 10^3$cells/mL) than the cell density of the water produced from surface water ($1.9 \pm 0.3 * 10^4$cells/mL). The cell density of the outgoing water was higher than the cell density of the incoming waters ($2.9 \pm 0.7 * 10^4$cells/mL). The water main works on April 24th caused a change in feed water composition (nearly 100% surface water origin), and resulted in the highest cell densities measured during the monitoring campaign (**figure 4.24,** red highlight). Due to the works on April 26th and April 27th, all of the incoming water was produced from groundwater. This resulted in a decrease of the cell density of the exiting water (**figure 4.24,** green highlight). Remark that the cell density of the incoming water

produced from surface water dropped during these periods as well, as "groundwater" was entering the tower through both feeders.

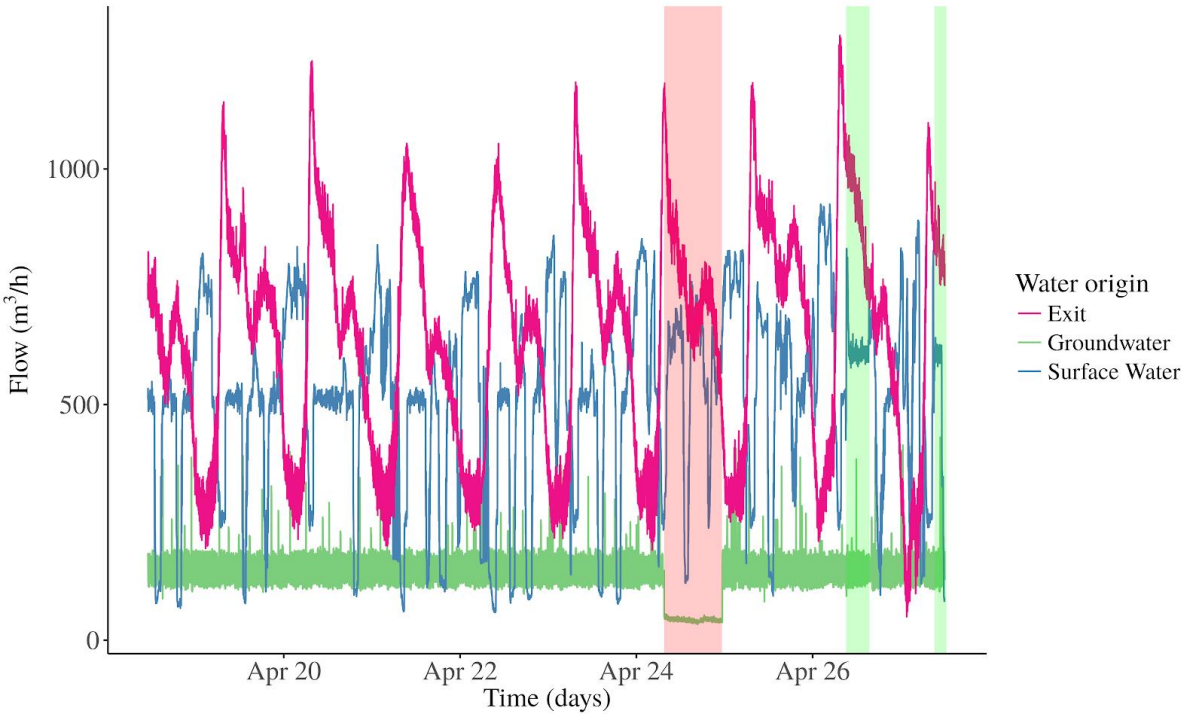

Figure 4.23 – Flow of incoming and outgoing streams of the water tower Kattenberg from April 18th until April 27th. The periods with drinking water produced from nearly 100% surface water and 100% groundwater are respectively highlighted in red and green.

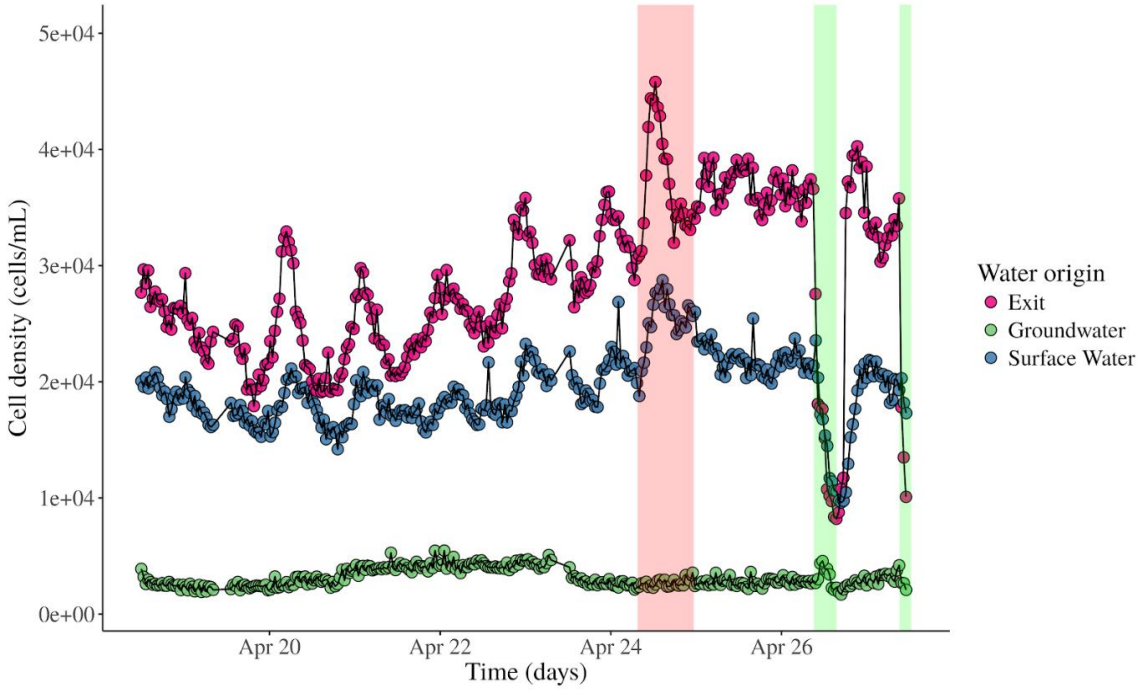

Figure 4.24 – Cell density over time of the incoming and outgoing water streams of the water tower Kattenberg. The periods with drinking water produced from nearly 100% surface water and 100% groundwater are respectively highlighted in red and green.

The results indicate a difference in cell density between drinking water produced from groundwater and surface water. This difference may be attributed to the difference in nutrient concentration, mainly total organic carbon (TOC) (**table 4.3**). Organic carbon is considered as the main limiting nutrient for microbial growth in drinking water (Liu et al. 2002). In literature, low bacterial cell concentrations (factor 10-100 lower) in groundwater are attributed to the lower nutrient concentration, with lower organic carbon concentrations in particular (Hofmann & Griebler 2018; Prest et al. 2016). More detailed variations of the non-purgeable organic carbon (NPOC) concentration of the incoming and outgoing streams are shown in **appendix 5** and **table 4.3**. The intervention on April 24th, resulting in a feed of nearly 100% surface water, was reflected in a short increase of the cell density of the exiting water. On the contrary, the switch to 100% groundwater was clearly observed as a decrease of the cell density. This may be due to the switch from 25% to 100% of incoming "groundwater", that is more drastic than switching from 75% to nearly 100% of "surface water".

Table 4.3 – NPOC concentration of the incoming and outgoing streams of the water tower Kattenberg. The data was provided by FARYS. More information can be found in **appendix 5**.

Stream	**NPOC concentration Kattenberg (mg/L)**
Incoming "groundwater"	0.8
Incoming "surface water"	2.0
Exit	1.4

Furthermore, the outgoing water had a higher cell density than both incoming water streams. This indicates that bacterial regrowth is occurring in the water tower. As both incoming water streams have a different nutrient composition (*e.g.* higher TOC in "surface water"), the mixed water is hypothesized to contain a more balanced nutrient composition and thus facilitate bacterial regrowth. Previous research showed that added nutrient mixtures with increased carbon concentration caused increased bacterial regrowth, even in demineralized water (Vermijs 2017). Furthermore, the average TOC concentration of the outgoing water stream (1.4mg/L) was lower than the weighted average of both incoming streams (1.7mg/L). This confirms the presence of bacterial regrowth in the water tower, as the organic carbon is incorporated in bacterial cells during growth. The hypothesis was confirmed in literature, where Niquette et al. (2001) attributed the significant decrease of biologically degradable organic carbon during distribution to consumption during bacterial regrowth. The observed regrowth in the water tower was limited, as the HRT was only 6.5h on average (**table 4.2**).

The bacterial cell density of the outgoing water was mainly determined by periodic fluctuations in the bacterial cell density of the incoming "surface water". This can be explained since this feed accounts for most of the exiting stream (72 ± 19%) and has the highest bacterial abundance under normal conditions. Besmer & Hammes (2016) studied the bacterial dynamics in groundwater and observed a diurnal pattern in the total cell counts, which was attributed to the production process, as groundwater extraction took place overnight. Seasonal fluctuations, such as precipitation, were also observed to cause changes in the microbial dynamics. Similarly, the observed fluctuations in the cell density of the surface water may be attributed to the changes in the source water quality and the production process.

The influence of the water temperature on the bacterial regrowth in the water tower was evaluated. The difference (delta) in cell density between the exiting water and the feed produced from surface water was calculated, since this feed accounts for around 75% of the entering stream under normal conditions. The delta cell density is shown in **figure 4.25, A**. An increase was observed during the first days of the monitoring campaign. The temperature of the incoming stream produced from surface water is shown in **figure 4.25, B**. The water temperature of the feed produced from surface water increased with 3°C during the first days of monitoring. These results suggest a positive relation between the "surface water" temperature and the bacterial regrowth in the water tower, definitely before April 24th.

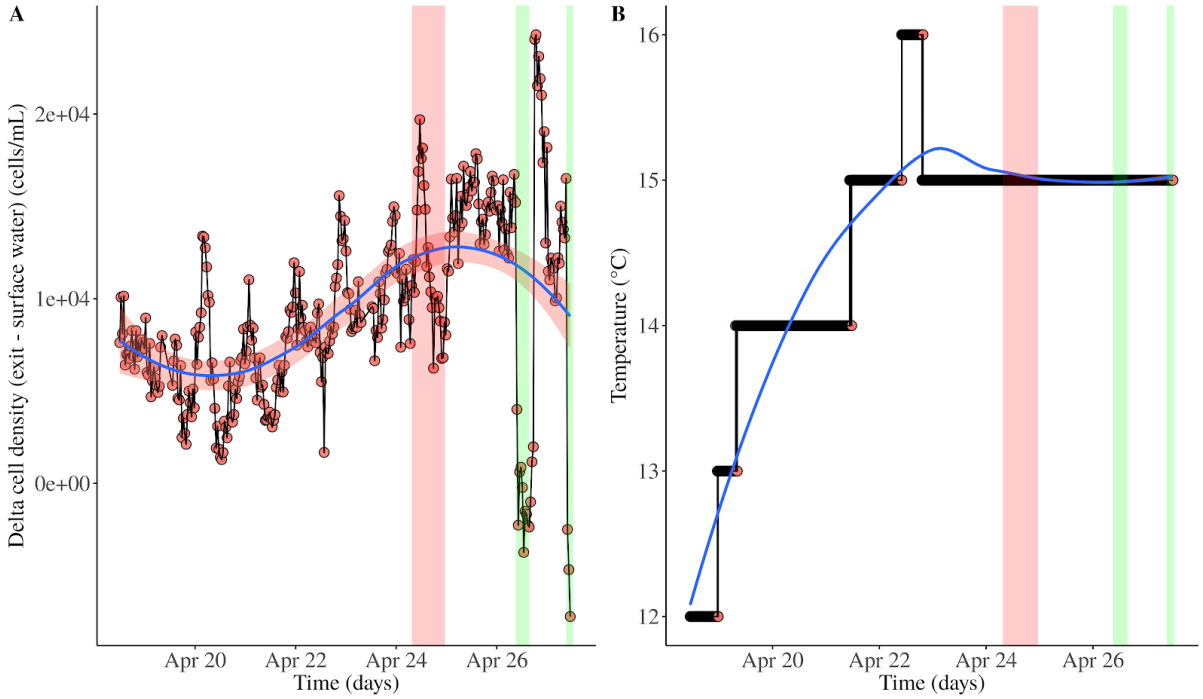

Figure 4.25 – (**A**) Difference in cell density between the exiting water and the feed water produced from surface water. A LOESS fitted trend line with standard deviation was added for visualization. (**B**) Temperature profile of the incoming water produced from surface water. The periods with drinking water produced from 100% surface water and 100% groundwater are respectively highlighted in red and green. A LOESS fitted trend line was added.

The results indicate that an increase in the water temperature of 3°C will result in an increase in bacterial regrowth. The difference in cell density between the incoming surface water stream and the exiting stream decreased after April 24th. This may be caused by the works indicated by the green highlights (**figure 4.25, A**), when the incoming feed consisted out of 100% drinking water produced from groundwater that had a stable temperature of 10 ± 2°C. This confirms the hypothesis, namely the relation between the drinking water temperature and bacterial regrowth. In literature, increasing drinking water temperatures have been shown to result in a general increase of the bacterial abundance (Chiao et al. 2014; McCoy & VanBriesen 2014; Nescerecka et al. 2018). Moreover, it has been demonstrated that rising water temperatures (*e.g.* caused by seasonal influences) will increase the bacterial richness and diversity (Chiao et al. 2014; McCoy & VanBriesen 2014).

To get a better insight in the bacterial community dynamics, the phenotypic alpha diversity D_2 was calculated (**figure 4.26**). The phenotypic diversity D_2 was highly correlated to the D_1 ($r_p(D_1,D_2)$ = 0.88, $p < 0.001$), therefore only the results of D_2 are shown and discussed. During the works on April 24th (nearly only "surface water" feed), D_2 of the surface water and the exiting water increased. During the works on April 26th (only "groundwater" feed), D_2 of the exiting water decreased drastically. D_2 of the surface water, which is replaced by groundwater during that period, increased up to the D_2 of the groundwater. The influence of the water works on April 27th on D_2 are less clear, as only three hours were measured during that period. After April 26th, D_2 of the "groundwater" changes, which indicates that the water quality of the incoming "groundwater" has changed. This change cannot be attributed to the main water works, since this feed was not affected, and D_2 did not return to its original level after the intervention. This may indicate that the water quality of the groundwater source changed at April 26th. FARYS confirmed that this was the case since other water sources were used at the production site in Espinette.

These results indicate that the phenotypic diversity of the exiting stream is similar to the phenotypic diversity of the incoming "surface water". Most importantly, D_2 confirms that the microbial community of the groundwater changed after April 26th, which could not be observed in the cell densities (**figure 4.24**).

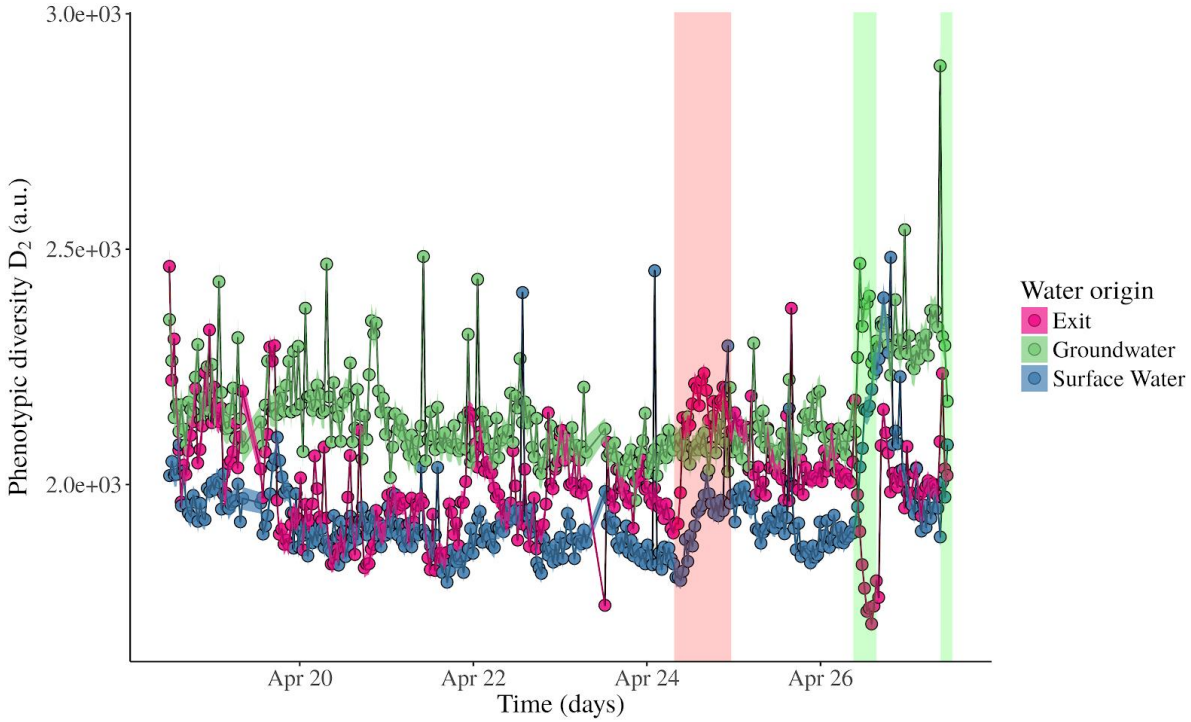

Figure 4.26 – Phenotypic diversity D_2 over time of the incoming and outgoing water streams of the water tower Kattenberg. The periods with nearly 100% drinking water produced from surface water and 100% groundwater are respectively highlighted in red and green.

To conclude, the phenotypic alpha diversity of the outgoing water is similar to the phenotypic alpha diversity of the incoming water produced from surface water. Flow cytometry was shown to be an effective and sensitive high-frequency monitoring tool, enabling the detection of changes in the microbial abundance and composition due to operational changes. Besides the cell counts, phenotypic diversity indices, which are calculated from the phenotypic fingerprint, may serve as indicators of changes in the microbial water quality. They have been shown to be a valuable addition to the FCM cell count measurements, since not all changes in the microbial community composition could be detected using cell counts (Besmer et al. 2017; El-Chakhtoura et al. 2015). The results from the present study demonstrate the additional value of phenotypic fingerprinting, as changes in the "groundwater" were observed that could not be deduced from solely cell density results.

2.2 Lab-scale water tower

To evaluate the effect of the mixing ratio on the water tower drinking water quality, a lab-scale water tower was built. Different mixing ratio regimes were consecutively run for 12 hours each (HRT = 4h), whilst increasing the percentage of groundwater. FCM samples were taken every 40 minutes of all streams.

The total cell density over time is given in **figure 4.27**. The cell density of the incoming water produced from surface water ($1.0 \pm 0.6 * 10^5$cells/mL) was higher than the water produced from groundwater ($3.9 \pm 2.0 * 10^4$cells/mL). The cell density of the lab-scale tower was intermediate at the start, but showed a strong increase towards the end of the experiment. The cell density of the "surface water" and water tower exit were observed to increase after two days (April 11th, 20:00), whereas the cell density of the "groundwater" only increased after three days (April 12th, 20:00).

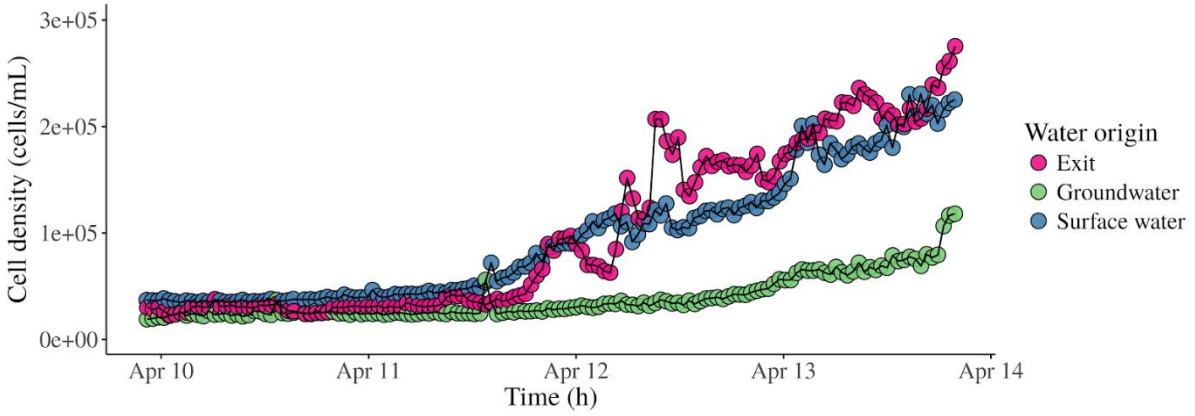

Figure 4.27 – Evolution of the cell densities over time of the incoming and outgoing streams of the lab-scale water tower.

These results seem counterintuitive and seem to be in contradiction with the previously discussed results of the full-scale water tower. First, the cell density of the lab-scale water tower was intermediate at the start of the experiment. This can be explained, as the setup was new and therefore did not contain any biofilm or contaminated parts. Thus, the cell densities in the lab-scale water tower are a result of the direct mixing of both waters. This is in compliance with a study performed by Prest et al. (2013) who mixed two types of drinking water and reported intermediate cell counts after direct measurement. Furthermore, as the percentage of "groundwater" in the water tower increased, the cell density in the water tower increased. This seems contradictory, as it was previously shown that the incoming "groundwater" contained lower cell densities. However, during the course of the experiment the water in the bottles was not renewed. Hence, this increase may be attributed to regrowth rather than to the changing mixing ratio of the incoming waters. The lag phase for regrowth in "groundwater" was longer than for "surface water" or the mixed water of the tower. As the temperature was the same for all streams (*i.e.* 15°C), the slower growth in the "groundwater" may be caused by a lack of nutrients, with carbon in particular (Hofmann & Griebler 2018; Prest et al. 2016). This was also observed at the full-scale water tower. In the lab-scale water tower, the fastest regrowth was observed in the exiting stream. As previously discussed, mixing of the different water steams may result in a larger variety of available nutrients, thus

facilitating bacterial growth. Also, plastic tubing was used to connect the incoming water bottles with the lab-scale water tower. Leaching of organic compounds, such as plasticizers, softeners and stabilizers, from the plastic tubing may be a nutrient source and hence promote bacterial growth in the water tower (Rożej et al. 2015). A study performed on plastic shower hoses, which have a similar diameter to the tubing used in the present setup, showed that leaching can occur to a high extent, hence facilitating bacterial regrowth. However, the extent of leaching and regrowth was shown to be highly dependent on the material specifications (Proctor et al. 2016).

To evaluate changes in the bacterial community during the experiment, the phenotypic alpha diversity indices were calculated from the FCM data. As the phenotypic alpha diversity D_2 was highly correlated to the phenotypic diversity D_1 ($r_p = 0.99$, $p < 0.001$) and the phenotypic richness D_0 ($r_p = 0.78$, $p < 0.001$), only the results for D_2 are shown and will be discussed. A decrease of D_2 was observed for all streams (**figure 4.28**).

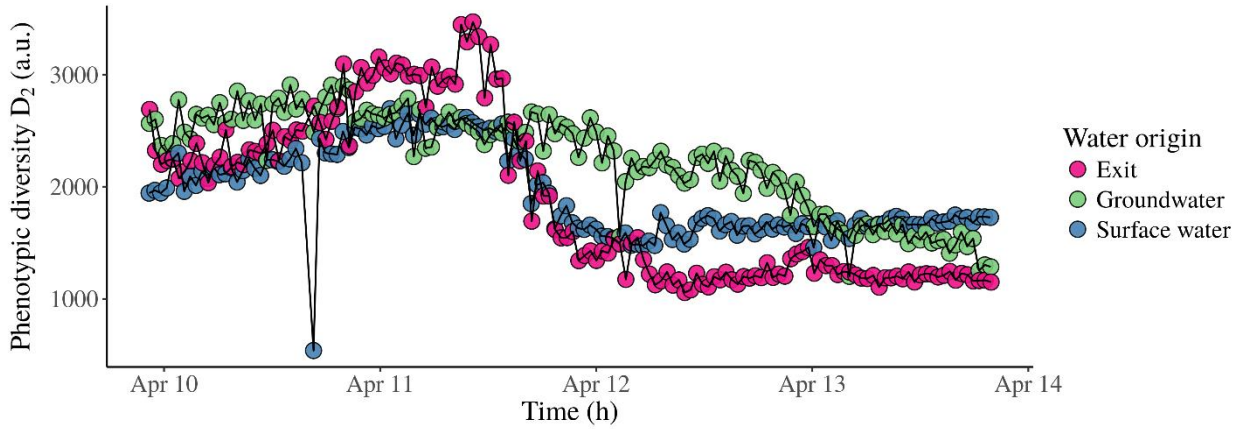

Figure 4.28 – Phenotypic diversity D_2 over time of the incoming and outgoing water streams of the lab-scale water tower.

These results indicate changes in the bacterial community of all streams during regrowth. The community evolved towards a community with a lower phenotypic diversity. This can be interpreted as the occurrence of selective regrowth. To address the changes in the bacterial community during the selective regrowth, a contrast analysis was performed for all streams (**figure 4.29**). The FCM fingerprints at the beginning and the end of the experiment were compared. The abundance of the HNA bacteria increased in all streams, whereas the abundance of the LNA bacteria was observed to decrease over the course of the experiment.

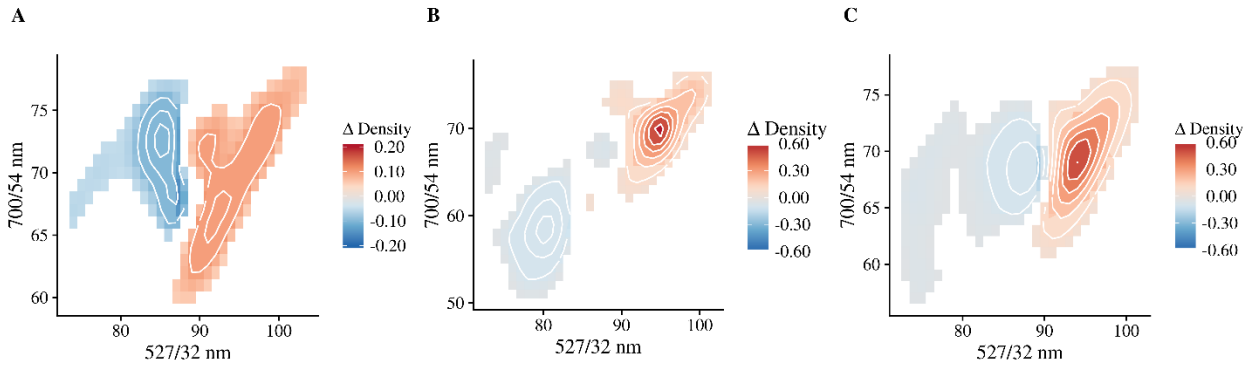

Figure 4.29 – Contrast analysis to compare the community structure at the beginning and the end of the lab-scale water tower experiment. Positive (red) bins indicate a higher abundance of these regions at the end of the experiment, whereas negative (blue) bins indicate a higher abundance of these regions at the beginning of the experiment for (**A**) surface water, (**B**) groundwater and (**C**) lab-scale water tower samples. The contrasts were calculated based on the average of three subsequent samples. Differences in density smaller than 0.05 are not displayed.

These results indicate that growth of HNA bacteria was favoured during selective regrowth. This is in compliance with the results of previously performed regrowth experiments in literature, where a community shift was observed due to the selective regrowth of HNA bacteria (Prest et al. 2013; Wang et al. 2009). However, these experiments were always performed in a nutrient-rich environment at optimal temperatures for bacterial growth (*e.g.* 30°C). Lautenschlager et al. (2010) studied changes in the bacterial community of overnight stagnated drinking water. Hence, these conditions were more similar to the present study. In accordance to our results, they observed an increase of the HNA bacteria after stagnation of 12h. Also, the results from the present study were confirmed by previously discussed findings from DC Water monitoring in this study, where an increase in HNA was observed after stagnation. *Vice versa*, as results from the lab-scale water tower were comparable, this may confirm the occurrence of selective regrowth at the DC Water hydrants.

To conclude, the increasing cell densities during the course of this experiment, indicate that bacterial regrowth, or the time factor, dominated the effect of the changing mixing ratio. Regrowth was the most prevalent in the water tower itself. This is believed to be attributed to an increased nutrient availability, which may be caused by a combination of plastic leaching and mixing of two streams. Selective regrowth of the HNA population resulted in a decrease of the phenotypic alpha diversity. This experiment illustrates the sensitivity of diversity indices and the FCM fingerprint as an additional source of information to HNA/LNA and cell count measurements. Based on the dynamics of the phenotypic alpha diversity, combined with fluctuations in the fingerprint it was possible to address the underlying cause of the increasing cell counts and get a better insight in the community dynamics.

To be able to draw conclusions concerning the effect of the mixing ratio on the bacterial community of the water tower, additional experiments are necessary. On the one hand, the experiment could be performed in reversed order, with an increasing percentage of "surface water", to evaluate the relative impact of the mixing ratio on bacterial regrowth. On the other hand, direct sampling from the water tower streams could be performed to avoid additional bacterial regrowth by continuously refreshing the incoming water.

2.3 Predictive modelling

Differential equations were used to calculate the percentage of surface water in the exiting water (see **section III.3.3.2**). Based on these equations, the percentage of surface water in the outgoing stream was modelled (**figure 4.30**).

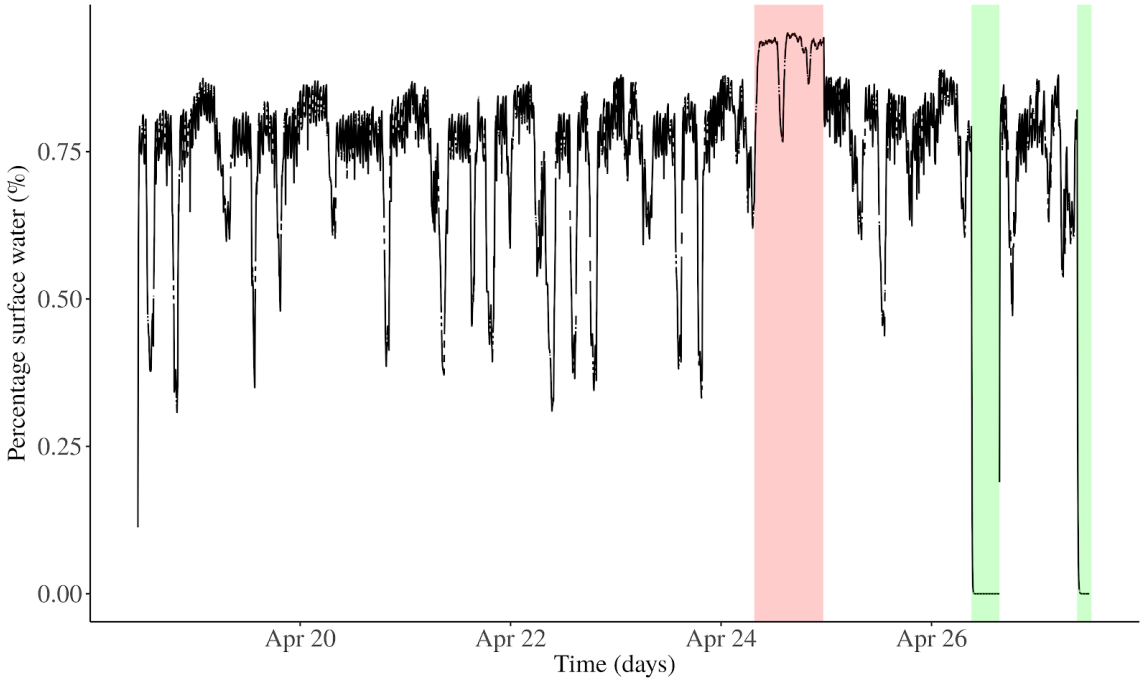

Figure 4.30 – Modelled percentage of water produced from surface water leaving the water tower Kattenberg, based on online measurements of the flows. The periods with drinking water produced from nearly 100% surface water and 100% groundwater entering the tower are respectively highlighted in red and green.

Using this approach, it was possible to model the mixing ratio of the exiting water, including the occurred events. In this method, however, perfect mixing was assumed. Yet, the mixing dynamics of the real water tower may be more complex as the tower consists out of four different storage tanks. Computational fluid dynamics (CFD) based models can alternatively be used to get an insight in the three-dimensional mixing of the water tower. Consequently, these models may provide a better estimation of the outgoing mixing ratio. They have been previously used to estimate the retention time of drinking water storage tanks (Hannoun & Boulos 1997; Templeton et al. 2006). Nevertheless, CFD models require knowledge of the problem's initial and boundary

conditions, and are computationally intensive. To overcome these drawbacks, an alternative approach was assessed in this study. In this method, the microbial community structure of the outgoing water was used to predict the mixing ratio. This way, there is no need to know the exact fluid dynamics of the water tower. In this study, the applicability of the microbial community structure as a basis to estimate the mixing ratio of the outgoing stream was evaluated.

A model was built using the FCM data, based on a Random Forest (RF) algorithm. RF was chosen because it can handle multivariate data sets such as FCM data (Breiman 2001). Also, RF algorithms have previously been shown to perform better on ecological data sets than linear analyses (*e.g.* LDA) (Cutler et al. 2007). More information about Random Forests can be found in **appendix 6**.

The model was based on the bacterial community structure, using the phenotypic fingerprint. This way, a model was created on a population level instead of on a single-cell level. The model was trained using *in silico* mixes with known mixing ratios. RF regression was used to predict the mixing ratio of the exiting water. Hereby, the percentage of "surface water" was predicted based on the phenotypic fingerprint of the bacterial community (**figure 4.31**).

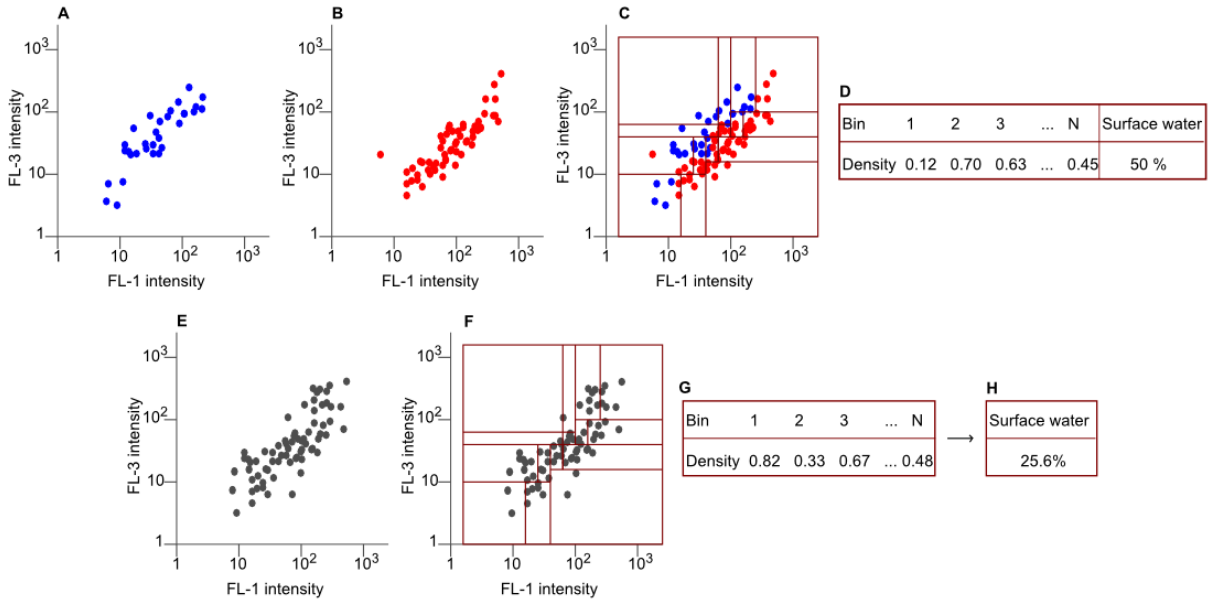

Figure 4.31 – Illustration of a regression algorithm on a population level, based on the structure of the bacterial community. (**A**) "Surface water" and (**B**) "groundwater" are mixed in silico (**C**) with a known mixing ratio. This in silico mix is discretized using probability binning. The resulting fingerprint (**D**), in combination with the known surface water concentration are used to train the RF model. A new sample from the exiting water (**E**) is subjected to the same binning grid (**F**). The obtained phenotypic fingerprint (**G**) is then used as a basis for the RF regression to predict (**H**) the percentage of "surface water".

The performance of the model was validated on *in silico* mixed samples (*i.e.* mixes made using the computer) and on *in vitro* mixed samples (*i.e.* lab mixtures) with a known mixing ratio (**figure 4.32, B**). Furthermore, D_2 was calculated in function of the mixing ratio (**figure 4.32, A)**.

To compare the accuracy of both models, the R^2 was calculated between the actual percentage "surface water" and the model predictions of the test sets (**table 4.4**).

Table 4.4 – R^2 of population based RF regression of both *in silico* and *in vitro* test data.

Data	R^2
In vitro	0.98
In silico	0.97

These results show that D_2 indicates changes in the mixing ratio, however, it is less valuable as a predictor for the mixing ratio. Using the RF model based on the phenotypic fingerprint, the mixing ratio of both *in silico* and *in vitro* mixes could be accurately predicted.

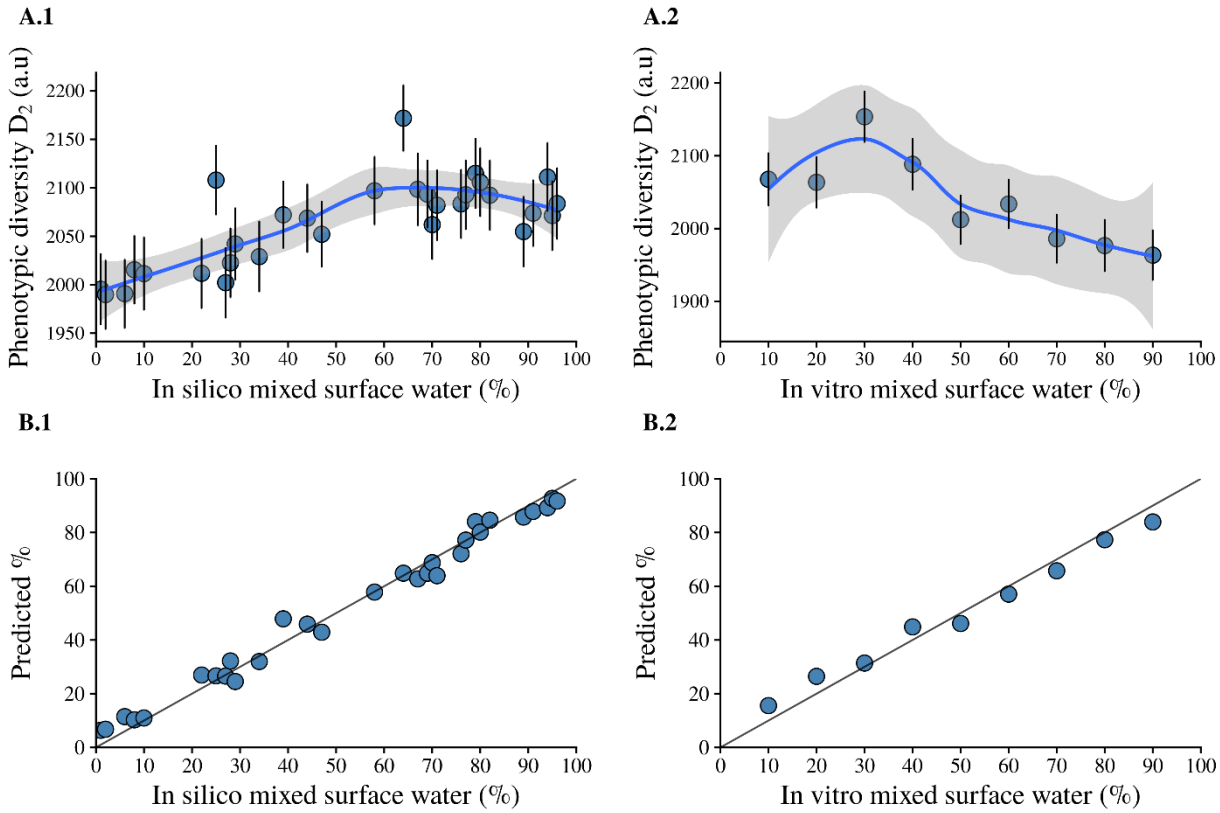

Fig 4.32 – Validation of the population model on a drinking water sample retrieved March 15th. (**A**) Phenotypic alpha diversity in function of the mixing ratio for the test set. A LOESS fitted trend line with standard deviation was added for visualisation. (**B**) Model prediction in function of the true mixing ratio. The validation was based on in silico mixes (**A.1, B.1**) and based on in vitro mixes (**A.2, B.2**). In vitro mixes were performed in eight replicates. Remark that the model required pooling of the in vitro mixed replicates per mixing ratio.

The population based model predictions were compared to the results obtained using differential equations for two grab samples from the outgoing water of the water tower Kattenberg, retrieved at March 8th and March 15th. The estimations are given in **table 4.5**. For both dates, the model was trained on *in silico* mixes of the incoming water stream samples of that day.

Table 4.5 – Population based RF regression of the percentage of surface water in the outgoing water stream, compared to the daily average of the results obtained using differential equations.

Date	Differential equations (SW %)	RF regression (SW %)
March 8th	71%	77%
March 15th	45%	23%

The model prediction at March 8th was close to the daily average estimation based on differential equations. However, at March 15th, the mixing ratio was altered due to upstream maintenance works, as described in **section IV.2.1**. The RF model indicated a change in the outgoing mixing ratio, however, its prediction was deviating from the estimation based on differential equations. Note that the estimation based on differential equations was the daily average, which may differ from the actual mixing ratio at the time the sample for RF regression was taken.

Rubbens et al. (2017) used Random Forest classification for single cell identification in axenic cultures. De Roy et al. (2012) used classification to determine the origin of pure water samples. The present research is a valuable extension to both approaches, as it demonstrates the use of the phenotypic fingerprint of the environmental drinking water community as a basis for predicting the mixing ratio of two drinking waters.

To conclude, this preliminary research is to be considered as a proof-of-concept. Population level RF regression has been shown to be capable of predicting the behaviour of environmental bacterial communities with high accuracy. RF population level regression based on the phenotypic fingerprint is a very promising approach that may serve as an additional source of information to trace the cause of contaminations in the drinking water distribution network. A better understanding of the sensitivity and increasing of the robustness is necessary future work. When this model can be successfully online implemented, it may serve as an early warning system for the detection of abnormal changes in the microbial drinking water community and mixing ratio in the future.

3. Pidpa water tower Kalmthout

As described in the materials and methods (**section III**), the rising pipe of the water tower of Kalmthout was monitored over 15 days using online FCM. Via this rising pipe, the water tower is emptied and filled, depending on the pressure in the drinking water network. The evolution of the bacterial abundance over time is given in **figure 4.33**. The cell density was stable over the course of the monitoring campaign ($9.0 \pm 0.5 * 10^5$cells/mL). Drinking water coming from the production ("network"), sampled when the water tower was filling, showed slightly higher and more variable cell densities ($9.1 \pm 0.7 * 10^5$cells/mL) compared to drinking water leaving the water tower ("water tower") ($8.9 \pm 0.3 * 10^5$cells/mL).

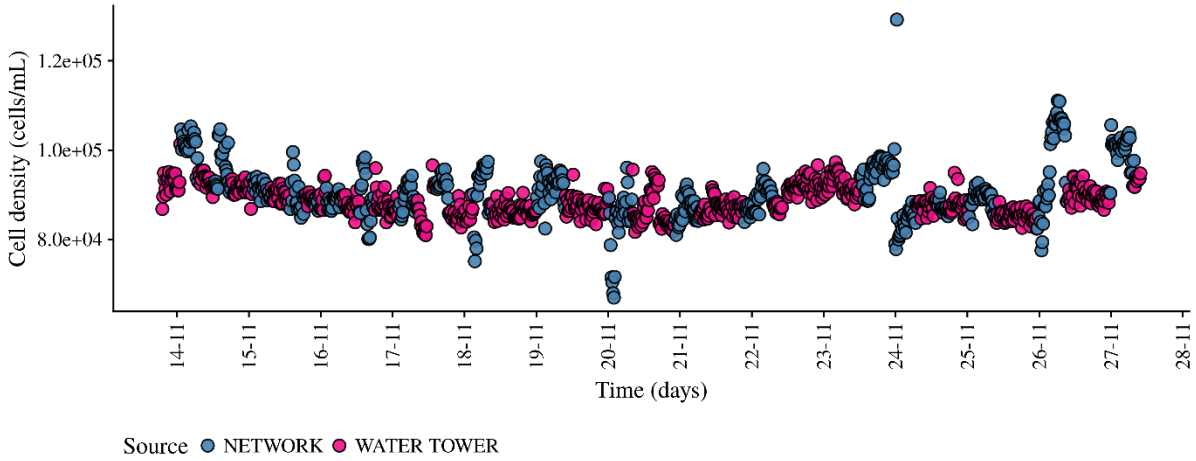

Figure 4.33 – Evolution of cell density over time, coloured according to the drinking water source. "Network" indicates samples that were taken from water coming from the transportation network when the water tower was filling. "Water tower" indicates samples that were taken when the water tower was emptied towards the distribution network. The dates on the x-axis indicate midnight of the respective day.

The cell density of the water leaving the tower is less variable, which may indicate good mixing in the water tower. Furthermore, cell densities are rather constant over time and are only slightly different between streams. This may indicate that regrowth is not taking place in the water tower. This is in contrast to observations at the water tower Kattenberg (**section IV.2.1**), where the cell density of the exiting stream was higher than those of the incoming feeds. This can be explained by the different drinking water sources, as in Kalmthout, only groundwater sources are used. These have typically a lower TOC concentration and bacterial cell density. Also, the water tower in Kalmthout was sampled in November instead of April (Kattenberg), thus the water temperature was lower. As previously discussed, this may be related to bacterial regrowth.

To detect changes in the microbial community, the phenotypic diversity was calculated. As D_2 was highly correlated to both D_0 and D_1 ($r_p(D_2,D_0) = 0.96$, $r_p(D_2,D_1) = 0.99$), only the results obtained from D_2 will be discussed. Over time, the phenotypic alpha diversity of the community was shifting

(**figure 4.34, A**). D_2 increased until November 18th, after which it started to decrease slightly. A sudden drop with immediate recovery was observed at November 17th. These dynamics occurred for both the incoming water (from the network) as well as the water from the water tower. This indicates that diversity shifts were occurring in the whole network and were not the result of storage inside the water tower itself.

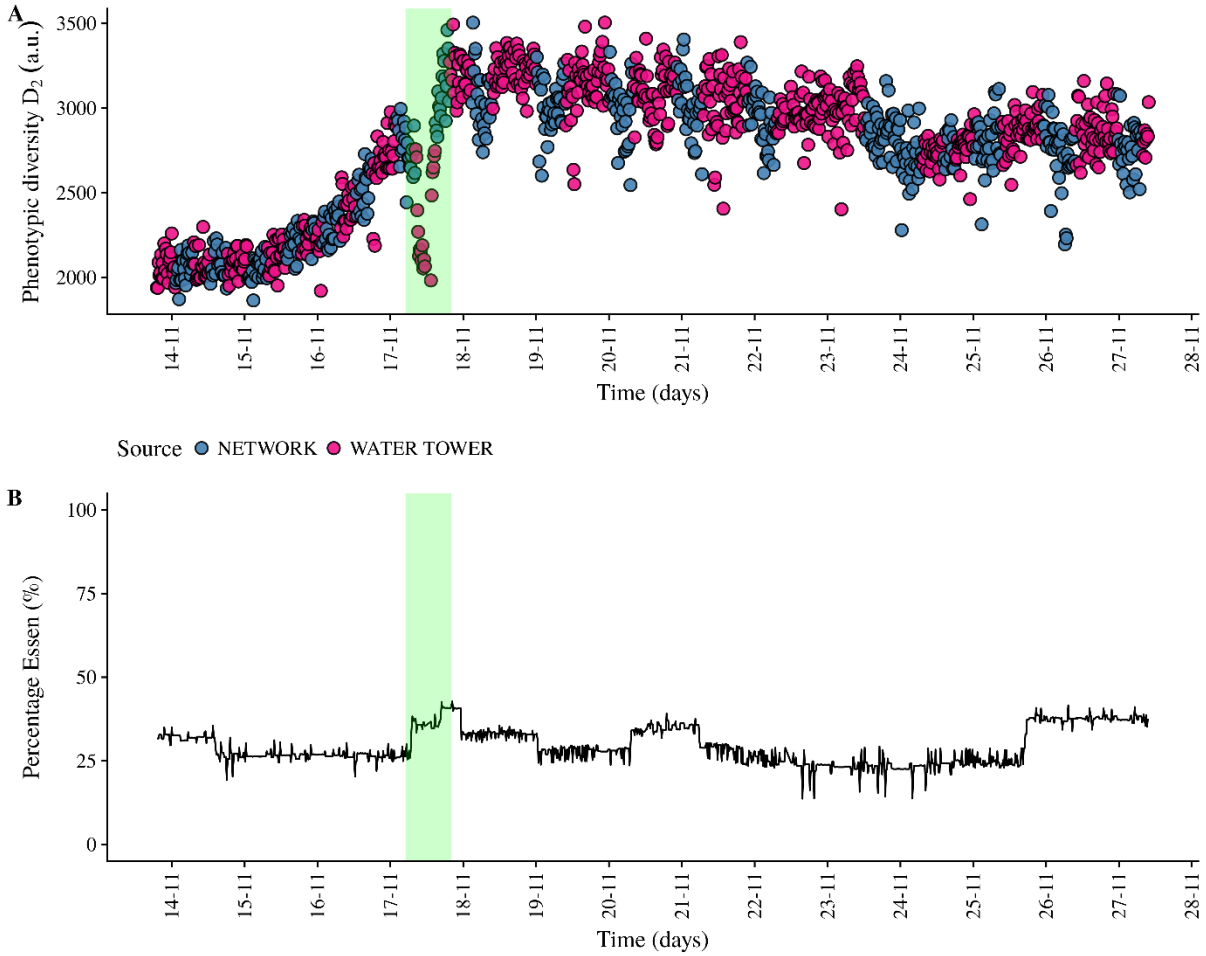

Figure 4.34 – (**A**) Evolution of D_2 over time. "Network" indicates samples that were taken from water coming from the transportation network when the water tower was filling. "Water tower" indicates samples that were taken when the water tower was emptied towards the distribution network. (**B**) Percentage of the total flow that is entering the storage reservoir, coming from the production at Essen. From the storage reservoir, drinking water is provided to the water tower Kalmthout. The dates on the x-axis indicate midnight of the respective day. The green rectangle indicates when the sudden drop with immediate recovery was observed in D_2.

These changes may be induced through the production process. Therefore, the incoming water origin and its flow dynamics were assessed. In short, two feeds ("Kapellen" and "Essen") produced from groundwater using a different production process, enter a storage reservoir. From this reservoir, the water tower Kalmthout is supplied. The flows of the incoming and outgoing streams of the reservoir were evaluated in order to detect changes in the mixing ratio of the water entering the water tower. The fraction of the flow entering the reservoir coming from Essen was plotted over time (**figure 3.34, B**). The percentage of water coming from Essen was rather constant (29 ±

5%) during the course of the monitoring campaign. During the event in D_2 at November 17th, there was a sudden increase in the percentage of drinking water coming from Essen observed (from around 25% to 37%). Furthermore, the total flow from the reservoir to the water tower was evaluated over time (**figure 4.35**). This flow was very variable (244 ± 89m³/h) and followed a diurnal pattern (high during the day and low overnight). At November 17th at 06:24, a flow of zero was registered.

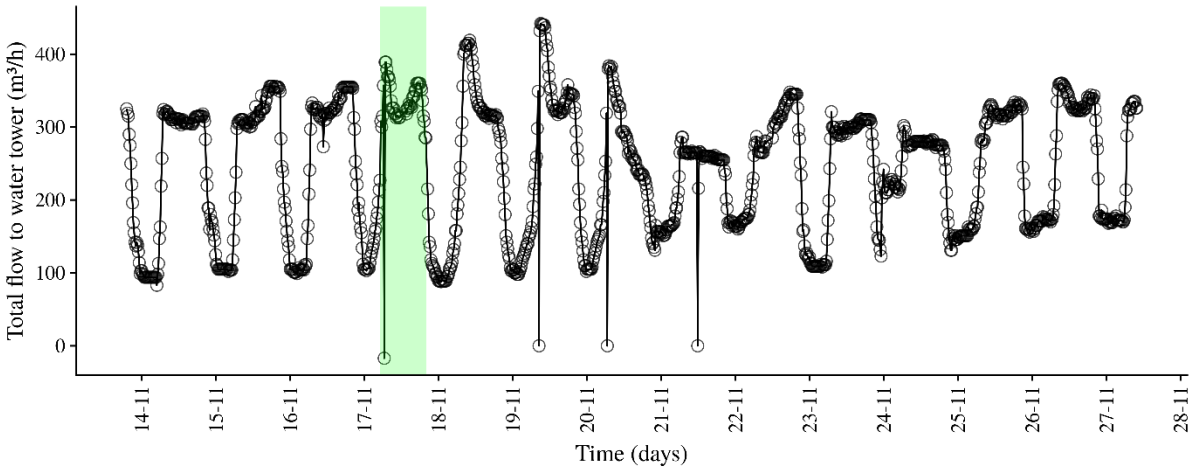

Figure 4.35 – Registered total flow from the reservoir to the water tower Kalmthout over the course of the monitoring campaign. The dates on the x-axis indicate midnight of the respective day. The green rectangle indicates when the sudden drop with immediate recovery was observed in D_2.

These results indicate that the influence of the retention in the water tower on the phenotypic alpha diversity was very limited, and was to a bigger extent influenced by the production process. The event registered in D_2 at November 17th was also observed in a change in the mixing ratio of the incoming streams at the reservoir (**figure 4.34, B**). Similarly to the observations in water tower Kattenberg, this may be reflected in a change in phenotypic diversity. However, other changes in mixing ratio were not reflected in the phenotypic alpha diversity (*e.g.* November 25th). Furthermore, a sudden drop in the total flow to the water tower was observed at that time (**figure 4.35**). The total registered flow was zero, which may have resulted in a precipitation of suspended particles such as iron. These may have been resuspended after restoring the flow. Consequently, this could have impacted the drinking water quality, as reflected in a change in phenotypic alpha diversity of the microbial community at the water tower. However, not all events (*e.g.* total flow of zero to the water tower at November 20th, 06:32) were reflected in the phenotypic alpha diversity, and *vice versa*, the overall trend in D_2 was not directly related to the studied flow dynamics.

To conclude, as both the bacterial abundance and the diversity were comparable for the incoming and outgoing stream of the water tower, bacterial regrowth may not be taking place. This could be

due to a combination of seasonal influences (*e.g.* colder water) and the sole groundwater origin (*e.g.* lower TOC and cell counts). The observed event in D_2 could be explained by a change in the drinking water quality upstream of the water tower. It is hypothesized to be caused by a change in production, such as changes in mixing ratio or flow magnitude. This monitoring campaign illustrates that phenotypic diversity indices are a valuable addition to cell density measurements when assessing the impact of operational on the microbial drinking water quality.

Conclusions and future perspectives

The main objective of this research was to assess the value of FCM as a tool for microbial drinking water quality monitoring.

In a first part, the objective was to relate changes in the physicochemical drinking water quality to the bacterial community by FCM measurements. This was evaluated on the basis of different research questions as defined in the objectives (**section II**). From these analyses, physicochemical parameters were linked to on the one hand the bacterial abundance and on the other hand the phenotypic alpha- and beta diversity. The bacterial cell density was shown to decrease significantly after flushing for most of the hydrants (**RQ 2**). Elevated cell densities "before" flushing were hypothesized to be caused by a combination of biofilm disruption and bacterial regrowth (**RQ 1**). Bacterial regrowth, and consequently an increase in the intact cell fraction, was attributed to a loss of disinfection residual in the system. Furthermore, iron was found to directly influence the bacterial abundance at low concentrations as a micronutrient (**RQ 5**). Changes in the phenotypic drinking water bacterial community structure were shown to be mainly related to either the flush duration (**RQ 2**) or to seasonal effects (**RQ 3**), depending on the water age at the hydrant. It was therefore concluded that the water age plays an important indirect role in the explanation of phenotypic changes in the bacterial community (**RQ 4**). Seasonal effects were demonstrated to have an influence on the changes in phenotypic community structure at all of the hydrants. However, this effect was dominated by the effect of flushing lower water age hydrants. At higher water age hydrants, the changes in phenotypic community structure were primarily related to seasonal changes, such as changes in temperature.

From this we conclude that FCM fingerprinting provides a valuable additional source of information to physicochemical analyses and classic microbial monitoring techniques. Practically, the phenotypic bacterial community structure and bacterial abundance can be used as additional factors when making operational decisions. Changes in the microbial community may indicate that the water is "refreshed", by means of restoring the microbial drinking water quality. These changes were not always reflected in the chlorine concentration, which means that operational decisions concerning microbial drinking water quality should not solely be based on chlorine concentrations. For example, the effectiveness of the flush regime may be evaluated and adapted based on chlorine data in combination with FCM data. When individualizing the flush regime for every hydrant, flushing can be done more effectively and both time and water will be saved. As a future perspective it is suggested to map the phenotypic bacterial community over a one-year timespan

in order to create a "baseline" of seasonally occurring bacterial community dynamics at each hydrant. This way, FCM can be applied as an early warning system when deviations from the baseline are detected.

In a second chapter, the aim was to assess to what extent online FCM can be used to determine the effect of operational changes on the drinking water bacterial community dynamics. The main finding of full-scale water tower measurements at Kattenberg was that changes in the mixing ratio of incoming streams were reflected in the cell density and/or phenotypic diversity (**RQ 6**). This was, to a lesser extent, also observed in the water tower at Kalmthout. Furthermore, bacterial regrowth was observed in the exiting stream of the water tower Kattenberg, which was attributed to a combination of the residence time, an increased nutrient concentration due to mixing and an increase in temperature (**RQ 6**). FCM was shown to be a sensitive high-frequency monitoring tool, enabling the detection of changes in the microbial abundance and composition due to operational changes. Moreover, the results from the present study demonstrate the additional value of phenotypic diversity indices as not all operational events were detected solely using cell counts or HNA/LNA, as demonstrated on the water tower at Kalmthout.

The initial aim in the lab-scale water tower experiment was to evaluate the effect of the mixing ratio on the bacterial community dynamics of the water tower by using FCM. However, no conclusions about the effect of the mixing ratio could be made, as bacterial regrowth during the course of the experiment dominated the effect of the changes in mixing ratio. Regrowth was the most prevalent in the lab-scale water tower, as the nutrient availability was believed to be higher, which may be caused by a combination of plastic leaching and mixing of two streams. Selective regrowth of the HNA population was reflected in a decrease of the phenotypic alpha diversity. This experiment emphasizes the usefulness of FCM fingerprinting as an additional source of information, as it was possible to address the underlying cause of the increasing cell counts, supported by the phenotypic diversity and HNA/LNA analyses.

The last objective of this study was to assess the use of flow cytometric data as a basis for predictive water composition modelling. Our study showed that it was possible to use the phenotypic microbial community structure as a basis for predicting the mixing ratio of different drinking waters (**RQ 7**). Population level RF regression has been shown to be capable of predicting the composition of environmental bacterial communities with high accuracy. This preliminary research should be considered as a proof-of-concept. A better understanding of the sensitivity and increasing of the robustness is necessary future work. It is a promising approach that, when

successfully applied on online measurements, may serve as an early warning system for the detection of abnormal changes in the microbial drinking water community and the mixing ratio in the future.

Bibliography

Allen, Edberg, & Reasoner. (2004). Heterotrophic plate count bacteria—what is their significance in drinking water? *International Journal of Food Microbiology*, *92*(3), 265–274.

Amann, Ludwig, & Schleifer. (1995). Phylogenetic identification and in situ detection of individual microbial cells without cultivation. *Microbiological Reviews*, *59*(1), 143–169.

Amy. (2007). USA to Europe: Who is the true world leader in drinking water technoloy (what can each learn from the other?). *59e Vakantiecursus in Drinkwatervoorziening & 26e in Riolering En Afvalwaterbehandeling: Grenzen Verleggen*, 19–27.

AWWA. (2002a). Effects of Water Age on Distribution System Water Quality. *American Water Works Association*.

AWWA. (2002b). Permeation and Leaching. *American Water Works Association*.

AWWA. (2013). Nitrification Prevention and Control in Drinking Water. *American Water Works Association*.

Bartram, Cotruvo, Exner, Fricker, & Glasmacher. (2003). Heterotrophic plate counts and drinking-water safety. London: IWA Publishing.

Bashashati, & Brinkman. (2009). A survey of flow cytometry data analysis methods. *Advances in Bioinformatics*.

BD biosciences. (2000). Introduction to Flow Cytometry: a learning guide. San Jose, CA.

BD biosciences. (2018). Spectrum Viewer. Retrieved March 5, 2018, from http://www.bdbiosciences.com/us/s/spectrumviewer

Beech, & Sunner. (2004). Biocorrosion: Towards understanding interactions between biofilms and metals. *Current Opinion in Biotechnology*, *15*(3), 181–186.

Benarde, Snow, Olivieri, & Davidson. (1967). Kinetics and mechanism of bacterial disinfection by chlorine dioxide. *Applied Microbiology*, *15*(2), 257–65.

Benedict, Reses, Vigar, Roth, Roberts, Mattioli, … Hill. (2017). Surveillance for Waterborne Disease Outbreaks Associated with Drinking Water — United States, *66*(44), 1216–1221.

Berney, Vital, Hülshoff, Weilenmann, Egli, & Hammes. (2008). Rapid, cultivation-independent assessment of microbial viability in drinking water. *Water Research*, *42*(14), 4010–4018.

Berry, Xi, & Raskin. (2006). Microbial ecology of drinking water distribution systems. *Current Opinion in Biotechnology*, *17*(3), 297–302.

Besmer, Epting, Page, Sigrist, Huggenberger, & Hammes. (2016). Online flow cytometry reveals microbial dynamics influenced by concurrent natural and operational events in groundwater used for drinking water treatment. *Scientific Reports*, 1–10.

Besmer, & Hammes. (2016). Short-term microbial dynamics in a drinking water plant treating groundwater with occasional high microbial loads. *Water Research*, *107*, 11–18.

Besmer, Sigrist, Props, Buysschaert, Mao, Boon, & Hammes. (2017). Laboratory-scale simulation and real-time tracking of a microbial contamination event and subsequent shock-chlorination in drinking water. *Frontiers in Microbiology*, *8*(10), 1–11.

Besmer, Weissbrodt, Kratochvil, Sigrist, Weyland, & Hammes. (2014). The feasibility of automated online flow cytometry for In-situ monitoring of microbial dynamics in aquatic ecosystems. *Frontiers in Microbiology*, *5*(6), 1–12.

Betancourt, & Rose. (2004). Drinking water treatment processes for removal of *Cryptosporidium* and *Giardia*. *Veterinary Parasitology*, *126*, 219–234.

Boe-Hansen, Albrechtsen, Arvin, & Jørgensen. (2002). Bulk water phase and biofilm growth in drinking water at low nutrient conditions. *Water Research*, *36*(18), 4477–4486.

Bolyard, Fair, & Hautman. (1992). Occurrence of chlorate in hypochlorite solutions used for drinking water disinfection. *Environmental Science & Technology*, *26*(8), 1663–1665.

Bray, & Curtis. (1957). An ordination of the upland forest communities of Southern Wisconsin. *Ecological Monographs*, *27*(4), 325–349.

Breiman. (1996). Bagging Predictors. *Machine Learning*, *140*, 123–140.

Breiman. (2001). Random Forests. *European Journal of Mathematics*, *45*, 5–32.

Buysschaert. (2018). *Single-cell optical fingerprinting for microbial community characterization*. Ghent University.

Buysschaert, Byloos, Leys, Van Houdt, & Boon. (2016). Reevaluating multicolor flow cytometry to assess microbial viability. *Applied Microbiology and Biotechnology*, *100*(21), 9037–9051.

Camper, Lechevallier, Broadaway, & Mcfeters. (1986). Bacteria associated with granular activated carbon particles in drinking water. *Applied and Environmental Microbiology*, *52*(3), 434–438.

Cantor, Denig-Chakroff, Vela, Pfeinik, & Lynch. (2000). Use of polyphosphate in corrosion control. *Journal / American Water Works Association*, *92*(2), 85–102.

Castro, & Neves. (2003). Chlorine decay in water distribution systems case study - Lousada network. *Electronic Journal of Environmental, Agricultural and Food Chemistry*, *2*(2), 261–266.

Cervero-Aragó, Rodríguez-Martínez, Puertas-Bennasar, & Araujo. (2015). Effect of common drinking water disinfectants, chlorine and heat, on free Legionella and amoebae-associated *Legionella*. *PLoS ONE*, *10*(8), 1–18.

Chappelle, & Levin. (1968). Use of the Firefly Bioluminescent and Counting of Reaction Bacteria. *Biochemical Medicine*, *52*(1), 41–52.

Characklis. (1988). *Bacterial regrowth in distribution systems*. American Water Works Association.

Chiao, Clancy, Pinto, Xi, & Raskin. (2014). Differential resistance of drinking water bacterial populations to monochloramine disinfection. *Environmental Science and Technology*, *48*(7), 4038–4047.

Choi, & Choi. (2010). The effects of UV disinfection on drinking water quality in distribution systems. *Water Research*, *44*(1), 115–122.

Choi, & Valentine. (2002). Formation of N-nitrosodimethylamine (NDMA) from reaction of monochloramine: A new disinfection by-product. *Water Research*, *36*(4), 817–824.

Chuang, Lin, Wang, & Tung. (2013). The contribution of dissolved organic nitrogen and chloramines to nitrogenous disinfection byproduct formation from natural organic matter. *Water Research*, *47*(3), 1308–1316.

Clark, Goodrich, & Wymer. (1993). Effect of the distribution system on the drinking water quality. *Journal of Water Supply: Research & Technology*, *42*(1), 30–38.

Clark, & Haught. (2005). Characterizing pipe wall demand: implications for water quality modeling. *Journal of Water Resources Planning and Management*, *131*(3), 208–217.

Courtens, Vandekerckhove, Prat, Vilchez-Vargas, Vital, Pieper, … Vlaeminck. (2016). Empowering a mesophilic inoculum for thermophilic nitrification: Growth mode and temperature pattern as critical proliferation factors for archaeal ammonia oxidizers. *Water Research*, *92*, 94–103.

Cutler, Edwards, Beard, Cutler, Hess, Gibson, … Lawler. (2007). Random Forests for Classification in Ecology. *Ecology*, *88*(11), 2783–2792.

DC Water. (2017). Drinking Water is Distributed by Elevation Levels. Retrieved April 13, 2018, from https://www.dcwater.com/water-distribution-system

De Roy. (2014). *Microbial resource management: introducing new tools and ecological theories*. Ghent University.

De Roy, Clement, Thas, Wang, & Boon. (2012). Flow cytometry for fast microbial community fingerprinting. *Water Research*, *46*(3), 907–919.

Decreet. (2002a). Besluit van de Vlaamse regering houdende reglementering inzake de kwaliteit en levering van water, bestemd voor menselijke consumptie. *Belgisch Staatsblad*, 2907–2923.

Decreet. (2002b). Decreet betreffende water bestemd voor menselijke aanwending. *Belgisch Staatsblad*, 32838.

Dewettinck, Hulsbosch, Van Hege, Top, & Verstraete. (2001). Molecular fingerprinting of bacterial populations in groundwater and bottled mineral water. *Applied Microbiology and Biotechnology*, *57*(3), 412–418.

Dickson. (1981). An exact definition of total alkalinity and a procedure for the estimation of alkalinity and total inorganic carbon from titration data. *Deep Sea Research Part A, Oceanographic Research Papers*, *28*(6), 609–623.

Douglas, Merrill, & Catlin. (1996). Water quality deterioration from corrosion of cement-mortar linings. *Journal American Water Works Association*, *88*(7), 99–107.

Douterelo, Boxall, Deines, Sekar, Fish, & Biggs. (2014). Methodological approaches for studying the microbial ecology of drinking water distribution systems. *Water Research*, *65*, 134–156.

Douterelo, Sharpe, & Boxall. (2013). Influence of hydraulic regimes on bacterial community structure and composition in an experimental drinking water distribution system. *Water Research*, *47*(2), 503–516.

Dufour. (1998). Grondwater in Nederland, onzichtbaar water waarop wij lopen. Nederlands Instituut voor Toegepaste Geowetenschappen TNO.

El-Chakhtoura, Prest, Saikaly, van Loosdrecht, Hammes, & Vrouwenvelder. (2015). Dynamics of bacterial communities before and after distribution in a full-scale drinking water network. *Water Research*, *74*, 180–190.

EPA. (2011). Water Treatment Manual: Disinfection. Wexford.

European Communities. (1998). Council Directive 98/83/EC of 3 November 1998 on the quality of water intended for human consumption. *Official Journal*, *41*, 32–54.

European Parliament. (2000). Directive 2000/60/EC of the European Parliament and of the Council of 23 October 2000 establishing a framework for Community action in the field of water policy. *Official Journal*, *43*, 1–73.

Fan, & Steinberg. (1996). Health implications of nitrate and nitrite in drinking water: An update on methemoglobinemia occurrence and reproductive and developmental toxicity. *Regulatory Toxicology and Pharmacology*, *23*(1 I), 35–43.

Frateur, Deslouis, Kiene, Levi, & Tribollet. (1999). Free chlorine consumption induced by cast iron corrosion in drinking water distribution systems. *Water Research*, *33*(8), 1781–1790.

Gatza, Hammes, & Prest. (2013). Assessing water quality with the BD Accuri™ C6 flow cytometer. *White Paper. BD Biosciences*.

George, Petit, & Servais. (2000). Use of enzymatic methods for rapid enumeration of coliforms in freshwaters. *Journal of Applied Microbiology*, *88*(3), 404–413.

Gillespie, Lipphaus, Green, Parsons, Weir, Juskowiak, … Nocker. (2014). Assessing microbiological water quality in drinking water distribution systems with disinfectant residual using flow cytometry. *Water Research*, *65*, 224–234.

Greenacre, & Primicerio. (2014). *Multivariate analysis of ecological data*. Fundacion BBVA.

Grégori, Citterio, Ghiani, Labra, Sgorbati, Brown, & Denis. (2001). Resolution of viable and membrane-compromised bacteria in freshwater and marine waters based on analytical flow cytometry and nucleic acid double staining. *Applied and Environmental Microbiology*, *67*(10), 4662–4670.

Grunditz, Gumaelius, & Dalhammar. (1998). Comparison of inhibition assays using nitrogen removing bacteria: application to industrial wastewater. *Water Research*, *32*(10), 2995–3000.

Hallam, West, Forster, Powell, & Spencer. (2002). The decay of chlorine associated with the pipe wall in water distribution systems. *Water Research*, *36*(14), 3479–3488.

Hammes, Berney, Wang, Vital, Köster, & Egli. (2008). Flow-cytometric total bacterial cell counts as a descriptive microbiological parameter for drinking water treatment processes. *Water Research*, *42*(1–2), 269–277.

Hammes, Broger, Weilenmann, Vital, Helbing, Bosshart, … Sonnleitner. (2012). Development and laboratory-scale testing of a fully automated online flow cytometer for drinking water analysis. *Cytometry Part A*, *81A*(6), 508–516.

Hammes, & Egli. (2007). *A flow cytometric method for AOC determination*. *Technau*.

Hammes, & Egli. (2010). Cytometric methods for measuring bacteria in water: Advantages, pitfalls and applications. *Analytical and Bioanalytical Chemistry*, *397*(3), 1083–1095.

Hammes, Goldschmidt, Vital, Wang, & Egli. (2010). Measurement and interpretation of microbial adenosine tri-phosphate (ATP) in aquatic environments. *Water Research*, *44*(13), 3915–3923.

Hannoun, & Boulos. (1997). Optimizing distribution storage water quality: a hydrodynamic approach. *Applied Mathematical Modelling*, *21*(8), 495–502.

Harms, Cognet, Lommerse, Blab, & Schmidt. (2001). Autofluorescent proteins in single-molecule research: applications to live cell imaging microscopy. *Biophysical Journal*, *80*(5), 2396–2408.

Harper, Manoharan, Mavinic, & Randall. (1996). Chromium and nickel toxicity during the biotreatment of high ammonia landfill leachate. *Water Environment Research*, *68*(1), 19–24.

Hill. (1973). Diversity and evenness: a unifying notation and its consequences. *Ecology*, *54*(2), 427–432.

Hoefel, Monis, Grooby, Saint, & Andrews. (2005). Culture-independent techniques for rapid detection of bacteria associated with loss of chloramine residual in a drinking water system. *Applied and Environmental Microbiology*, *71*(11), 6479–6488.

Hofmann, & Griebler. (2018). DOM and bacterial growth efficiency in oligotrophic groundwater: Absence of priming and co-limitation by organic carbon and phosphorus. *Aquatic Microbial Ecology*, *81*(1), 55–71.

IARC. (2010). Ingested nitrate and nitrite, and cyanobacterial peptide toxins. *IARC Monographs on the Evaluation of Carcinogenic Risks to Humans*, *94*, 412.

Jacangelo, Rhodes Trussell, & Watson. (1997). Role of membrane technology in drinking water treatment in the United States. *Desalination*, *113*(2–3), 119–127.

Jones. (2006). The effect of environmental factors on estimated viable and total populations of planktonic bacteria in lakes and experimental enclosures. *Freshwater Biology*, *7*(1), 67–91.

Karim, Abbaszadegan, & Lechevallier. (2003). Potential for pathogen intrusion during pressure transients. *Journal American Water Works Association*, *95*(5), 134–146.

Karl. (1980). Cellular nucleotide measurements and applications in microbial ecology. *Microbiological Reviews*, *44*(4), 739.

Keen, & Prosser. (1987). Steady state and transient growth of autotrophic nitrifying bacteria. *Archives of Microbiology*, *147*(1), 73–79.

Kirmeyer. (2004). *Optimizing chloramine treatment*. American Water Works Association.

Kirmeyer, Odell, Jacangelo, Wilczak, & Wolfe. (1995). Nitrification occurrence and control in chloraminated water systems. American Water Works Association.

Koch. (1883). Über die neuen Untersuchungsmethoden zum Nachweis der Mikrokosmen in Boden, Luft und Wasser. *Ärztliches Vereinsblatt Für Deutschland*, (137), 274–284.

Koch, Harnisch, Schröder, & Müller. (2014). Cytometric fingerprints: Evaluation of new tools for analyzing microbial community dynamics. *Frontiers in Microbiology*, *5*, 1–12.

Koninklijk besluit. (2002). Koninklijk besluit betreffende de kwaliteit van voor menselijke consumptie bestemd water dat in voedingsmiddeleninrichtingen verpakt wordt of dat voor de fabricage en/of het in de handel brengen van voedingsmiddelen wordt gebruikt. *Belgisch Staatsblad*, 11443–11458.

Kool, Carpenter, & Fields. (1999). Effect of monochloramine disinfection of municipal drinking water on risk of nosocomial Legionnaires' disease. *Lancet*, *353*(9149), 272–277.

Lankford, & Byers. (1973). Bacterial assimilation of iron. *Critical Reviews in Microbiology*, *2*(3), 273–331.

Lautenschlager, Boon, Wang, Egli, & Hammes. (2010). Overnight stagnation of drinking water in household taps induces microbial growth and changes in community composition. *Water Research*, *44*(17), 4868–4877.

Lautenschlager, Hwang, Liu, Boon, Köster, Vrouwenvelder, … Hammes. (2013). A microbiology-based multi-parametric approach towards assessing biological stability in drinking water distribution networks. *Water Research*, *47*(9), 3015–3025.

LeChevallier. (1999). The case for maintaining a desinfectant residual. *Journal American Water Works Association*, *91*(1), 86–94.

Lee, Pressman, & Wahman. (2018). Three-dimensional free chlorine and Monochloramine biofilm penetration: correlating penetration with biofilm activity and viability. *Environmental Science and Technology*, *52*(4), 1889–1898.

Lee, Tong, Millero, Sabine, Dickson, Goyet, … Key. (2006). Global relationships of total alkalinity with salinity and temperature in surface waters of the world's oceans. *Geophysical Research Letters*, *33*(19), 1–5.

Lee, Wahman, Bishop, & Pressman. (2011). Free chlorine and monochloramine application to nitrifying biofilm: Comparison of biofilm penetration, activity, and viability. *Environmental Science and Technology*, *45*(4), 1412–1419.

Lehtola, Laxander, Miettinen, Hirvonen, Vartiainen, & Martikainen. (2006). The effects of changing water flow velocity on the formation of biofilms and water quality in pilot distribution system consisting of copper or polyethylene pipes. *Water Research*, *40*(11), 2151–2160.

Lehtola, Miettinen, Hirvonen, Vartiainen, & Martikainen. (2007). Estimates of microbial quality and concentration of copper in distributed drinking water are highly dependent on sampling strategy. *International Journal of Hygiene and Environmental Health*, *210*(6), 725–732.

Lipponen, Suutari, & Martikainen. (2002). Occurrence of nitrifying bacteria and nitrification in Finnish drinking water distribution systems, *36*, 4319–4329.

Liu, Gunawan, Barraud, Rice, Harry, & Amal. (2016). Understanding, monitoring, and controlling biofilm growth in drinking water distribution systems. *Environmental Science and Technology*, *50*(17), 8954–8976.

Liu, Wu, Wang, Ong, Hu, & Ng. (2002). Investigation of assimilable organic carbon (AOC) and bacterial regrowth in drinking water distribution system. *Water Research*, *36*(4), 891–898.

Lorenzo-Lorenzo, Are-Mazas, Villacorta-Martinez de Maturana, & Duran-Oreiro. (1993). Effect of ultraviolet disinfection of drinking water on the Viability of *Cryptosporidium parvum* oocysts. *The Journal of Parasitology*, *79*(1), 67–70.

Makris, Andra, & Botsaris. (2014). Pipe scales and biofilms in drinking-water distribution systems: undermining finished water quality. *Critical Reviews in Environmental Science and Technology*, *44*(13), 1477–1523.

Manuel, Nunes, & Melo. (2007). Dynamics of drinking water biofilm in flow/non-flow conditions. *Water Research*, *41*(3), 551–562.

Masters, Wang, Pruden, & Edwards. (2015). Redox gradients in distribution systems influence water quality, corrosion, and microbial ecology. *Water Research*, *68*, 140–149.

McCoy, & VanBriesen. (2014). Comparing spatial and temporal diversity of bacteria in a chlorinated drinking water distribution system. *Environmental Engineering Science*, *31*(1), 32–41.

McCoy, Vanbriesen, & Asce. (2012). Temporal variability of bacterial diversity in a chlorinated drinking water distribution system. *Journal of Environmental Engineering*, *138*(7), 786–795.

Melcer. (2004). *Methods for wastewater characterization in activated sludge modelling*. IWA Publishing.

Moritz, Flemming, & Wingender. (2010). Integration of *Pseudomonas aeruginosa* and *Legionella pneumophila* in drinking water biofilms grown on domestic plumbing materials. *International Journal of Hygiene and Environmental Health*, *213*(3), 190–197.

Morton, Zhang, & Edwards. (2005). Implications of nutrient release from iron metal for microbial regrowth in water distribution systems. *Water Research*, *39*(13), 2883–2892.

Müller, & Nebe-Von-Caron. (2010). Functional single-cell analyses: Flow cytometry and cell sorting of microbial populations and communities. *FEMS Microbiology Reviews*, *34*(4), 554–587.

Muster, Gotama, Gould, De Silva, Beale, Burn, & Davis. (2011). *Cement mortar linings in cast and ductile iron pipes: Life expectancy and dependence upon water chemistry* (Vol. 2).

Muyzer. (1999). DGGE/TGGE a method for identifying genes from natural ecosystems. *Current Opinion in Microbiology*, *2*(3), 317–322.

Nescerecka, Juhna, & Hammes. (2018). Identifying the underlying causes of biological instability in a full-scale drinking water supply system. *Water Research*, *135*, 11–21.

Neville. (2001). Effect of cement paste on drinking water. *Materials and Structures*, *34*(240), 367–372.

Nie, Liu, Chen, Liu, & Ao. (2016). Flow cytometric assessment of the effects of chlorine, chloramine, and UV on bacteria by using nucleic acid stains and 5-cyano-2,3-ditolyltetrazolium chloride. *Frontiers of Environmental Science and Engineering*, *10*(6).

Niquette, Servais, & Savoir. (2001). Bacterial dynamics in the drinking water distribution system of Brussels. *Water Research*, *35*(3), 675–682.

Oki, & Kanae. (2006). Global Hydrological Cycles and Water Resources. *Freshwater Resources*, *313*, 1068–1072.

Prest, Hammes, Kötzsch, van Loosdrecht, & Vrouwenvelder. (2013). Monitoring microbiological changes in drinking water systems using a fast and reproducible flow cytometric method. *Water Research*, *47*(19), 7131–7142.

Prest, Hammes, van Loosdrecht, & Vrouwenvelder. (2016). Biological stability of drinking water: Controlling factors, methods, and challenges. *Frontiers in Microbiology*, *7*(2).

Proctor, Besmer, Langenegger, Beck, Walser, Ackermann, … Hammes. (2018). Phylogenetic clustering of small low nucleic acid-content bacteria across diverse freshwater ecosystems. *ISME Journal*, 1–16.

Proctor, Gächter, Kötzsch, Rölli, Sigrist, Walser, & Hammes. (2016). Biofilms in shower hoses – choice of pipe material influences bacterial growth and communities. *Environmental Science: Water Research and Technology*, *2*(4), 670–682.

Props, Monsieurs, Mysara, Clement, & Boon. (2016). Measuring the biodiversity of microbial communities by flow cytometry. *Methods in Ecology and Evolution*, *7*(11), 1376–1385.

Rabaey, & Verstraete. (2015). *Biotechnological processes in environmental sanitation*. Ghent Univeristy.

Rahman. (2014). *Introduction to Flow Cytometry*. Oxford: AbD Serotec.

Ramseier, von Gunten, Freihofer, & Hammes. (2011). Kinetics of membrane damage to high (HNA) and low (LNA) nucleic acid bacterial clusters in drinking water by ozone, chlorine, chlorine dioxide, monochloramine, ferrate(VI), and permanganate. *Water Research*, *45*(3), 1490–1500.

Reasoner. (2004). Heterotrophic plate count methodology in the United States. *International Journal of Food Microbiology*, *92*(3), 307–315.

Reiff. (1995). Balancing the chemical and microbial risks in the disinfection of drinking water supplies in developing countries. International Association Hydrological Sciences Publications.

Rice, Baird, Eaton, & Clesceri. (2012). *Standard Methods for the Examination of Water and Wastewater* (22nd ed.). American Public Health Association, American Water Works Association, Water Environment Federation.

Rogers, & Holyst. (2009). FlowFP: A Bioconductor Package for Fingerprinting Flow Cytometric Data. *Advances in Bioinformatics*, *2009*, 1–11.

Rogers, Moser, Holyst, Bantly, Mohler, Scangas, & Moore. (2008). Cytometric fingerprinting: Quantitative characterization of multivariate distributions. *Cytometry Part A*, *73*(5), 430–441.

Rompré, Servais, Baudart, De-Roubin, & Laurent. (2002). Detection and enumeration of coliforms in drinking water: current methods and emerging approaches. *Journal of Microbiological Methods*, *49*(1), 31–54.

Rossman, Clark, & Grayman. (1995). Modelling chlorine residuals in drinking-water distribution systems. *Journal of Environmental Engineering*, *120*(4), 803–820.

Rożej, Cydzik-Kwiatkowska, Kowalska, & Kowalski. (2015). Structure and microbial diversity of biofilms on different pipe materials of a model drinking water distribution systems. *World Journal of Microbiology & Biotechnology*, *31*(1), 37–47.

Rusin, Rose, Haas, & Gerba. (1997). *Reviews of Environmental Contamination and Toxicology*. (Ware, Ed.) (1st ed., Vol. 152). New York: Springer.

Sakakibara, Murakami, Hattori, Nakajima, & Imai. (1997). Enzymatic treatment to eliminate the extracellular ATP for improving the detectability of bacterial intracellular ATP. *Analytical Biochemistry*, *250*(2), 157–161.

Sarin, Snoeyink, Lytle, & Kriven. (2004). Iron corrosion scales: model for scale growth, iron release, and

colored water formation. *Journal of Environmental Engineering*, *130*(4), 364–373.

Sarker, Patel, Heitz, & Anwar. (2018). Evaluation of zinc and copper for co-inhibition of nitrification in mild nitrified drinking water. *Journal of Environmental Chemical Engineering*, *6*(2), 2939–2943.

Sedlak. (2014). *Water 4.0: the past, present, and future of the world's most vital resource*. Yale University Press.

Shang, Uber, & Rossman. (2008). Modeling reaction and transport of multiple species in water distribution systems. *Environmental Science and Technology*, *42*(3), 808–814.

Shapiro. (2005). *Practical Flow Cytometry*. Wiley.

Shuler, Aris, & Tsuchiya. (1972). Hydrodynamic focusing and electronic cell-sizing techniques. *Applied Microbiology*, *24*(3), 384–388.

Staley, & Konopka. (1985). Measurement of in situ activities of nonphotosynthetic microorganisms in aquatic and terrestrial habitats. *Annual Reviews in Microbiology*, *39*(1), 321–346.

Stocks. (2004). Mechanism and use of the commercially available viability stain, BacLight. *Cytometry Part A*, *61*(2), 189–195.

Templeton, Hofmann, & Andrews. (2006). Case study comparisons of computational fluid dynamics (CFD) modeling versus tracer testing for determining clearwell residence times in drinking water treatment. *Journal of Environmental Engineering*, *5*(6), 529–536.

Teunis, Medema, Kruidenier, & Havelaar. (1997). Assessment of the risk of infection by *Cryptosporidium* or *Giardia* in drinking water from a surface water source. *Water Research*, *31*(6), 1333–1346.

Tryby, Boccelli, Koechling, Uber, Summers, & Rossman. (1999). Booster chlorination for managing disinfectant residuals. *Journal American Water Works Association*, *91*(1), 95–108.

United Nations. (1997). *Comprehensive assessment of the freshwater resources of the world*. Stockholm.

USACE. (2013). Baltimore district: water treatment process. Retrieved December 27, 2017, from http://www.nab.usace.army.mil/Missions/Washington-Aqueduct/Treatment-Process/

US Congress. (1996). Safe Drinking Water Act (SDWA). *Public Health Service Act*, 964–1043.

US EPA. (1998). National Primary Drinking Water Regulations: Disinfectant and Disinfection byproducts. *Federal Register*, *63*(241), 69390–69476.

US EPA. (2001). Potential Contamination Due to Cross-Connections and Backflow and the Associated Health Risks. Washington DC: United States Environmental Protection Agency.

US EPA. (2002a). Health Risks from Microbial Growth and Biofilms in Drinking Water Distribution Systems. Washington DC: United States Environmental Protection Agency.

US EPA. (2002b). National Primary Drinking Water Regulations: Long Term 1 Enhanced Surface Water Treatment Rule. *Federal Register*, *69*(9), 1812–1817.

US EPA. (2003a). The potential for health risks from intrusion of contmainants into the distribution system from pressure transients. *Distribution System Issue Paper*.

US EPA. (2003b). Water on tap: what you need to know.

US EPA. (2004a). National Primary Drinking Water Regulations. In *Code of Federal Regulations* (40th ed.). Washington DC: United States Environmental Protection Agency.

US EPA. (2004b). National Secondary Drinking Water Regulations. In *Code of Federal Regulations* (40th ed.). Washington DC: United States Environmental Protection Agency.

US EPA. (2006). National Primary Drinking Water Regulations: Ground Water Rule. *Federal Register*, *71*(216), 65573–65660.

US EPA. (2010). Priorities of the Distribution System Research and Information Collection Partnership. Washington DC: United States Environmental Protection Agency.

US EPA. (2013). National Primary Drinking Water Regulations: Revisions to the Total Coliform Rule. *Federal Register*, *78*(30), 10270–1365.

van der Hoek, Bertelkamp, Verliefde, & Singhal. (2014). Drinking water treatment technologies in Europe: state of the art – challenges – research needs. *Journal of Water Supply: Research and Technology*, *63*(2), 124.

van der Kooij, Visser, & Hijnen. (1982). Determining the concentration of easily assimilable organic carbon in drinking water. *Journal American Water Works Association*, *V 74*(N 10), 540–545.

van der Wielen, & van der Kooij. (2013). Nontuberculous mycobacteria, fungi, and opportunistic pathogens in unchlorinated drinking water in the Netherlands. *Applied and Environmental Microbiology*, *79*(3), 825–834.

Van Nevel. (2014). *Growth and flow cytometric monitoring of bacteria in drinking water*. Ghent University.

Van Nevel, Buysschaert, De Gusseme, & Boon. (2016). Flow cytometric examination of bacterial growth in a local drinking water network. *Water and Environment Journal*, *30*(1–2), 167–176.

Van Nevel, Buysschaert, De Roy, De Gusseme, Clement, & Boon. (2017). Flow cytometry for immediate follow-up of drinking water networks after maintenance. *Water Research*, *111*, 66–73.

Van Nevel, Koetzsch, Proctor, Besmer, Prest, Vrouwenvelder, … Hammes. (2017). Flow cytometric bacterial cell counts challenge conventional heterotrophic plate counts for routine microbiological drinking water monitoring. *Water Research*, *113*, 191–206.

Vandekerckhove. (2014). *Ontwikkelingsstrategieën voor thermofiele nitrificatie ter behandeling van warm afvalwater*. Ghent University.

Veal, Deere, Ferrari, Piper, & Attfield. (2000). Fluorescence staining and flow cytometry for monitoring microbial cells. *Journal of Immunological Methods*, *243*(1–2), 191–210.

Venkobachar, Iyengar, & Prabhakara Rao. (1977). Mechanism of disinfection: effect of chlorine on cell membrane functions. *Water Research*, *11*(8), 727–729.

Vermijs. (2017). *Flow cytometric monitoring of process water*. Ghent University.

Vikesland, Ozekin, & Valentine. (2001). Monochloramine decay in model and distribution system waters. *Water Research*, *35*(7), 1766–1776.

Volk, Dundore, Schiermann, & Lechevallier. (2000). Practical evaluation of iron corrosion control in a drinking water distribution system. *Water Research*, *34*(6), 1967–1974.

Wade Miller. (2006). Integrated concepts in water reuse: Managing global water needs. *Desalination*, *187*(1–3), 65–75.

Wang, Edwards, Falkinham III, & Pruden. (2013). Probiotic approach to pathogen control in premise plumbing systems? A review. *Environmental Science and Technology*, *47*(18), 10117–10128.

Wang, Hammes, Boon, Chami, & Egli. (2009). Isolation and characterization of low nucleic acid (LNA)-content bacteria. *ISME Journal*, *3*(8), 889–902.

Wang, Hu, Hu, Yang, & Qu. (2012). Effects of disinfectant and biofilm on the corrosion of cast iron pipes in a reclaimed water distribution system. *Water Research*, *46*(4), 1070–1078.

Water in the West. (2013). Water Energy Nexus: Literature Review, 146.

Westbrook, & Digiano. (2009). Rate of chloramine decay at pipe surfaces. *Journal American Water Works Association*, *101*(7).

Whitehead, Kricka, Carter, & Thorpe. (1979). Analytical luminescence: its potential in the clinical laboratory. *Clinical Chemistry*, *25*(9), 1531–1546.

Whittaker. (1972). Evolution and Measurement of Species Diversity. *Taxon*, *21*(2/3), 213–251.

WHO. (2005a). *Bromate in Drinking-water*. *Background document for development of WHO Guidelines for Drinking-water Quality*. Geneva.

WHO. (2005b). *Chlorite and Chorate in Drinking-water*. *Background document for development of WHO Guidelines for Drinking-water Quality*. Geneva.

WHO. (2011). Guidelines for drinking-water quality. *World Health Organization*. Geneva.

Williams, LeBel, & Benoit. (1997). Disinfection by-products in Canadian drinking water. *Chemosphere*, *34*(2), 299–316.

Yang, Cheng, Li, Yu, Gin, Chen, & Reinhard. (2017). Effects of monochloramine and hydrogen peroxide on the bacterial community shifts in biologically treated wastewater. *Chemosphere*, *189*, 399–406.

Zhang, & DiGiano. (2002). Comparison of bacterial regrowth in distribution systems using free chlorine and chloramine: A statistical study of causative factors. *Water Research*, *36*(6), 1469–1482.

Zhang, & Edwards. (2010). Nutrients and metals effects on nitrification in drinking water systems. *Journal American Water Works Association*, *102*(7), 56–66.

Zhang, Love, & Edwards. (2009). Nitrification in drinking water systems. *Critical Reviews in Environmental Science and Technology*, *39*(3), 153–208.

Appendix 1: Calibration of pumps

Both of the pumps used in the experimental setup of the lab scale water tower were calibrated within the range of interest, using the Masterflex® 6404-13 tubing. Peristaltic pumps, which are generally less sensitive to pressure gradients, were used. However, to minimize calibration errors, the pumps were calibrated only after the experimental setup. The calibration itself was performed by setting a number of revolutions per minute (rpm) on the pump head and measuring the pumped volume after a certain time interval. The flow rate can be calculated. The linear relation between the flow rate and the revolutions per minute allows an easy conversion of the desired flow rates to rpm by the use of a linear trend line (**figure A1.1** and **figure A1.2**).

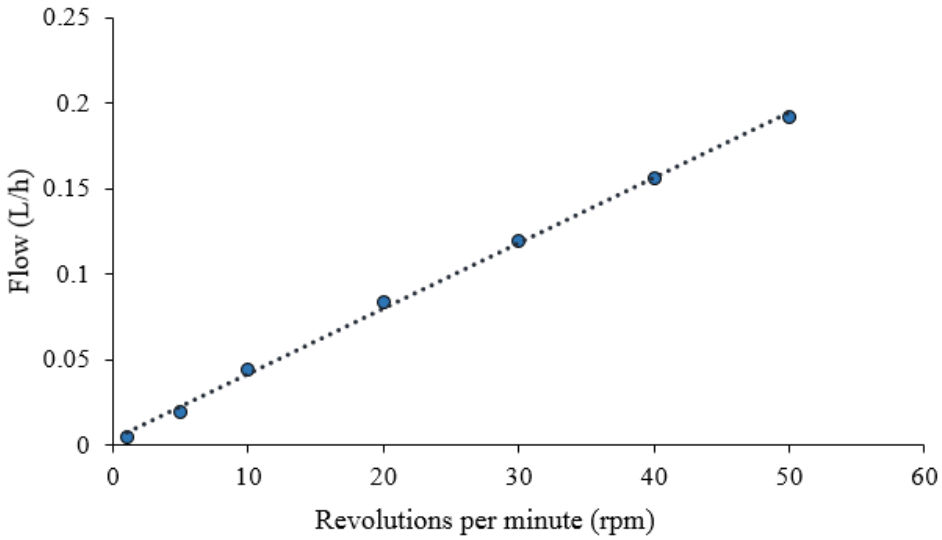

Figure A1.1 – Calibration of the Watson-Marlow® 101U pump with Masterflex® 6404-13 tubing.

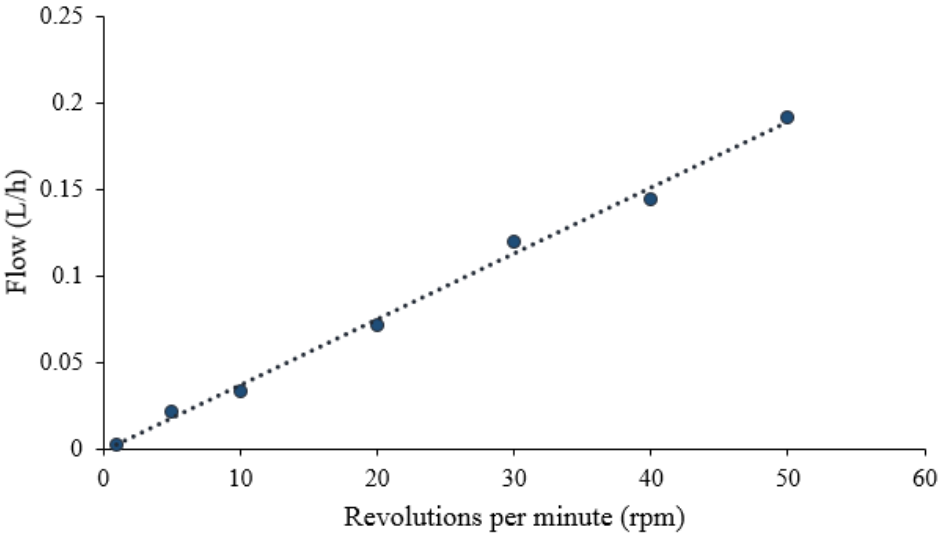

Figure A1.2 – Calibration of the Masterflex® L/S® pump with Masterflex® 6404-13 tubing.

The used flow rates are together with the revolutions per minute (rpm) given in **table A1.1** for each incoming stream.

Table A1.1 – Flow rates at each "surface water"/"groundwater" ratio of drinking water feed streams expressed in L/h and the revolutions per minute (rpm). The Watson-Marlow® 101U pump was used for the feed produced from surface water, and the Masterflex® L/S® pump was used for pumping of the feed produced from groundwater.

Q_{surf} (%)	Q_{surf} (L/h)	Revolutions per minute (rpm)	Q_{ground} (%)	Q_{ground} (L/hr)	Revolutions per minute (rpm)
90	0.122	31	10	0.014	4
80	0.108	28	20	0.027	7
70	0.095	24	30	0.041	11
60	0.081	20	40	0.054	15
50	0.068	17	50	0.068	18
40	0.054	13	60	0.081	22
30	0.041	10	70	0.095	25
20	0.027	6	80	0.108	29

Appropriate gates were chosen based on heat killed samples that were SGPI stained (**figure A2.1**). The same gate was applied on the SG-stained samples as on the SGPI-stained samples. The gate for the permeabilized cells is located above the intact cell gate.

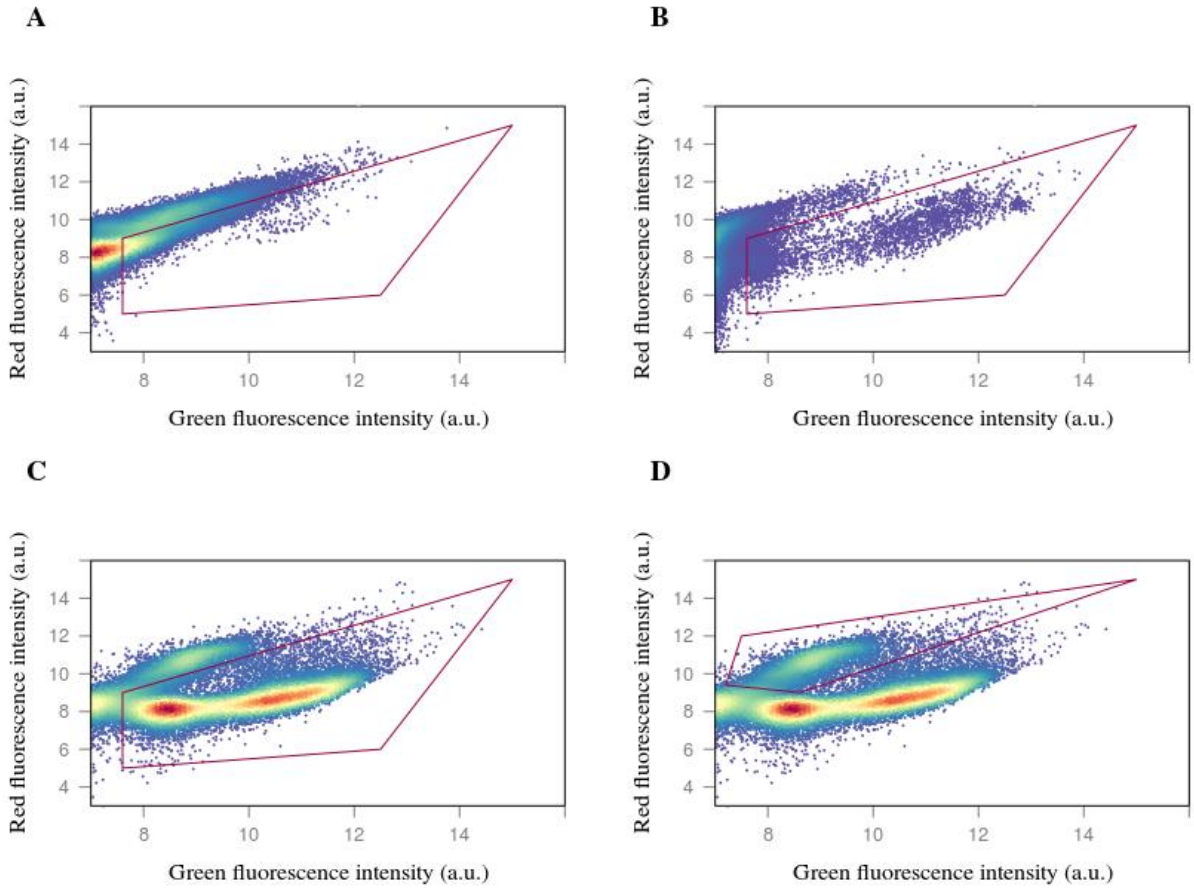

Figure A2.1 – Gating step. (**A**) Heat killed sample with gate for total/intact cells. (**B**) SG stained sample with gate for total cells. (**C**) SGPI stained sample with gate for intact cells. (**D**) SGPI stained sample with gate for permeabilized cells.

The alpha (*i.e.* within sample), and beta (*i.e*. between sample) diversities are calculated from the SG stained sample, since the SG dataset is more extended. Furthermore, the phenotypic diversity profiles are similar for the SGPI and SG fingerprints.

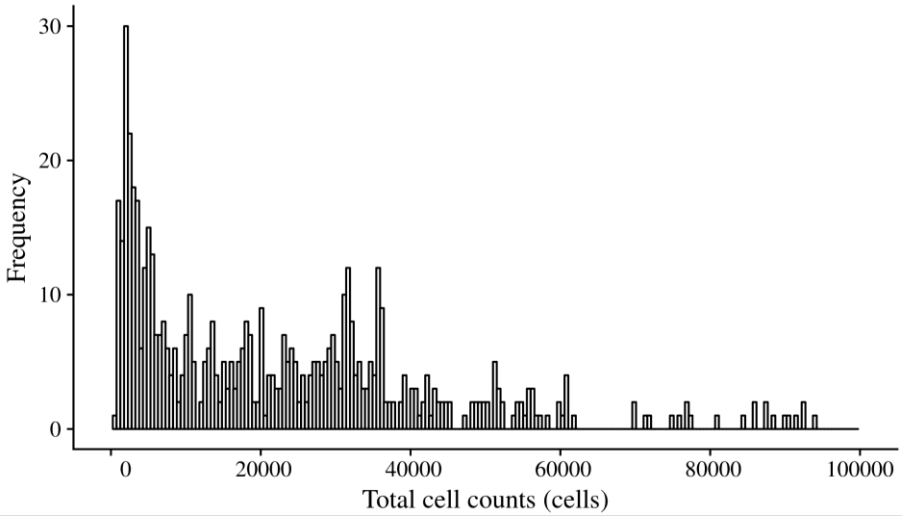

Figure A2.2 – Histogram of the total cell counts for all samples. The total cell counts are the total events that have been detected within the respective gate. One outlying sample (total cell counts > 250000) was removed from the dataset.

One sample was randomly selected from the DC Water dataset and used as a test sample to evaluate the sensitivity of the diversity metrics towards low sample sizes (*i.e.* number of cells). The sample was subsampled to different sample sizes and subsequently the diversity metrics were calculated (**figure A2.3**). For each of the selected sample sizes, the diversity for 100 bootstrap samples (sampling with replacement) was evaluated. This analysis indicated the highest sensitivity for D_0 and a lower sensitivity for D_1 and D_2.

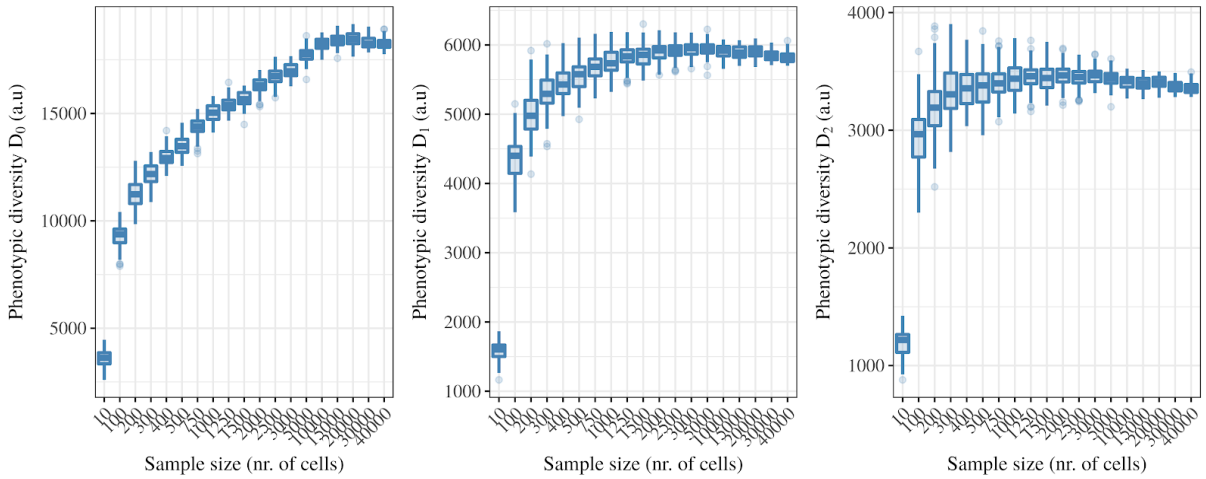

Figure A2.3 – The effect of the sample size on the phenotypic alpha diversity (n = 100).

Since the cell counts in the drinking water are low (**figure A.2.2**), the selected threshold for the calculation of the phenotypic alpha diversity is 3,000 cells instead of the desired threshold of 10,000 cells. All samples with lower cell counts were excluded for phenotypic diversity analysis. Using this threshold, the phenotypic alpha diversity metrics D_1 and D_2 can be calculated accurately (**figure A2.3**). They are strongly correlated (r_p = 0.97, p < 0.001). At this level the calculated phenotypic richness D_0 is an underestimation of the true phenotypic richness. The phenotypic

richness is also correlated to the D_2 ($r_p = 0.75$, $p < 0.001$). The D_2 phenotypic alpha diversity is thus considered to be representative as a phenotypic alpha diversity metric for this dataset. In this work, discussion and conclusions are thus solely based on D_2 analysis.

Appendix 3: Activity test of nitrifying bacteria in drinking water

An activity test was performed to estimate the maximal growth rate (μ_{max}) and the initial biomass concentration (X_o) of the nitrifiers present in the bulk drinking water.

Materials and methods

A sample (16 - 18L) from all hydrants was taken to the lab, and covered by a perforated film to prevent contamination and at the same time avoiding oxygen limitation. At the start of the experiment, chlorine was measured and was quenched using a sodium thiosulfate concentrate solution if > 0.1mg Cl_2/L was present. The pH was followed up throughout the experiment using a Hach® SL1000 equipped with pH probe (Hach, Colorado, United States), and was corrected when < 7, using NaOH. The temperature was constant throughout the experiment (23.7 ± 0.4°C). Ammonia, in the form of the salt NH_4Cl, was spiked at the beginning of the experiment, as 5mg N/L. The ammonia consumption, and nitrite and nitrate production were followed up over time using Hach® TNTplus Vial Tests (Hach, Colorado, United States).

The activity test was performed as a high F/M (food/mass, or ammonia/nitrifying biomass) test, based on Melcer (2004). This way, substrate limitation is avoided, and the growth rate during the exponential phase of the experiment will consequently equal the μ_{max}. A few assumptions were made in order to calculate μ_{max} and X_o. First, as the substrate was added in excess, the growth rate during the exponential phase of the experiment was assumed to equal the maximal growth rate. Also, the dissolved oxygen in the water is assumed to not be growth limiting. Furthermore, it was assumed that only autotrophic nitrification was taking place.

Based on Melcer (2004), equations that describe the ammonia consumption and the nitrite and nitrate production were derived to estimate μ_{max} and X_o. The autotrophic nitrifier growth rate $r_{X,AUT}$ (g biomass/L/d) was described as in **eq. A5.1**, with μ_{max} the maximal growth rate (1/d), X_{AUT} the biomass concentration (g biomass/L), S_{Am} the ammonia concentration (mg N/L) and $K_{s,Am}$ the half saturation constant (mg N/L).

$$r_{X,AUT} = \frac{\mu_{max} * S_{Am}}{S_{Am} + K_{s,Am}} * X_{AUT} \quad \textbf{(eq. A5.1)}$$

As the growth rate equalled the maximal growth rate μ_{max} in the high F/M test, this could be rewritten based on the Monod equation (**eq. A5.2**).

$$r_{X,AUT} = \mu_{max} * X_{AUT} \quad \textbf{(eq. A5.2)}$$

The nitrite/nitrate production rate and the ammonia consumption rate was obtained by dividing through the nitrification yield coefficient Y_{AUT} (g N/g biomass) (**eq. A5.3**).

$$r_{Nx} = \sum \frac{\mu_{max}}{Y_{AUT}} * X_{AUT} \quad \textbf{(eq. A5.3)}$$

r_{Nx} represents the production rate for nitrite or nitrate (g N/L/d), and can be written out for each nitrogen compound depending on the contributing nitrifying organisms (**eq. A5.4 - eq. A5.6**).

$$\frac{dNH_3}{dt} = \frac{-\mu_{max,AOB}}{Y_{AOB}} * X_{AOB} \quad \textbf{(eq. A5.4)}$$

$$\frac{dNO_2^-}{dt} = \frac{\mu_{max,AOB}}{Y_{AOB}} * X_{AOB} - \frac{\mu_{max,NOB}}{Y_{NOB}} * X_{NOB} \quad \textbf{(eq. A5.5)}$$

$$\frac{dNO_3^-}{dt} = \frac{\mu_{max,NOB}}{Y_{NOB}} * X_{NOB} \quad \textbf{(eq. A5.6)}$$

Also, the biomass concentrations X_{AOB} and X_{NOB} were variable as both growth and decay were assumed to occur during the course of the experiment. Both biomass concentrations could be described by **eq. A5.7**, in which X_{AUT} indicated general biomass concentration (g biomass/L) and b_{AUT} the decay coefficient (1/d).

$$\frac{dX_{AUT}}{dt} = (\mu_{AUT} - b_{AUT}) * X_{AUT} \quad \textbf{(eq. A5.7)}$$

Integration of **eq. A5.7** with $t_o = 0$, gave (**eq. A5.8**):

$$X_{t,AUT} = X_{o,AUT} * [e^{(\mu_{AUT} - b_{AUT}) * t} - 1] \quad \textbf{(eq. A5.8)}$$

Substitution of **eq. A5.8** in **eq. A5.4 - eq. A5.6** resulted in three general equations that describe the change of ammonia, nitrite and nitrate concentrations over time (**eq. A5.9 - A5.11**).

$$[NH_3]_t = [NH_3]_o - \frac{\mu_{max,AOB}}{Y_{AOB}} * X_{o,AOB} * [e^{(\mu_{max,AOB} - b_{AOB}) * t} - 1] \quad \textbf{(eq. A5.9)}$$

$$[NO_2^-]_t = [NO_2^-]_o + \frac{\mu_{max,AOB}}{Y_{AOB}} * X_{o,AOB} * \left[e^{(\mu_{max,AOB} - b_{AOB}) * t} - 1\right] - \frac{\mu_{max,NOB}}{Y_{NOB}} * X_{o,NOB} * [e^{(\mu_{max,NOB} - b_{NOB}) * t} - 1] \quad \textbf{(eq. A5.10)}$$

$$[NO_3^-]_t = [NO_3^-]_o \frac{\mu_{max,NOB}}{Y_{NOB}} * X_{o,NOB} * [e^{(\mu_{max,NOB} - b_{NOB}) * t} - 1] \quad \textbf{(eq. A5.11)}$$

The obtained equations were used to estimate μ_{max} and X_o. Based on the detailed research performed by Melcer (2004), the following estimations for decay rates and nitrification yield coefficients were used:

$b_{AOB} = b_{NOB} = 0.17$ (1/d) at 20°C

$Y_{AOB} = 0.15, Y_{NOB} = 0.09$ (g N/g biomass)

Note that the decay coefficient was temperature dependent, so a correction was applied using an Arrhenius constant of 1.029 (Melcer 2004). The final decay rate was calculated depending on the mean temperature T (°C) of the hydrant sample during the course of the experiment as described in **eq. A5.12**.

$$b_{AOB} = b_{NOB} = b_{AUT,20°C} * 1.029^{(T-20°C)} \quad \textbf{(eq. A5.12)}$$

Results and discussion

Based on the parameter estimations and the obtained equations, μ_{max} and X_o were predicted by minimizing the sum of the squared residual between the measured concentrations and the calculations (Excel v2013 Solver). Only the exponential growth phase was taken into account for the predictions. As the nitrate measurements showed interference, only the AOB growth rate and initial biomass concentration could be calculated (**table A5.1**). The initial ammonia and nitrite concentration was also estimated as a cross-validation.

Table A5.1 - Estimations of the maximal growth rate and the initial biomass concentration of autotrophic AOB based on the outcome of the activity test. Also the NH_3 and NO_2^- concentrations at the start of the experiment were estimated.

Hydrant	**$\mu_{max,AOB}$ (1/d)**	**$X_{o,AOB}$ (mg COD/L)**	**$[NH_3]_o$ (mg N/L)**	**$[NO_2^-]_o$ (mg N/L)**
West	0.76	0.05	5.10	0.26
South	0.57	0.05	5.87	0.07
NE 1	0.90	0.02	4.93	0.10
NE 2	0.90	0.02	4.98	0.31
SE 1	0.76	0.05	5.12	0.10
SE 2	0.87	0.03	5.02	0.07
NW 1	0.90	0.05	5.11	0.32
NW 2	0.90	0.04	5.05	0.21

The initial ammonia and nitrite concentration were resp. approximately 5mg N/L and 0.2mg N/L, which was close to the model predictions. They were consequently assumed to be accurate. Melcer (2004) noted that the μ_{max} would be around $0.9d^{-1}$. The obtained results were close to this number. Furthermore, the results were similar to the maximal growth rate of *Nitrosomonas* (μ_{max} = $0.84d^{-1}$), an AOB genus that is prevalent in drinking water, as determined by Keen & Prosser (1987). These results indicate that the autotrophic AOB may be present and active in the drinking water bulk. To be able to estimate the NOB activity, it is suggested to repeat the experiment and use a different nitrate measurement method. Note that theoretically, it would be possible to only use nitrite measurements for NOB activity tests. In practice it has not been feasible to obtain plausible results solely based on nitrite measurements in this experimental setup.

Appendix 4: Preliminary evaluation of zinc as nitrifying activity inhibitor

The goal of this preliminary experiment was to evaluate the inhibitory effect of zinc on the activity of nitrifying drinking water biofilm. With an eye on future applications in drinking water, zinc may be dosed as its phosphate salt, since phosphate is currently added in DWDS as corrosion inhibitor. Therefore, the effect of (zinc) phosphate on nitrifying activity was also evaluated.

Materials and methods

The experiment was performed in a 96 well plate, with a working volume of 250µL. 50µL hereof consisted of a nitrifying biomass concentrate. This concentrate was extracted from a drinking water sand filter biofilm by vortexing and subsequent isolation of the supernatant three times. The remaining volume (200µL) consisted of tap water containing three concentrations of zinc (1, 2 and 3mg Zn/L), zinc phosphate (1, 2 and 3 mg Zn/L) or phosphate (equivalent of 1, 2 and 3mg Zn/L). All solutions were tested in triplicates. Zinc was dosed as the salt $ZnCl_2$ and phosphate as KH_2PO_4. Three controls were evaluated in triplicates as well: MilliQ without nitrifying biomass, and drinking water with and without nitrifying biomass. Samples were kept at a constant temperature of 15°C to eliminate temperature-dependent fluctuations. Initially, ammonium was spiked at 15mg N/L in all samples. Liquid samples (2µL) were taken for ammonium analyses during two weeks. The ammonium concentration was determined in a high-throughput measurement as optimized by Vandekerckhove (2014) and described by Courtens et al. (2016). Results were obtained colorimetrically using a Tecan infinite plate reader (Tecan Trading AG, Switzerland).

Results and discussion

The results are shown in **table A4.1**. From the control samples, it was observed that nitrification was also taking place, to a lesser extent, without addition of nitrifying biomass. The zinc samples showed a lower ammonium conversion than the control "DW + nitr.", but the difference was not significant when taking the standard deviations into account. This makes it hard to base reliable conclusions on the preliminary data. These results indicate that lower concentrations of zinc are not effective against nitrifying activity in drinking water. Moreover, dosing of zinc phosphate even seemed to increase the nitrification activity. Furthermore, zinc inhibition is hypothesized to be attributed to precipitation of phosphorus nutrients and by delaying chloramine decay (Harper et al. 1996; Sarker et al. 2018). Thus when adding zinc phosphate, the effect of zinc would be negated. Moreover, the added phosphate may even be used as nutrient by nitrifying bacteria, as almost all

samples with additional phosphate showed an increased ammonium conversion.

Table A4.1 - Ammonium concentrations at the beginning and at the end (after two weeks) of the experiment. Concentrations are expressed as the average of three replicates ± standard deviation. The last column indicates the difference in ammonium concentration between day 0 and day 14. DW = drinking water. Control samples consisted out of MilliQ, and drinking water with and without nitrifying biomass, without zinc or phosphate addition. Phosphate was added in "equivalents" zinc, *i.e.* the amount of phosphate that would be present when the respective concentration of zinc phosphate was added.

	$[NH_4^+]$ at 0 days (mg N/L)	**$[NH_4^+]$ at 14 days (mg N/L)**	**Δ $[NH_4^+]$ (mg N/L)**
Control			
MilliQ	13.21 ± 0.04	12.89 ± 0.99	0.31 ± 0.45
DW + nitr.	10.54 ± 0.17	0.98 ± 0.34	9.56 ± 0.92
DW - nitr.	10.59 ± 0.96	2.09 ± 0.14	8.50 ± 1.05
Zn^{2+}			
1 mg/L Zn	11.56 ± 0.60	2.29 ± 0.37	9.27 ± 0.34
2 mg/L Zn	11.71 ± 0.29	2.84 ± 0.82	8.86 ± 0.76
3 mg/L Zn	12.04 ± 0.36	2.58 ± 0.97	9.46 ± 1.22
PO_4^{3-}			
eq. 1 mg/L Zn	10.59 ± 0.47	0.00 + 0.22	10.59 ± 0.53
eq. 2 mg/L Zn	11.97 ± 0.46	1.87 ± 1.55	10.11 ± 0.62
eq. 3 mg/L Zn	10.92 ± 0.41	2.06 ± 0.34	8.85 ± 1.92
$Zn_3(PO_4)_2$			
1 mg/L Zn	10.79 ± 0.45	0.00 + 0.18	10.79 ± 0.68
2 mg/L Zn	11.09 ± 0.02	0.00 + 0.20	11.09 ± 1.53
3 mg/L Zn	11.27 ± 0.22	1.05 ± 1.53	10.22 ± 0.46

Appendix 5: TOC of water tower Kattenberg

The total organic carbon (TOC) concentrations and their fluctuations over time were provided by FARYS. The TOC is expressed as non-purgeable organic carbon (NPOC). At the water tower itself, only the outgoing stream is sampled (**figure A5.1**). The TOC values during the measurement period for the exiting stream, the feed produced from ground and surface water are resp. 1.4, 0.8 and 2.0mg/L TOC. The feed produced from groundwater is sampled at Merelbeke, which is the closest sampling point to the water tower. The feed produced from surface water is sampled in Buggenhout. At the water tower itself, only the outgoing water is sampled.

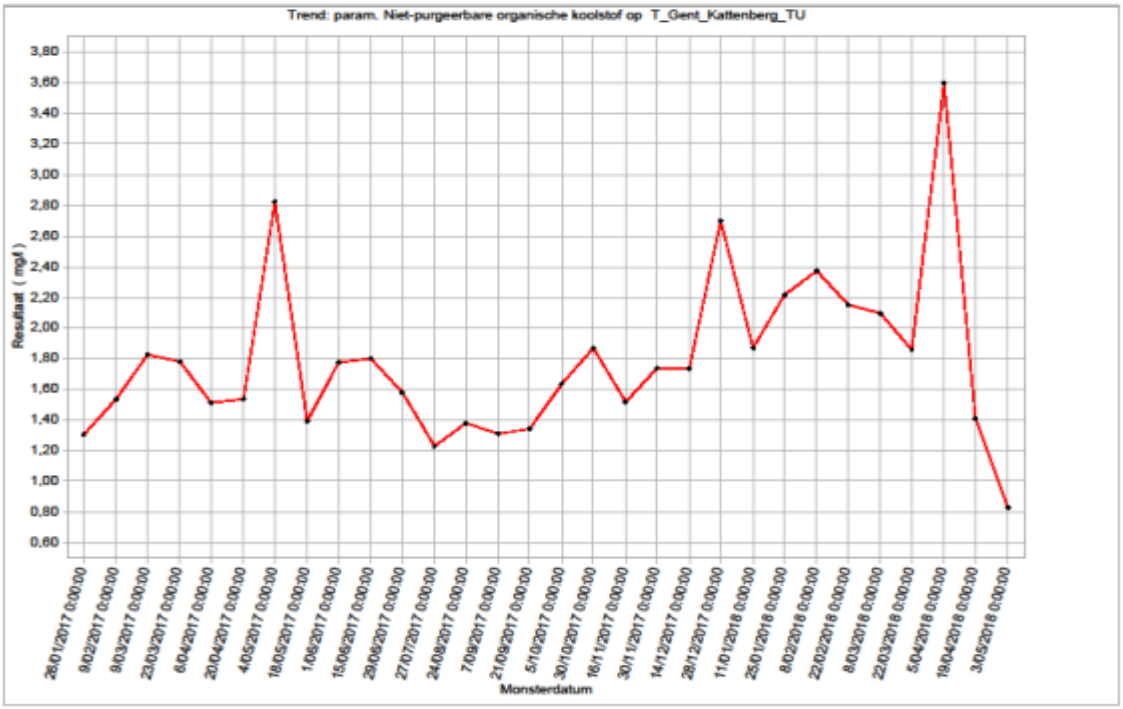

Figure A5.1 - Fluctuations in TOC over time of the outgoing water of the water tower Kattenberg (Gent). The values are expressed as NPOC.

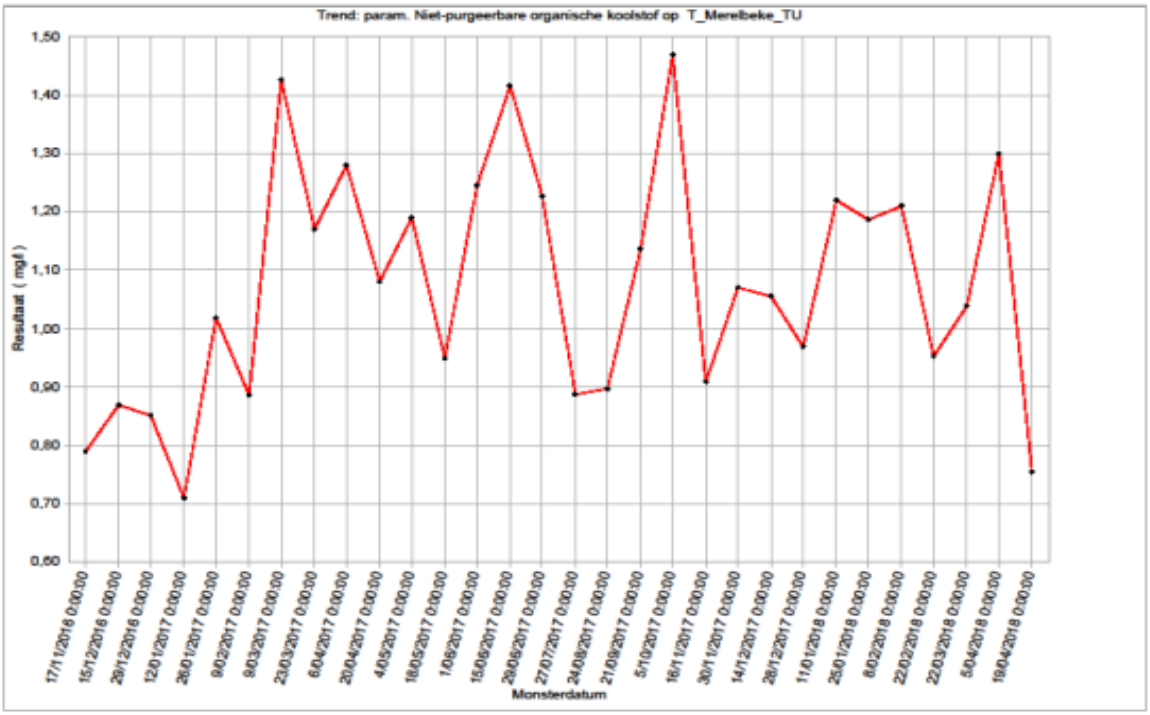

Figure A5.2 - Fluctuations in TOC of the water coming from Brakel over time, produced from groundwater. The values are expressed as NPOC.

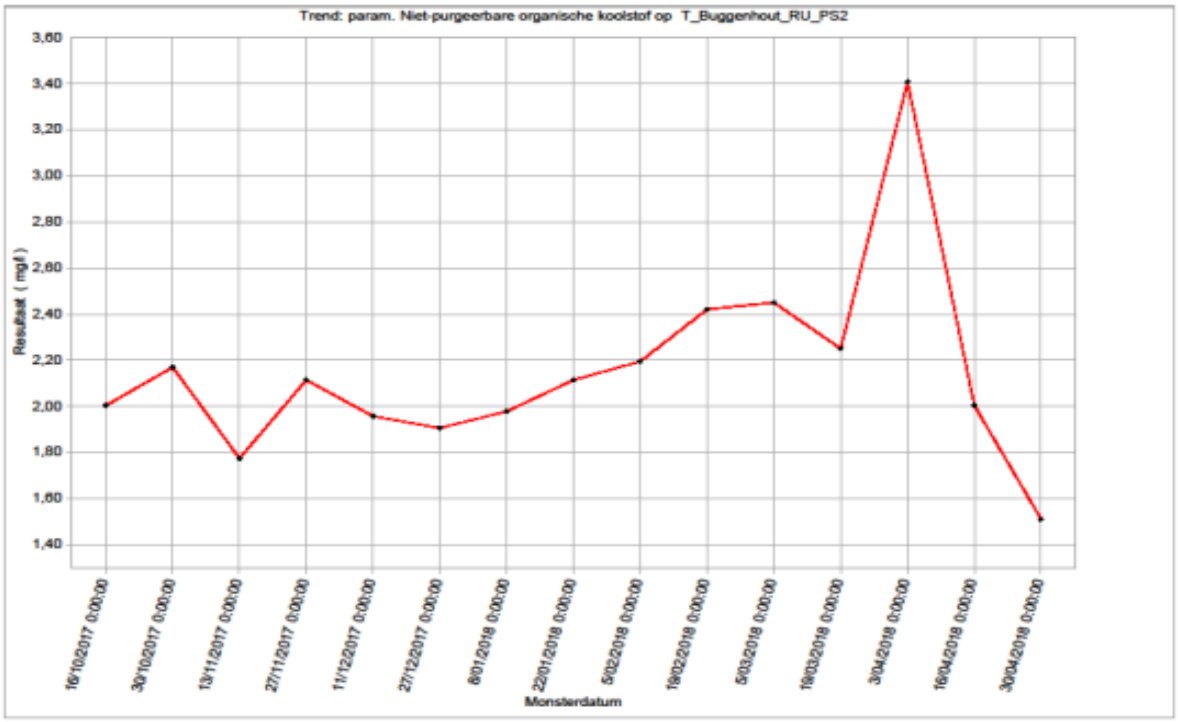

Figure A5.3 - Fluctuations in TOC of the water coming from Buggenhout over time, produced from surface water. The values are expressed as NPOC. The value at April 30th is unreliable due to a technical defect.

Appendix 6: Random Forest

The Random Forest (RF) algorithm is based on the creation of a large number of decision trees (Breiman 2001). It incorporates "bagging" as meta-algorithm, by building each tree based on a random subset (bootstrap) of the training data set (Breiman 1996). This way, the accuracy will increase and overfitting will be avoided. Overfitting means that the model is too adapted to the training data, so that extrapolation to new data results in bad predictions. The trees consist out of nodes at which a binary decision is taken based on a predictor of the data set. At each node, the algorithm is limited in its choice of predictors. Thus, only a subset of the predictor set is available at each split, *e.g.* two out of four parameters. This way, bias towards one predictor is avoided and the generated trees are decorrelated. When the trees are fully grown, they will all have obtained their own solution to the problem.

In Random Forest classification, feature space will be divided using decision boundaries. The outcome of Random Forest classifier is a set of trees, that all have "labelled" the new data point according to their outcome (**figure A6.1, A**). The outcome of the RF classification is the majority vote of all trees. For example, to determine the origin of a bacterial cell, all trees will either vote "surface water" or "groundwater". The final classification of the origin is thus the label that was predicted by most of the decision trees.

Random Forest regression is based on the same decorrelated tree-growing principle. However, the outcome of RF regression is the average of the outcomes of the trees. For example, when determining the percentage of surface water, all trees will obtain a predicted percentage (**figure A6.1, B**). The final output of the RF regression is the average of the predictions of all trees.

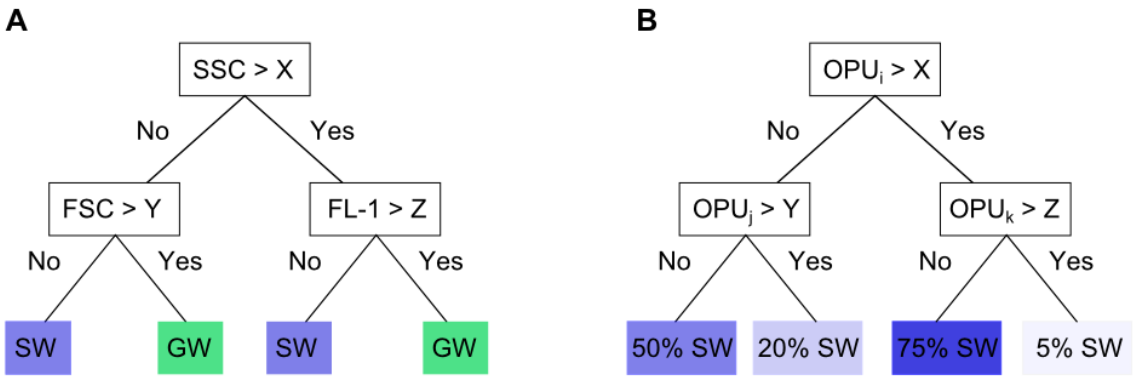

Figure A6.1 - Example of decision tree using (**A**) RF classification or (**B**) RF regression. The output of RF classification is a label, either "SW" (surface water) or "GW" (groundwater). The output of RF regression is an exact percentage surface water. When applied on FCM data, classification on a single-cell level will label cells according to their fluorescence or scatter characteristics, whereas regression on a population level will make decisions based on the density of the operational phenotypic units (OPU's).

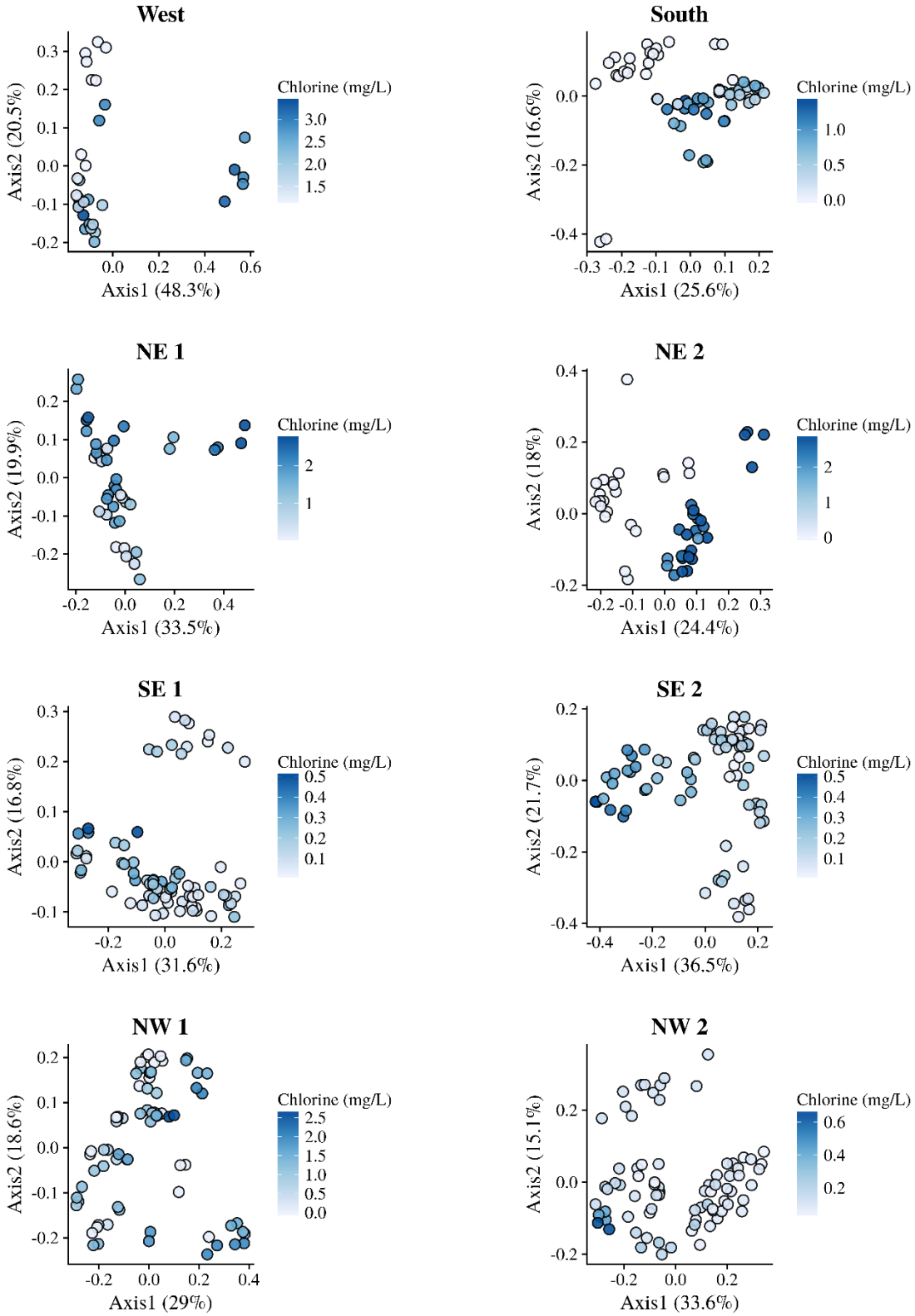

Figure A7.1 – PcoA ordination of phenotypic fingerprints for every hydrant (all flush times), coloured according to total chlorine concentration. Since the total chlorine concentration range is different for every hydrant, the scale is adapted for each hydrant.

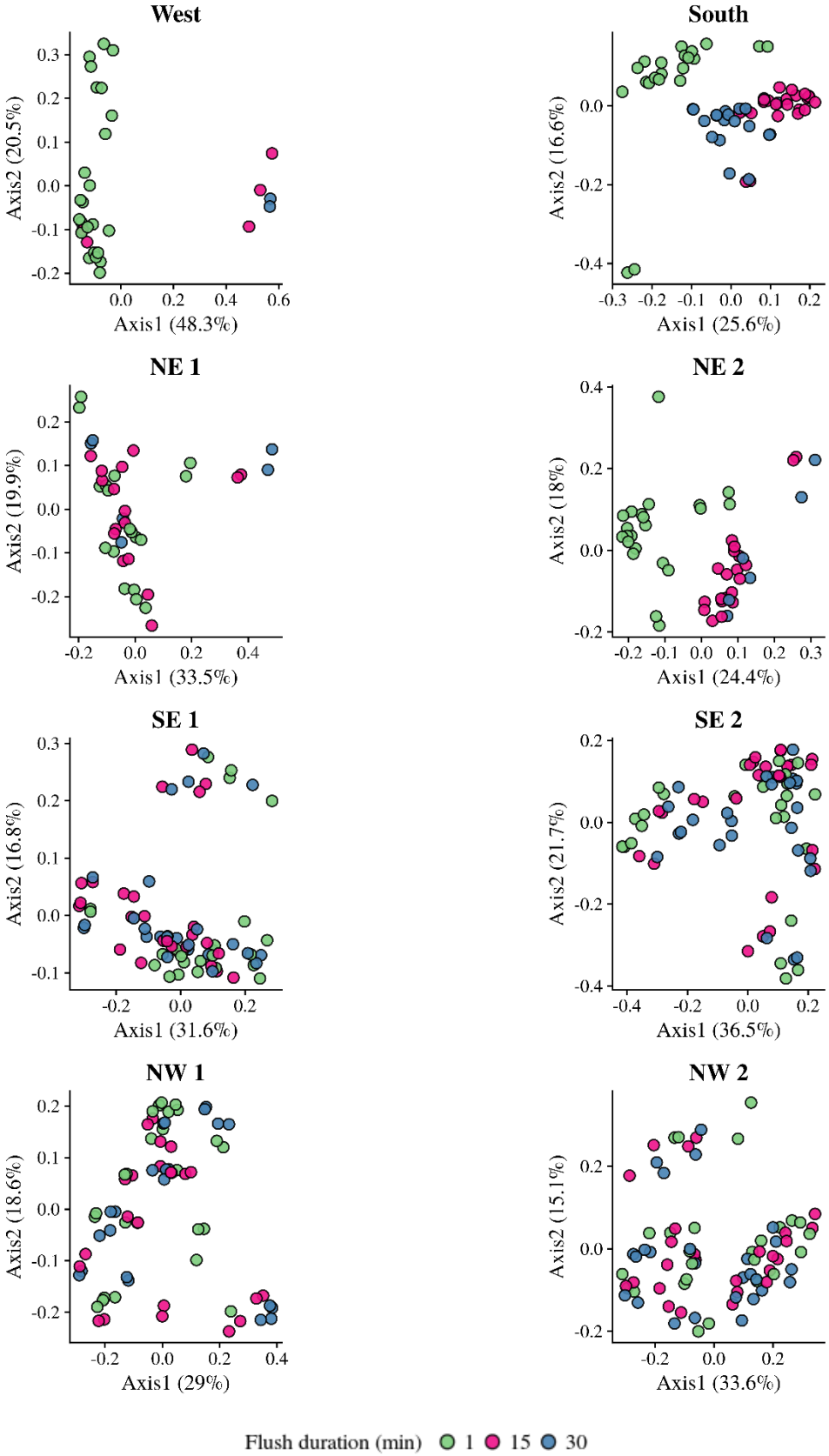

Figure A7.1 – PcoA ordination of phenotypic fingerprints for every hydrant, coloured according to flush duration. The phenotypic fingerprints after 1 minute of flushing of hydrants West, NE 2 and South are clearly separated. For the other hydrants, the distinction between phenotypic fingerprints is not explained by the flush duration.

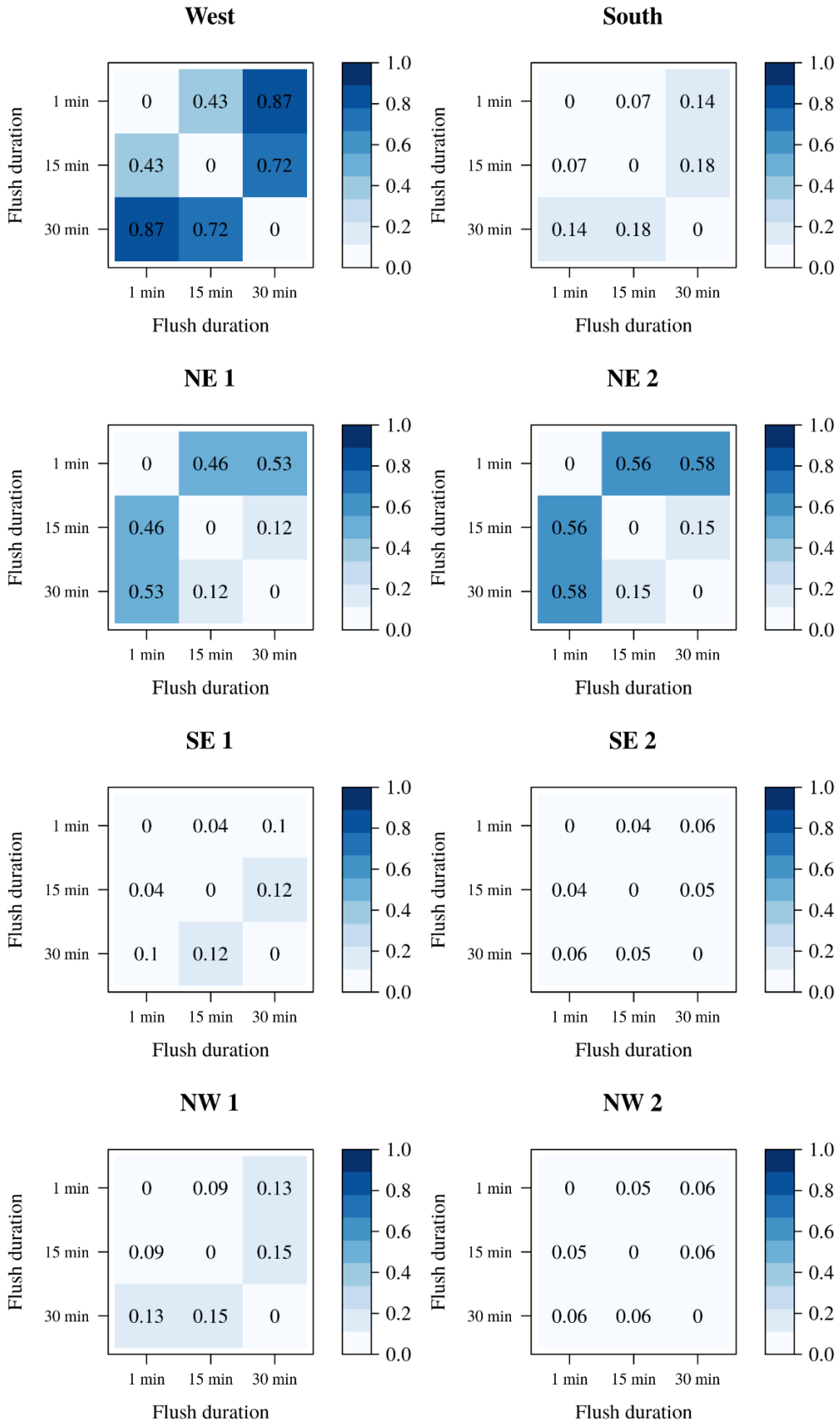

Figure A7.3 – Heatmap of the Bray-Curtis dissimilarity matrix for each hydrant, calculated between flush durations. The Bray-Curtis dissimilarity ranges from 0 to 1. Blue: higher dissimilarity, indicating more different fingerprints, white: lower dissimilarity, indicating more similar fingerprints. The fingerprints of the samples were pooled per flush duration.

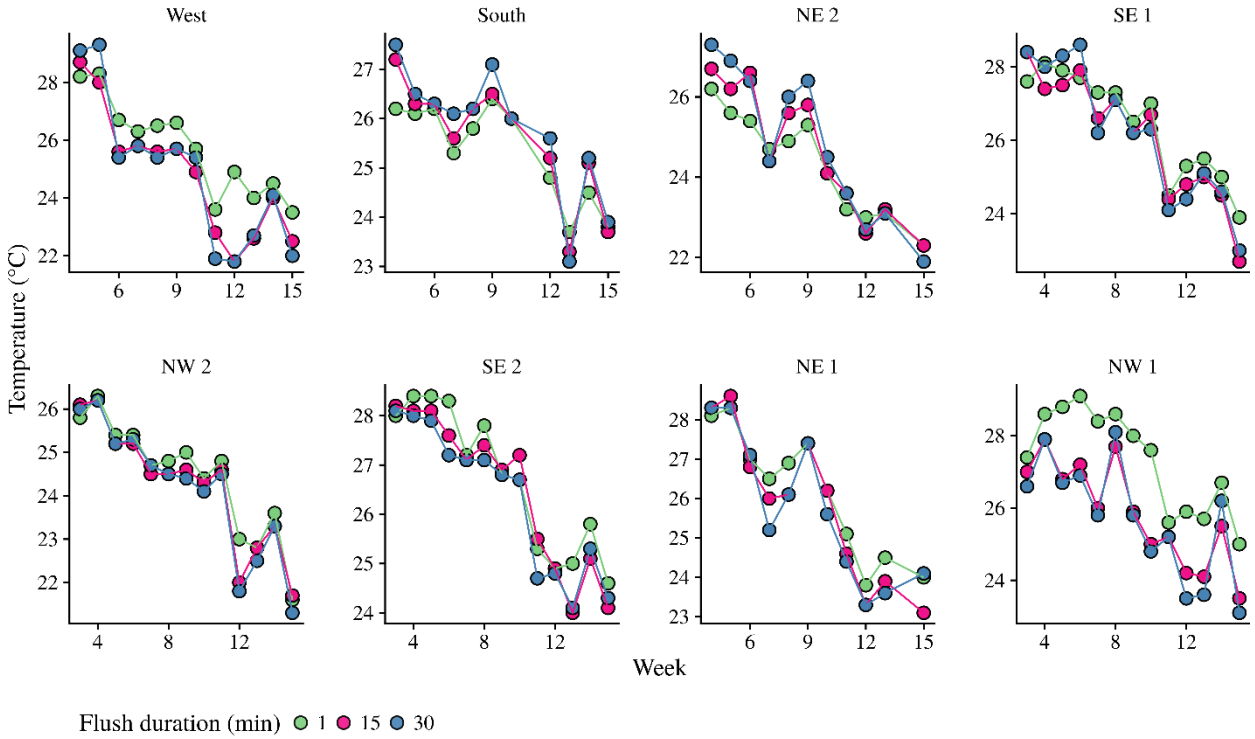

Figure A7.4 – Evolution of the temperature over time for all hydrants, coloured according to flush duration. The x-axis indicates the week, starting from June 26th.

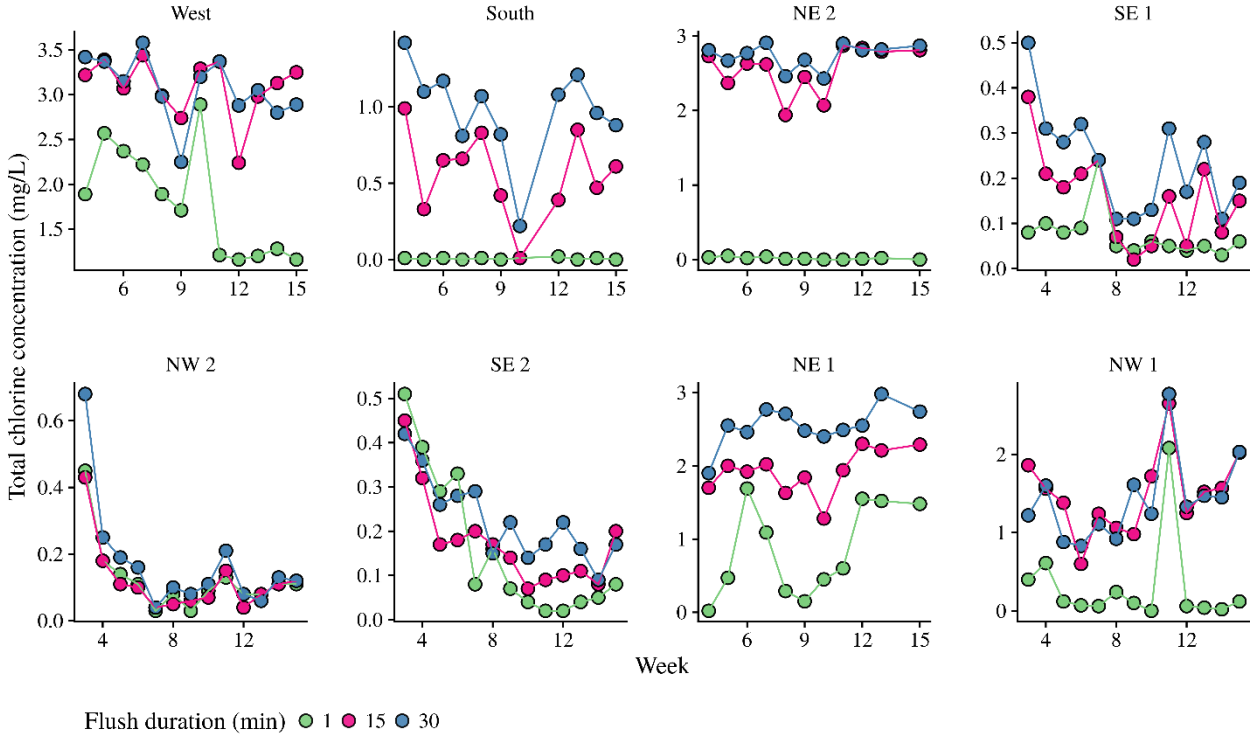

Figure A7.5 – Evolution of the total chlorine concentration over time for all hydrants, coloured according to flush duration. The x-axis indicates the week, starting from June 26th. To clearly show the hydrant-specific fluctuations, the axis are different for each hydrant.

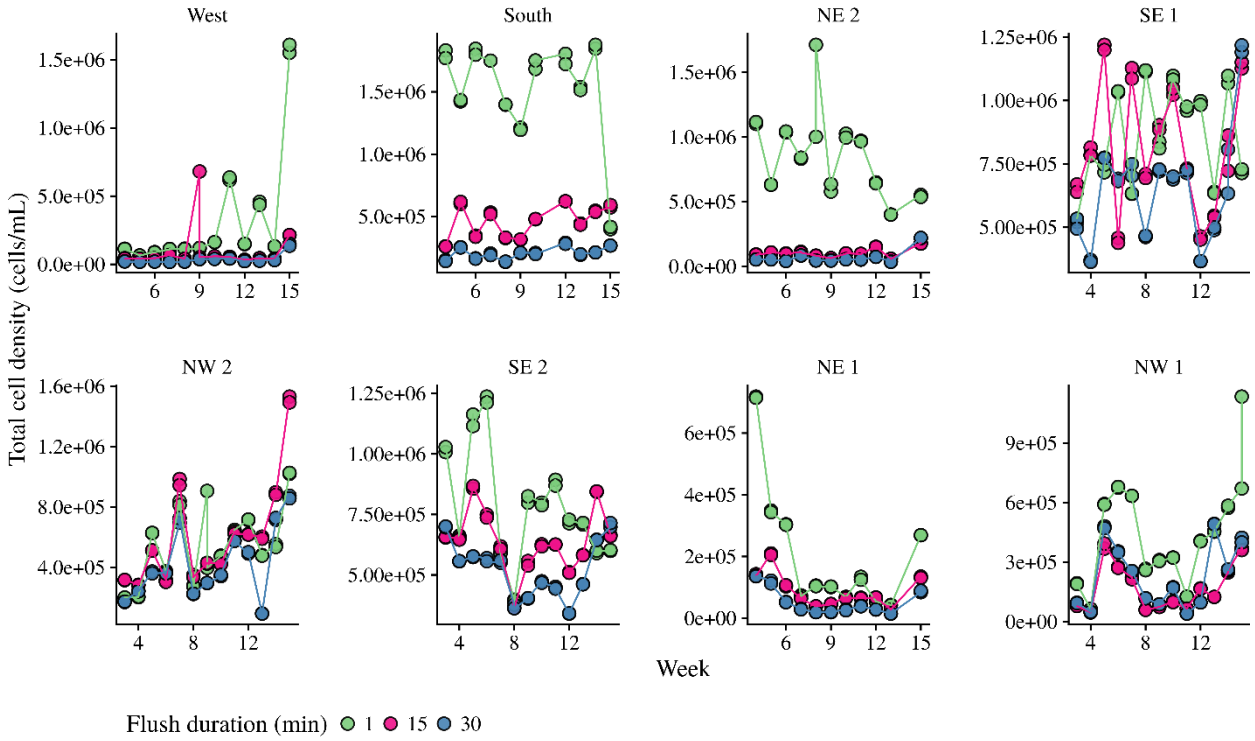

Figure A7.6 – Evolution of the total cell density over time for all hydrants, coloured according to flush duration. The x-axis indicates the week, starting from June 26th. To clearly show the hydrant-specific fluctuations, the axis are different for each hydrant.

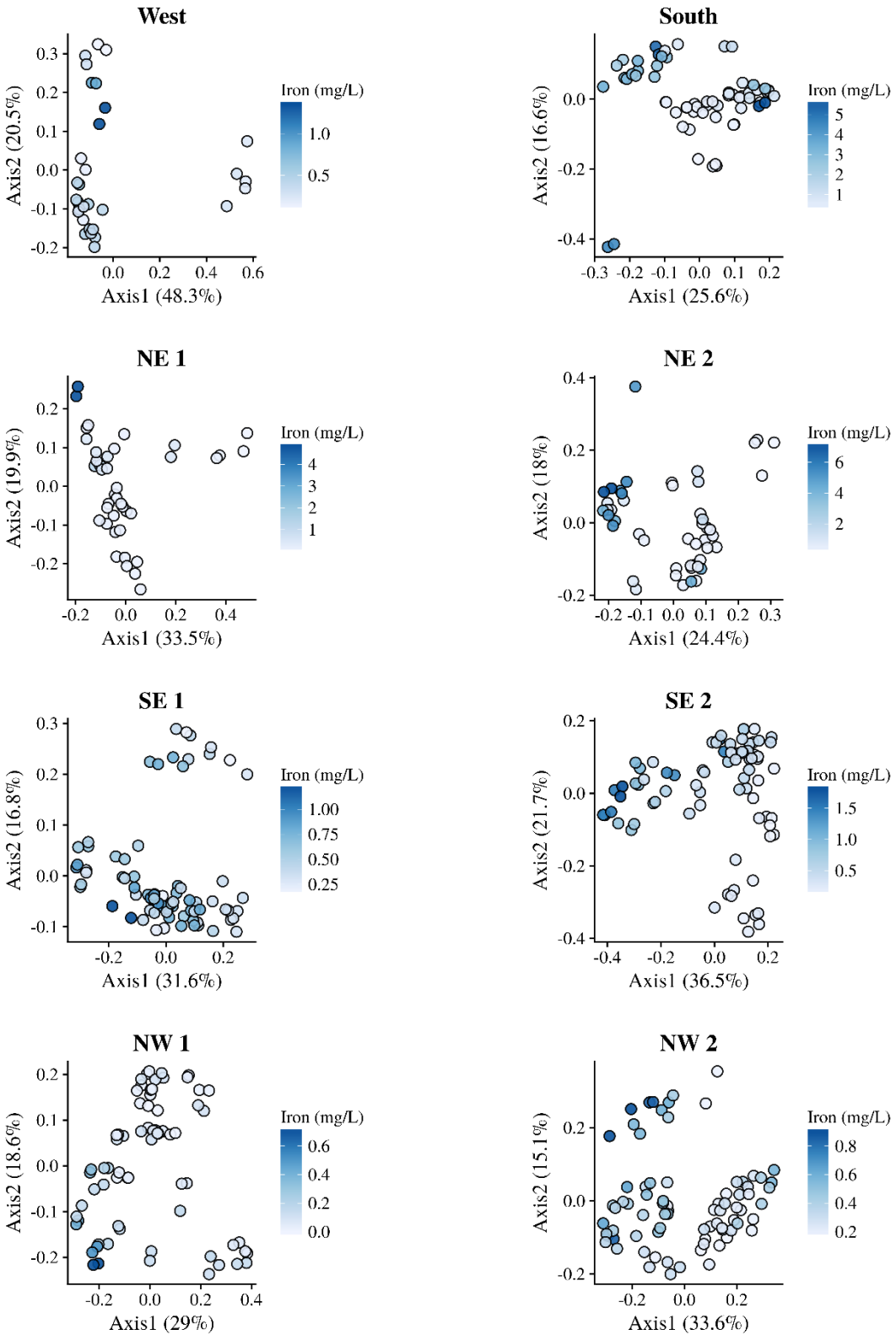

Figure A7.7 – PcoA ordination of phenotypic fingerprints for every hydrant (all flush times), coloured according to total iron concentration. Since the total iron concentration range is different for every hydrant, the scale is adapted for each hydrant.

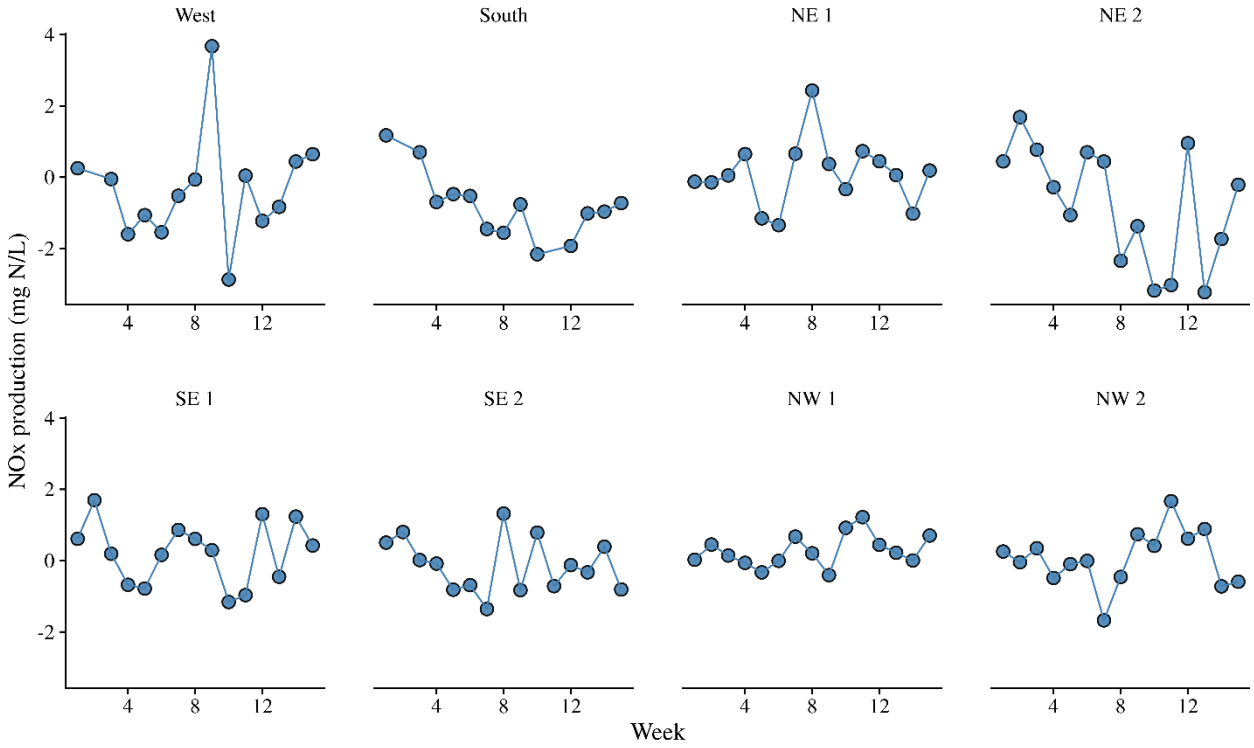

Figure A7.8 – NO_x production over time between subsequent sampling times. The NO_x production was calculated as the NO_2 + NO_3 concentration at 1 minute of flushing minus the NO_2 + NO_3 concentration at 30 minutes of flushing. Negative values indicate that the NOx concentration at 30 minutes of flushing was higher than the concentration at 1 minute of flushing.

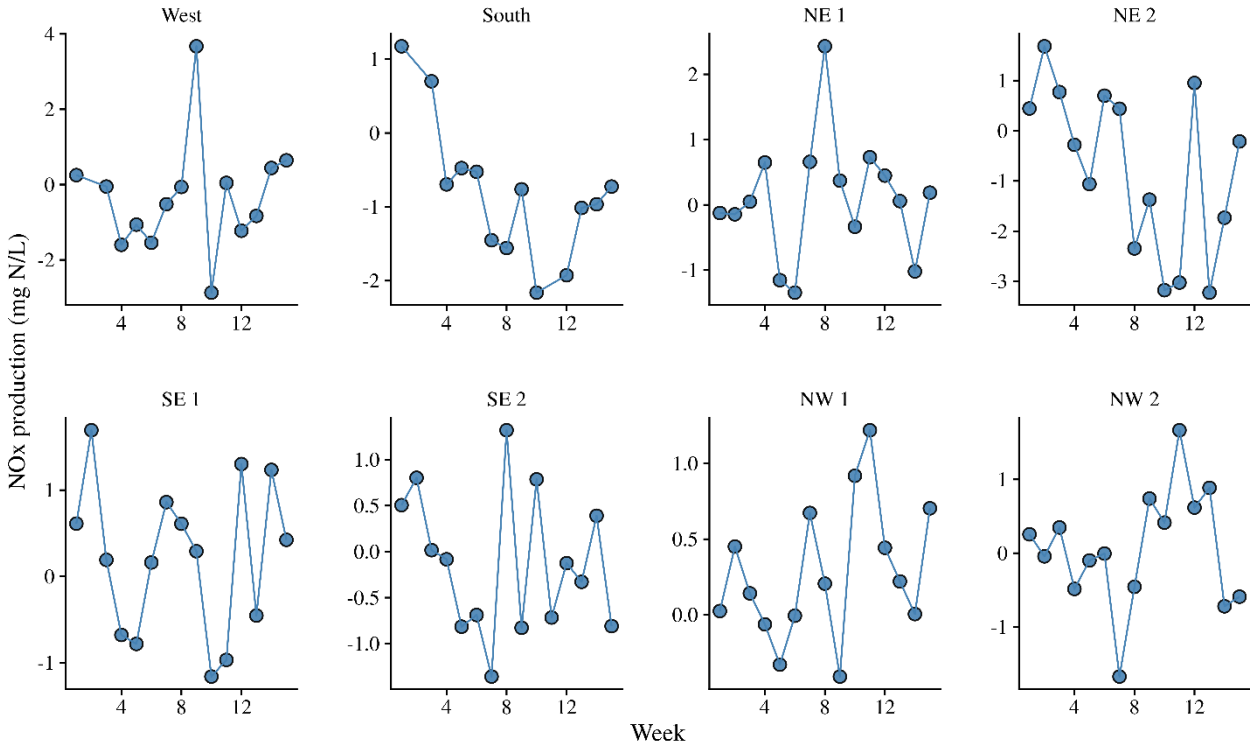

Figure A7.9 – Ammonia consumption over time between subsequent sampling times. The ammonia consumption was calculated as the TAN concentration at 30 minutes of flushing minus TAN concentration at 1 minute of flushing. Negative values indicate that the TAN concentration at 1 minute of flushing was higher than the concentration at 30 minutes of flushing.